Rare events in cluster-cluster aggregation

By

Subashri V

PHYS10201804002

The Institute of Mathematical Sciences, Chennai

A thesis submitted to the

Board of Studies in Physical Sciences

In partial fulfillment of requirements

for the Degree of

DOCTOR OF PHILOSOPHY

of

HOMI BHABHA NATIONAL INSTITUTE

Homi Bhabha National Institute

Recommendations of the Viva Voce Committee

As members of the Viva Voce Committee, we certify that we have read the dissertation prepared by Subashri V entitled "Rare events in cluster-cluster aggregation" and recommend that it may be accepted as fulfilling the thesis requirement for the award of Degree of Doctor of Philosophy.

_____   Date: 28/11/2024

Chairperson - Pinaki Chaudhuri

_____   Date: 28/11/2024

Guide/Convenor - Rajesh Ravindran

_____   Date: 28/11/2024

Examiner - Anupam Kundu

_____   Date: 28/11/2024

Member 1 - Satyavani Vemparala

_____   Date: 28/11/2024

Member 2 - Sitabhra Sinha

_____   Date: 28/11/2024

Member 3 - Manjari Bagchi

_____   Date: 28/11/2024

Member 4 - Sanjib Sabhapandit

Final approval and acceptance of this thesis is contingent upon the candidate's submission of the final copies of the thesis to HBNI.

I hereby certify that I have read this thesis prepared under my direction and recommend that it may be accepted as fulfilling the thesis requirement.

Date: 28/11/2024

Place: Chennai   Guide

STATEMENT BY AUTHOR

This dissertation has been submitted in partial fulfillment of requirements for an advanced degree at Homi Bhabha National Institute (HBNI) and is deposited in the Library to be made available to borrowers under rules of the HBNI.

Brief quotations from this dissertation are allowable without special permission, provided that accurate acknowledgement of source is made. Requests for permission for extended quotation from or reproduction of this manuscript in whole or in part may be granted by the Competent Authority of HBNI when in his or her judgement the proposed use of the material is in the interests of scholarship. In all other instances, however, permission must be obtained from the author.

Subashri V

DECLARATION

I hereby declare that the investigation presented in the thesis has been carried out by me. The work is original and has not been submitted earlier as a whole or in part for a degree / diploma at this or any other Institution / University.

Subashri V

LIST OF PUBLICATIONS ARISING FROM THE THESIS

<u>**Publications:**</u>

- <u>**Published**</u>

  1. A Monte-Carlo algorithm to measure probabilities of rare events in cluster-cluster aggregation, Rahul Dandekar, R. Rajesh, V. Subashri and Oleg Zaboronski, Computer Physics Communications 288, 108727 (2023)

  2. Exact calculation of the probabilities of rare events in cluster-cluster aggregation, R. Rajesh, V. Subashri, and Oleg Zaboronski, Physical Review Letters 133, no. 9 (2024): 097101.

- <u>**Submitted**</u>

  1. Exact calculation of the probabilities of rare events in $k-$nary coalescence, R. Rajesh, V. Subashri, Oleg Zaboronski, arXiv:2410.24118 (2024) (under review)

- <u>**In Preparation**</u>

  1. Instanton mass distributions for constant and sum kernel aggregation, R. Rajesh, V. Subashri and Oleg Zaboronski

List of presentations and participations at conferences

1. Poster on **Rare events in aggregation** at 'Building a bridge between non-equilibrium statistical physics and biology', Isaac Newton Institute for Mathematical Sciences, Cambridge, UK (2023)

2. Talk on **Exact calculation of the probabilities of rare events in cluster-cluster aggregation** at 'Frontiers in non-equilibrium physics, IMSc, India (2023)

3. Poster on **Rare events in aggregation** at StatPhys-Kolkata XI, IISER Kolkata, India (2022)

4. Statistical physics of complex systems, ICTS, Bengaluru, India (2022)

5. Frontiers in statistical physics, RRI, Bengaluru, India (2023)

6. Bangalore school of statistical physics, conducted by ICTS and RRI (2019)

Research visits and seminars

1. Visited Prof. Oleg Zaboronski at University of Warwick, UK (2023)

2. Talk on **Rare events in aggregation** for Institute Seminar Days, IMSc, India (2024)

3. Seminar talk on **Rare events in aggregation** at University of Warwick, UK (2023)

Thesis dedicated to (late) Prof. S.V.M. Sathyanarayana

ACKNOWLEDGEMENTS

am today.

I express my heartfelt gratitude to my Guru, Dr. S. Sowmya, who has always encouraged me to pursue academics with as much seriousness as music, and instilled in me the important skill of time management at an early age. I am forever grateful to her for the crucial role she plays in my life.

The person who opened my eyes to the wonders of physics, and inspired me to pursue PhD was late Prof. S.V.M. Sathyanarayana. He inspired hundreds of others from various socio-economic backgrounds to pursue physics, through his free Sunday classes at Madras University, the annual Physics Training and Talent Search (PTTS) and many more initiatives. He left us too soon, but his work is continued by many of his students and colleagues. At this juncture, I also thank thank Dr. Joseph Prabhagar, Dr. M. Sivakumar, Dr. H. S. Mani, (late) Dr. K.P.N. Murthy and Dr. Kamalesh Kar for mentoring me on various topics through Sunday class and PTTS. I also thank Prof. D. Indumathi (IMSc) for guiding me in my masters thesis. The period with her gave me a taste of working in a research institute, and further inspired me to pursue research in physics.

I found my life partner in my fellow PhD student, Himanshu Badhani. I am deeply grateful to him for his unconditional support in all my endeavours, and for making my time in IMSc memorable. I am especially thankful to him for listening to all my rants over the past few years, and bolstering my confidence when I was frustrated.

IMSc provided the environment for me to develop friendships with a variety of people. I thank Nishant Gupta for always being there for me. I thank Vinay Vaibhav for teaching me the basics of parallel computing, and helping me in various other ways, during the initial days of my PhD. I would also like to express my gratitude to my colleagues Amit, Apurba, Amir, Dipanjan, Asweel, Prasad, Goutham, Arup, Reshmi and Hitesh for the useful discussions that we have had regarding our work, and otherwise. I thank Dr. Varuni Prabhakar, Dr. R. Ramanujam and Dr. K. N.

Contents

7 Conclusions and Outlook

Synopsis

Interacting, many particle systems exhibit a wide range of complex behaviour including emergent phenomena that are not evident at the microscopic scale. These systems may be in thermal equilibrium or out of equilibrium. Equilibrium phenomena obey detailed balance and there exists a well-defined set of principles for calculating thermodynamic quantities, for instance the weight of a configuration is proportional to its Boltzmann weight. However, most of the physical phenomena around us are far from equilibrium, and characterised by non-zero currents, lack of detailed balance and often irreversible dynamics.

A well-studied example of nonequilibrium phenomena is cluster-cluster aggregation (CCA), a far-from-equilibrium, irreversible stochastic process where particles or clusters aggregate on contact to form larger clusters. The rates of collision depend on both on the transport properties of the clusters as well as the details of aggregation, and in general depend on the colliding masses. The study of CCA has a long history since the pioneering work of Smoluchowski in 1917 [1], and its omnipresence in many natural phenomena such as cloud formation [2], prion coagulation [3], polymers [4], etc., continue to make it an active area of research. The most common approach to study the kinetics of aggregation is the mean field Smoluchowski equation, which describes the time evolution of the mean number of clusters of a given mass. This first order non-linear differential equation is exactly solvable for a few special forms of the collision kernel, and specialised numerical techniques are required to solve for arbitrary kernels [5]. In lower dimensions, spatial fluctuations become important, and have been studied using renormalisation group techniques, exact solutions and simulations.

In this thesis, we study rare events or large fluctuations in CCA, *i.e.,* those trajectories that are far from the mean or typical trajectory, thereby characterizing

the process completely. These rare events correspond to the tails of a probability distribution. Although they have low likelihood, they may have high impact, such as natural disasters, epidemics or formation of a plaque in a brain affected by a neurodegenerative condition such as Alzheimer's disease. Large deviation theory forms a general mathematical framework for rare events, and is based on the insight that the probability of rare events decays exponentially with respect to a rate. The quantity of interest in characterizing rare events in this framework is the large deviation function or rate function, which is, in general, difficult to compute.

Large deviation theory forms a general framework in which the entire formulation of equilibrium statistical mechanics can be cast. The main outcomes of this are that a large deviation principle for the probability of occurrence of a macrostate exists, in the thermodynamic limit. Additionally, the large deviation function is equivalent to the negative of the entropy in the microcanonical ensemble, and to the free energy in the canonical ensemble. On the other hand, for systems out of equilibrium, large deviation theory provides a consistent framework in which the large deviation function can be interpreted as a nonequilibrium generalization of entropy, while the scaled cumulant generating function associated with the distribution can be interpreted as a nonequilibrium generalization of free energy.

Questions

1. Can an efficient numerical algorithm to compute the probabilities of rare events in CCA be designed and implemented?

2. Can an analytical formalism to obtain the rate functions, as well as most probable trajectories for arbitrary collision kernels be developed?

3. Can the formalism be generalised to cases when the collisions are not binary, but multiparticle?

Model

We study the following model for CCA, also known as the Marcus-Lushnikov model [6, 7]. Consider a collection of particles which are labeled by their masses. Given a configuration, the system evolves stochastically in time through mass-conserving binary aggregation:

$$A_i + A_j \xrightarrow{K(i,j)} A_{i+j}, \tag{1}$$

where A_k denotes a particle of mass k, and the collision kernel $K(i,j)$ is the rate at which two particles of masses i and j aggregate. In an infinitesimal time dt, the probability of collision of two particles having masses i and j is given by $K(i,j)dt$. Since each aggregation event reduces the number of particles, $N(t)$, by 1, $N(t)$ decreases monotonically with time. Initially, there are $N(0) = M$ particles with equal mass m_0. We set $m_0 = 1$, so that all masses are measured in units of m_0. We note that the collision kernel $K(i,j)$ is dependent on the physical process being modelled.

We also study $k-$nary coalescence, where collisions are not binary. Consider a system of particles, which evolves in time through the generalized coalescence process,

$$kA \xrightarrow{\lambda} \ell A, \quad \ell < k \tag{2}$$

where A denotes a particle. Equation (6.1) describes the aggregation of k particles into ℓ particles at constant rate λ. Each collision reduces the number of particles, $N(t)$, by $(k - \ell)$. The final absorbing state of this process contains $\ell, \ell + 1, \ldots k - 1$ particles, depending on the value of the initial number of particles, M.

In both the models described above, we compute $P(M, N, t)$, the probability that exactly N particles remain at time t, given that there are M particles initially. Here

the time t is fixed, and N is the random variable. We also compute the quantity $\tilde{P}(M, N, t)$, the probability that the $C-$th collision, where $C = M - N$ for the binary aggregation model, and $C = (M - N)/(k - \ell)$ for $k-$nary coalescence, occurs at time t. Here N is fixed and t is the random variable. In the large deviation limit,

$$\tilde{P}(M, N, t) \approx P(M, N, t), \tag{3}$$

and we will not make the distinction between $P(M, N, t)$ and $\tilde{P}(M, N, t)$ henceforth. We also compute the most probable trajectory for a given M, N, t.

Findings of the thesis

The answers to the questions posed above are enumerated below.

1. **A Monte-Carlo algorithm to measure probabilities of rare events in CCA**

   A biased Monte Carlo algorithm to measure probabilities of rare events in cluster-cluster aggregation for arbitrary collision kernels is developed. Given a trajectory, the algorithm flips between trajectories by modifying the waiting times between collisions, the sequence of collisions, as well as the number of collisions, all using local moves.

   - The waiting times are modified by weighting them with a bias parameter, such that they are biased towards the tails of $P(M, N, t)$.

   - The sequence of collisions is modified by reassigning a randomly chosen collision in a rejection-free manner, such that the trajectory is only modified locally, as shown in Fig. 1.

   - The number of collisions is modified either by adding a collision after the $C-$th collision, or by deleting the $C-$th collision, with rates that satisfy
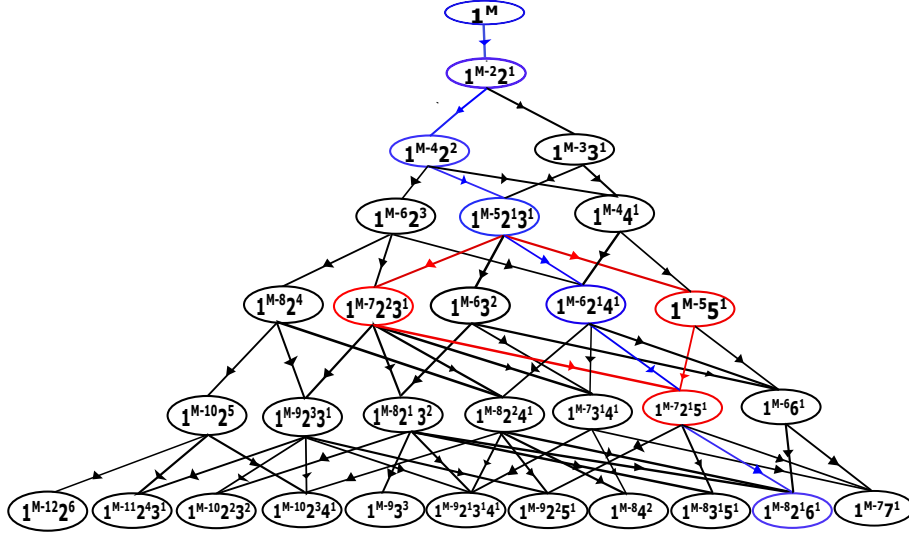
Figure 1: All possible configurations and trajectories for 6 collisions. The configurations after each collision are shown inside the bubbles. For the trajectory shown in blue, the red lines denote possible alternate paths that alter only the 4th configuration.

detailed balance.

- We prove the ergodicity of the algorithm by specifying a protocol that transforms an arbitrary trajectory to a standard trajectory using valid Monte Carlo moves.

- Rare events with probabilities of the order of 10^{-40} and lower are sampled, as shown in Fig. 2. The algorithm is shown to be independent of the initial configuration of clusters.

- The algorithm is tested for constant kernel aggregation $[K(i,j) = 1]$ by benchmarking the large deviation function with the exact answer (Fig. 2).

- The algorithm is characterized by measuring the autocorrelation times corresponding to the waiting times as well as the configurations. We find that the optimum fraction of Monte Carlo moves corresponding to waiting time changes should be close to 1, as the autocorrelation time corresponding to waiting time changes shows at most a weak dependence on M, while the autocorrelation time corresponding to configuration changes is proportional to M^2.
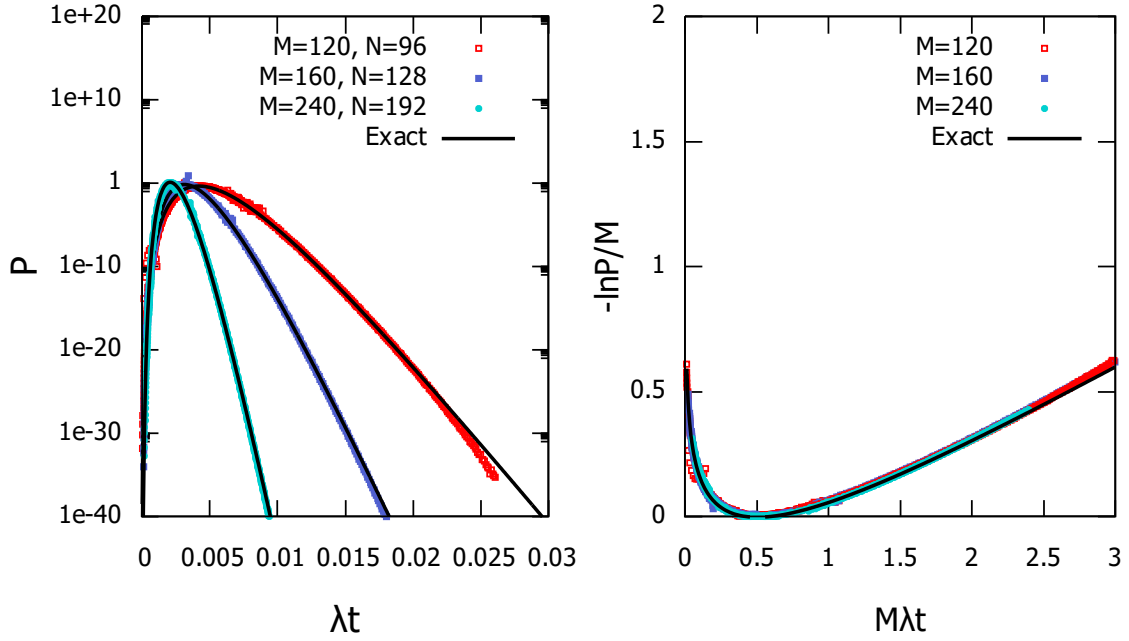
Figure 2: (a) $P(M, N, t)$ for the constant kernel for different M, keeping $\phi = N/M = 0.8$ fixed are compared with the exact solution. (b) The data in (a) for different M collapse onto one curve when scaled, to give the large deviation function.

2. **Exact calculation of the probabilities of rare events in CCA**

- **Calculation using Doi-Peliti-Zeldovich formalism**

  We develop a formalism to calculate the probabilities of rare events in cluster-cluster aggregation for arbitrary collision kernels, using the Doi-Peliti-Zeldovich formalism of writing the master equation in terms of an action.

  - By rewriting these probabilities in terms of minimizing an effective action, we establish, for any arbitrary collision kernel, a large deviation principle with the total mass M being the rate,

  $$P(M, N, t) \approx e^{-Mf(\phi, \tau)}, \tag{4}$$

  where $\phi = N/M$, $\tau = tM$, and $f(\phi, \tau)$ is the large deviation function.

6

- The large deviation functions of constant, sum and product kernels are as follows.

  * Constant kernel $[K(i,j) = 1]$:

$$f(\phi,\tau) = \tag{5}$$

$$\begin{cases} \phi \ln \frac{\phi^2}{-2E+\phi^2} + \ln(1-2E) - E\tau, & E < 0, \\[2mm] 0 & E = 0, \\[2mm] -E\tau - 2\phi \ln \frac{2E}{\phi} - (1-\phi) \ln \frac{\sinh \tau \sqrt{E/2}}{1-\phi} + \\[2mm] (1+\phi) \ln(\sqrt{2E} \cosh \tau \sqrt{E/2} + \sinh \tau \sqrt{E/2}), & E > 0, \end{cases}$$

  where E is a parameter of the theory that is determined in terms of ϕ, τ, and is a constant of motion.

  * Sum kernel $[K(i,j) = (i+j)/2]$:

$$f(\phi,\tau) = -(1-\phi) \ln \frac{1-e^{-\frac{\tau}{2}}}{1-\phi} + \frac{\tau \phi}{2} + \phi \ln \phi. \tag{6}$$

  * Product kernel $[K(i,j) = ij]$:

$$f(\phi,\tau) = \ln \frac{\phi^\phi e^{\tau/2+1-\phi}}{\tau^{1-\phi}} + \min_x \{\ln x - \phi\, h(x)\}, \tag{7}$$

$$h(x) = \sum_{k=1}^{k^*} \frac{x^k F_{k-1}(e^{\tau/M})}{k!}, \tag{8}$$

  where $F_k(x)$ are the Mallows-Riordan polynomials.

- The large deviation functions are in excellent agreement with large-scale Monte Carlo simulations, as shown in Fig. 3.

- We show that the large deviation function for the product kernel is singular. In particular, we show that $\partial^2 f / \partial \phi^2$ is discontinuous at a $\tau-$dependent critical ϕ, suggesting the presence of a second order phase transition. This singular behaviour corresponds to the

7
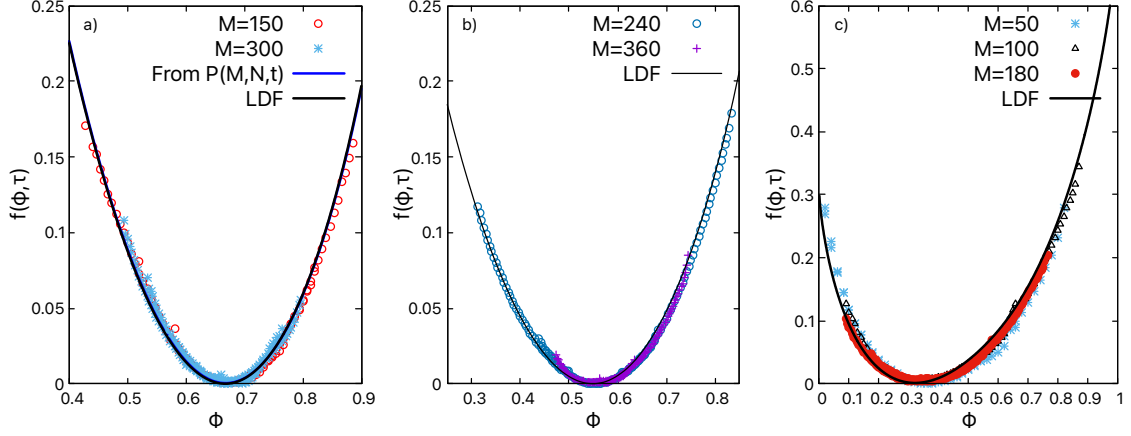
Figure 3: The LDF $f(\phi, \tau)$ with respect to ϕ (a) for constant kernel, $\tau_f = 1$, (b) for sum kernel, $\tau = 1.2$, and (c) product kernel, $\tau = 1.4$.

formation of a gel.

– The instanton trajectories for constant and sum kernels are calculated exactly and found to match well with the simulations. However, for the product kernel, the equation for the instanton trajectory involves higher order moments of the mass distribution, and hence is difficult to solve.

– Instanton mass distributions:

* Using the algorithm described in Point 1, the instanton mass distributions at typical and atypical times can be determined for any collision kernel.

* We obtain the exact expressions for the mass distributions of constant and sum kernels.

* For a given number of collisions, the instanton mass distribution at the final time for both the constant and sum kernels is shown to be invariant, and equal to the typical mass distribution.

• **Exact calculation of large deviation function for the product kernel**

For the product kernel, the calculation of the large deviation function

8

using the Doi-Peliti-Zeldovich formalism has an issue, which is the non-uniqueness of the action. We provide an alternate exact solution that bypasses the Doi-Peliti-Zeldovich formalism and instead relies on the replica trick.

3. **Exact calculation of the large deviation function for k-nary coalescence**

- For arbitrary k, ℓ, we derive the large deviation function describing the probability of finding N particles at time t, when starting with M particles initially.

- The asymptotic behaviour of the large deviation function for $\tau \to 0$ and $\tau \to \infty$ is computed exactly.

- The instanton trajectories for rare and typical events are obtained.

Chapter 1

Introduction

Interacting, many particle systems exhibit a wide range of complex behaviour including emergent phenomena that are not evident at the microscopic scale, which may be in thermal equilibrium or out of equilibrium. Equilibrium phenomena obey detailed balance and there exists a well-defined set of principles for calculating thermodynamic quantities, However, most of the physical phenomena around us are far from equilibrium, and characterised by non-zero currents, lack of detailed balance and often irreversible dynamics. One such phenomenon is cluster-cluster aggregation (CCA), in which particles, or clusters coalesce on contact to form larger clusters. The rates of collision depend on the transport properties of the clusters, as well as the details of aggregation, and in general, on the colliding masses. The study of cluster-cluster aggregation has a long history dating back to Smoluchowski in 1917 [1]. There are many physical phenomena in which the dominant dynamic process is coalescence or aggregation. Examples include blood coagulation [8], cloud formation [9, 10], aerosol dynamics [11], dynamics of Saturn's rings [12, 13], aggregation of particulate matter in oceans [14], protein aggregation [15, 3], coagulation of soot particles [16, 17, 18], colloids [19], charged polymers [20, 21], etc. CCA also finds applications in applied fields such as river networks [22], mobile networks [23],

population genetics [24] and explosive percolation [25, 26], etc. In addition to direct applications, CCA is also of interest as a nonequilibrium process obeying self-similar scaling at large times with exponents that are universal and dependent only on generic details of the transport.

CCA has been analyzed using different approaches. The most common approach is to solve the deterministic mean-field Smoluchowski equation that describes the change in the number of clusters of a given mass due to coagulation events (see Refs. [27, 28, 29, 30] for reviews). The Smoluchowski equation for the mean mass distribution is exactly solvable when the rate of collision is independent of the masses (constant kernel), is the sum of the masses (sum kernel), and product of the masses (product kernel). For the product kernel, a sol-gel transition is observed wherein the total mass is not conserved beyond a gelling time. For the sum kernel, the gelling occurs at infinite time [29]. In lower dimensions, spatial density fluctuations become important and have been studied using both analytical and numerical techniques [31, 32, 33, 34]. These approaches are, however, restricted to studying the mean or typical mass distribution and the low order moments of the mean mass distributions and do not give information about either the probabilities of rare or atypical events or the trajectories that lead to atypical events.

Rare events are those which occur at the tails of a probability distribution, and have a low likelihood of occurrence. In a stochastic process, although rare events occur infrequently, they often have a large impact. Examples include cyclones, tsunamis, earthquakes [35], giant rogue waves in the middle of the ocean [36], heat waves [37, 38], financial black swan events [39], neurological disorders [40] and pandemics like COVID-19. For predicting their occurrence in order to plan for them, it is important to have an estimate of the probability of occurrence as well as the atypical trajectories that lead to rare events. Also, knowing the probabilities gives complete information about the large fluctuations of a system around its most prob-

able states. The behaviour of the tails of the probability distributions describing these large fluctuations are captured by the large deviation function [41]. The large deviation function is the central focus of study of large deviation theory. Large deviation theory forms a general framework in which the entire formulation of equilibrium statistical mechanics can be cast. It has been applied successfully to many established models in equilibrium such as the Potts model and $2D$ Ising model. The main outcomes of this are that a large deviation principle for the probability of occurrence of a macrostate exists, in the thermodynamic limit. Additionally, the large deviation function is equivalent to the negative of the entropy in the microcanonical ensemble, and to the free energy in the canonical ensemble. On the other hand, for systems out of equilibrium, large deviation theory provides a consistent framework in which the large deviation function can be interpreted as a nonequilibrium generalization of entropy, while the scaled cumulant generating function associated with the distribution can be interpreted as a nonequilibrium generalization of free energy.

Numerically, many sophisticated techniques have been developed for studying rare events, such as importance sampling [5, 42, 43] and splitting algorithms. In importance sampling, the original probability distribution is biased so that the rare event occurs more frequently. The distribution is then unbiased to obtain the true probability of the event. Different kinds of importance sampling methods have been developed to sample rare events, such as instanton based importance sampling [44] and adaptive importance sampling [45]. In splitting algorithms, events close to the rare event of interest are realized many times while other events are allowed with a certain probability, in the course of the simulation. Different types of splitting algorithms include static and dynamic splitting, and adaptive splitting algorithms [46]. A review of the different numerical methods available for calculating probability of rare events may be found in Refs. [47, 48].

However, there are no algorithms in the literature which measure the probabilities

of rare events in aggregation. The study of rare events in aggregation is a challenging problem, because the number of possible configurations after each collision increases rapidly, which implies that sampling these configurations would be a computationally expensive task. Can an efficient numerical algorithm to compute the probabilities of rare events in CCA be designed and implemented? Can an analytical formalism to obtain the rate functions, as well as most probable trajectories for arbitrary collision kernels be developed? Can we analytically obtain the probabilities of rare events? Can the algorithm and formalism be used to study the optimal evolution trajectories, and mass distributions contributing to a given rare event? Can the formalism be generalised to cases when the collisions are not binary, but multiparticle?

Questions

1. Can an efficient numerical algorithm to compute the probabilities of rare events in CCA be designed and implemented?

2. Can an analytical formalism to obtain the rate functions, as well as most probable trajectories for arbitrary collision kernels be developed?

3. Can the formalism be generalised to cases when the collisions are not binary, but multiparticle?

In this thesis, we develop a Monte Carlo algorithm to measure probabilities of rare events in CCA for arbitrary collision kernels, based on importance sampling, whuch can sample events with probabilities as low as 10^{-40}, and smaller. We also develop an action formalism to calculate probabilities of rare events for arbitrary collision kernels and establish a pathwise large deviation principle with total mass being the rate. As an application, the rate function for the number of surviving particles as

well as the optimal evolution trajectory are calculated exactly for the constant, sum and product kernels. We also calculate the full mass distributions for the constant and sum kernels. We apply this formalism to find the large deviation function for the general coalescence process, $kA \to \ell A$.

The remainder of the thesis is organized as follows. In Chapter 2, we provide brief reviews of the Smoluchowski equation and large deviation theory. We decribe the Smoluchowski solutions for the constant, sum and product kernels, and a remarkable exact solution by Lushnikov for the product kernel. In Chapter 3, we describe in detail the algorithm developed to access the tails of probability distributions in CCA. In Chapter 4, we develop a general analytical formalism to obtain the probabilities of rare events for arbitrary collision kernels. We explicitly calculate these probabilities for the constant, sum and product kernels. In Chapter 5, we obtain the full mass distribution for the constant and sum kernels. In Chapter 6, we apply this formalism to obtain the probabilities of rare events to the case of $k-$nary coalescence, when more than two particles collide.

Chapter 2

Review

In this chapter, we provide detailed reviews of the two cornerstones of this thesis - aggregation and large deviation theory. The reviews include historical background, and the existing results that are relevant to the work done as part of this thesis.

2.1 Review of aggregation

Much of the work on aggregation has concentrated on solving the Smoluchowski equation for various kernels, using analytical and numerical methods. In this chapter, we provide a review of the important results obtained by solving this equation, and also some other results beyond the Smoluchowski equation.

2.2 Marcus-Lushnikov model

Consider a collection of particles which are labeled by their masses. Given a configuration, the system evolves in time through mass-conserving binary aggregation

(also known as Marcus-Lushnikov model [6, 7, 49, 50]):

$$A_i + A_j \xrightarrow{\lambda K(i,j)} A_{i+j}, \qquad (2.1)$$

where A_k denotes a particle of mass k, and $\lambda K(i,j)$ is the rate at which two particles of masses i and j aggregate. In an infinitesimal time dt, the probability of collision of two particles having masses i and j is given by $\lambda K(i,j)dt$. The collision kernel, $K(i,j)$, is dependent on the transport properties of the clusters and their collisional area of cross-section. We note that all the spatial information has been encoded into the collision kernel. Since each aggregation event reduces the number of particles, $N(t)$, by 1, $N(t)$ decreases monotonically with time. Initially, there are $N(0) = M$ particles with equal mass m_0. We set $m_0 = 1$, so that all masses are measured in units of m_0.

The Smoluchowski equation is a mean-field, integro-differential equation which describes the time evolution of $n(m,t)$, the mean number of clusters of mass m:

$$\frac{dn_m(t)}{dt} = \frac{1}{2} \sum_{i=1}^{m-1} \lambda K(i, m-i) n_i(t) n_{m-i}(t) - n_m(t) \sum_{i=1}^{\infty} \lambda K(m,i) n_i(t). \qquad (2.2)$$

On the right hand side of Eq. (2.2), the first term describes the formation of clusters of mass m, while the second term describes the depletion of clusters of mass m, by coagulating with other clusters. Note that this is a mean field equation, *i.e.*, correlations higher than first order are ignored. In other words,

$$\langle n_i(t) n_j(t) \rangle = \langle n_i(t) \rangle \langle n_j(t) \rangle. \qquad (2.3)$$

The dimensions of the rate λ are the inverse of time. In the following analysis, we make the transformation $\lambda t \to t$.

Equation (2.2) has been solved exactly only for three kernels - constant [$K(i,j) = 1$],

sum $[K(i,j) = i + j]$ and product $[K(i,j) = ij]$. Although Eq. (2.2) is defined for infinite mass, it explicitly conserves mass for an arbitrary $K(i,j)$, *i.e.*,

$$\frac{d}{dt} \sum_m m n_m(t) = 0. \tag{2.4}$$

However, the solution $n(m,t)$ for certain kernels does not conserve mass. The simplest kernel which exhibits this behaviour, known as gelation, is the product kernel.

In Sec. 2.3, 2.4 and 2.5, we provide a review of the solution of the Smoluchowski kernels for these three kernels. The detailed calculations can be found in [29, 27]. In Sec. 2.6, we describe Lushnikov's remarkable exact solution for the mass distribution of the product kernel.

2.3   Constant kernel $[K(i,j) = 1]$

The constant kernel is the simplest kernel that can be solved exactly. The mass distribution for the constant kernel has been obtained by solving for the moments of the mass distribution recursively. The Smoluchowski equation in this case is

$$\frac{dn_i}{dt} = \frac{1}{2} \sum_{j=1}^{i-1} n_j n_{i-j} - \sum_{j=1}^{\infty} n_i n_j, \tag{2.5}$$

with the initial condition set to be $n_i(0) = M\delta_{i,1}$, where M is the total mass of the system. The evolution of the zeroth moment of $n(m,t)$, denoted by $n(t)$, which corresponds to the total number of clusters remaining, is evolution is given by

$$\frac{dn}{dt} = -\frac{n^2}{2}. \tag{2.6}$$

Solving the equation for $n(t)$,

$$n(t) = \frac{2M}{2 + Mt} \xrightarrow[M \to \infty]{} \frac{2}{t}. \tag{2.7}$$

The first moment corresponds to the total mass M, which is conserved, *i.e.*,

$$\frac{dM}{dt} = 0. \tag{2.8}$$

Substituting Eq. (2.7) into the Smoluchowski equation for $n_1(t)$,

$$\frac{dn_1}{dt} = -n_1 n(t). \tag{2.9}$$

Solving for $n_1(t)$, we obtain

$$n_1(t) = \frac{4M}{(2 + Mt)^2}. \tag{2.10}$$

Using the answer for $n_1(t)$ in the Smoluchowski equation for $n_2(t)$, we obtain the result for $n_2(t)$. Solving recursively in this way, we obtain the typical mass distribution for the constant kernel,

$$n_i(t) = \frac{M(t/2)^{i-1}}{(1 + t/2)^{i+1}}. \tag{2.11}$$

Equivalence to binary coalescence

The collision rates for constant kernel aggregation do not explicitly depend on the colliding masses. This suggests that constant kernel aggregation is equivalent to the phenomenon of binary coalescence, $A + A \to A$. The rate equation for the time evolution of number of particles in binary coalescence is

$$\frac{dn}{dt} = -\frac{n^2}{2}, \tag{2.12}$$

which is the same as Eq. (2.6). This equation can be obtained from the exact master equation for the probability of n particles at time t, and ignoring second and higher order correlations.

2.4   Sum kernel $[K(i,j) = (i + j)]$

The next kernel for which the exact mean mass distribution can be obtained is the sum kernel. The Smoluchowski equation is given by

$$\frac{dn_i}{dt} = \frac{1}{2} \sum_{j=1}^{i-1} i n_j n_{i-j} - n_i[in(t) + M], \tag{2.13}$$

where $n(t) = \sum_j n_j(t)$, $M = \sum_j j n_j(t)$ and the initial condition is $n_m(0) = M\delta_{m,1}$. The equations for the moments are

$$\frac{dn}{dt} = -Mn(t), \tag{2.14}$$

$$\frac{dM}{dt} = 0, \tag{2.15}$$

$$\frac{dM_2}{dt} = 2MM_2, \tag{2.16}$$

$$\frac{dM_3}{dt} = 3MM_3 + 3M_2^2, \tag{2.17}$$

and so on, with the initial condition for all the moments being $M_k(0) = M$. These equations can be solved recursively to yield $n(t) = Me^{-Mt}$, $M_2(t) = Me^{2Mt}$ etc. The second and higher moments diverge in the limit $t \to \infty$, implying that a macroscopic cluster known as gel, forms at infinite time. In order to obtain the mass distribution $n_i(t)$, we define:

$$n_m(t) = \Psi_m(t)e^{-\int_0^t dt'(mn(t)+M)}, \tag{2.18}$$

Then, from Eq. (2.13), we obtain,

$$\frac{\partial \Psi_m(\tau)}{\partial \tau} = \sum_i i \Psi_i \Psi_{m-i}, \tag{2.19}$$

where $\frac{d\tau}{dt} = e^{-Mt}/2$. In other words, $\tau = (1 - e^{-Mt})/2M$. Substituting the ansatz

$$\Psi_m(\tau) = a_m \tau^{m-1}, \tag{2.20}$$

we obtain

$$a_m = \frac{m}{m-1} \sum_i a_i a_{m-i}. \tag{2.21}$$

The generating function for a_m is written as

$$F(x) = \sum_m a_m x^m. \tag{2.22}$$

The equation for $F(x)$ is

$$x \frac{\partial F}{\partial x} - F(x) = 2F(x)x \frac{\partial F}{\partial x}. \tag{2.23}$$

Rearranging the terms and integrating,

$$\ln F - 2F = \ln \left(\frac{x}{x_0} \right), \tag{2.24}$$

and hence

$$Fe^{-2F} = \frac{x}{x_0}. \tag{2.25}$$

The left hand side can be rewritten in terms of the Lambert W function, $z = W(z)e^{W(z)}$ by multiplying both sides by -2,

$$-2Fe^{-2F} = \frac{-2x}{x_0}, \tag{2.26}$$

20

where $W(z) = -2F, z = \frac{-2x}{x_0}$. The Lambert function can be expanded as a series in z:

$$W(z) = \sum_{n=1}^{\infty} \frac{(-n)^{n-1}z^n}{n!}. \qquad (2.27)$$

That is,

$$2F = \sum_{m=1}^{\infty} \frac{m^{m-1}}{m!} \left(\frac{2x}{x_0}\right)^m. \qquad (2.28)$$

Hence,

$$a_m = \frac{(2m)^{m-1}a^m}{m!}, \qquad (2.29)$$

where $a = 1/x_0$. Substituting this result in the ansatz Eq. (2.20), and the resulting answer in Eq. (2.18), we obtain the final mass distribution,

$$n_k(t) = M\frac{k^{k-1}}{k!}(1 - e^{-Mt})^{k-1}e^{-Mt}e^{-k(1-e^{-Mt})}. \qquad (2.30)$$

2.5   Product kernel $[K(i, j) = ij]$

We now present the solution for the product kernel. The Smoluchowski equation for the product kernel is

$$\frac{dn_i}{dt} = \frac{1}{2}\sum_{j} j(i - j)n_j n_{i-j} - in_i M, \qquad (2.31)$$

where $M = \sum_j jn_j(t)$. Defining the generating function $G(x, t) = \sum_m mn_m(t)e^{mx}$ with the initial condition

$$G_0 = G(x, 0) = Me^x, \qquad (2.32)$$

we obtain

$$\frac{\partial G}{\partial t} = G\frac{\partial G}{\partial x} - M\frac{\partial G}{\partial x}. \qquad (2.33)$$

The characteristic curves for this partial differential equation have the slope

$$\frac{dx}{dt} = M - G. \tag{2.34}$$

But, it can also be verified from the partial differential equation that the generating function $G(x,t)$ remains constant along the characteristic curve. Hence,

$$x = (M - G)t + f(G), \tag{2.35}$$

where the function $f(G)$ is determined from the initial condition Eq. (2.32). From the initial condition, we obtain

$$x(t = 0) = \ln\left(\frac{G_0}{M}\right). \tag{2.36}$$

Substituting in the characteristic curve and rearranging, we obtain

$$Gte^{-Gt} = Mte^{-Mt}e^x. \tag{2.37}$$

In order to obtain Gt as a power series in e^x, we use the Lagrange inversion formula [29]: given a function $X = f(Y)$, and $X \approx Y$ for small Y, Y is given in terms of a power series in X, $Y = \sum_{n=1}^{\infty} b_n X^n$, with the coefficients:

$$b_n = \frac{1}{2\pi i} \oint \frac{Y}{X^{n+1}} dX. \tag{2.38}$$

Here, $Y = Gt, X = Mte^{-Mt}e^x$. Using Lagrange inversion formula and solving,

$$b_m = \frac{m^{m-1}}{m!}. \tag{2.39}$$

Now, writing $G(x,t)$ in terms of a power series in e^x,

$$G(x,t) = \sum_m m n_m(t) e^{mx} = \sum_m \frac{m^{m-1}}{m!} (Mt)^m e^{-mMt} e^{mx}. \tag{2.40}$$

The final mass distribution is

$$n_m(t) = M \frac{m^{m-2}}{m!} e^{-mMt} (Mt)^{m-1}. \tag{2.41}$$

We now consider the moments of the mass distribution:

$$\frac{dn}{dt} = -\frac{M^2}{2}, \tag{2.42}$$

$$\frac{dM}{dt} = 0. \tag{2.43}$$

Solving Eq. (2.42), we obtain

$$n(t) = M - \frac{M^2 t}{2}. \tag{2.44}$$

we note that $n(t) = 0$ at $Mt = 2$, and is negative when $Mt > 2$. Naively solving for the second moment $M_2(t)$, we obtain

$$M_2(t) = \frac{M}{1 - Mt}. \tag{2.45}$$

It is evident from this result that there is a singularity at $Mt = 1$, where $M_2(t)$ diverges. Further, we see that all the higher moments exhibit this singularity at $Mt = 1$.

We compare the mass distribution Eq. (2.41) with Monte-Carlo simulations. The solution matches with Monte Carlo simulations for $t < 1$. But, for $t > 1$, Fig. (2.1) shows that this solution cannot be true, as it does not capture the behaviour of the gel, and hence breaks mass conservation.
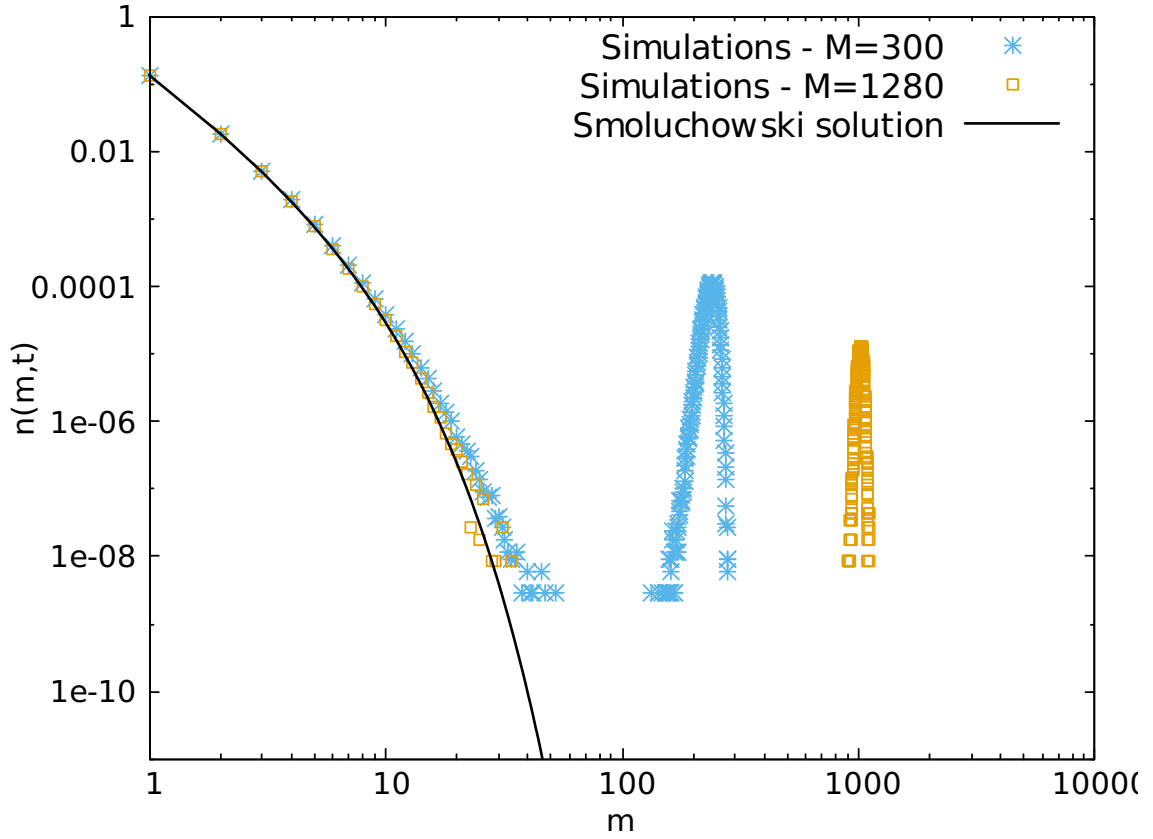
Figure 2.1: Smoluchowski solution for mean $n(m,t)$ [Eq. (2.41)] is compared with Monte-Carlo simulations for $M = 300, 1280$. It is evident that the behaviour of the gel is not captured.

This singularity is explained in terms of a phase transition known as gelation. The product kernel is the simplest kernel to exhibit gelation/gel formation, in which a macroscopic fraction of particles coagulates to form a gel at finite time. When the gel forms, a phase separation occurs, such that the dominant aggregation process is the aggregation of the gel with the small masses. The discrepancy between theory and simulations arises because the Smoluchowski equation is defined for infinite total mass, whereas the gel is a finite, macroscopic mass, whose number density vanishes in the limit of infinite M.

2.6   Lushnikov's solution

Many attempts were made to obtain $n_m(t)$ for the product kernel from the Smolu-chowski equation, using perturbative techniques, scaling solutions etc. But, in order to obtain the exact solution, one must account for the gel, whose behaviour cannot be explained in the thermodynamic limit of infinite total mass for which the Smoluchowski equation is defined. To capture gelling behaviour, it is essential to work in the limit of finite M. The exact solution for the mean mass distribution, $n_m(t)$ for the product kernel was obtained by Lushnikov [7, 49, 50], by considering such a finite system. The aggregation process is defined in terms of an exact master equation for the probability of a configuration $N = \{N_1, N_2, \ldots N_M\}$ at time t, for arbitrary collision kernels:

$$\frac{dP(N,t)}{dt} = \sum_{N^-} \mathcal{R}(N, N^-)P(N^-, t) - \sum_{N^+} \mathcal{R}(N^+, N)P(N, t), \qquad (2.46)$$

where N^- is a state from which the state N can be attained by a single aggregation, N^+ is a state which can be attained from N through a single aggregation, and $\mathcal{R}(N, N^-)$ and $\mathcal{R}(N^+, N)$ are the respective rates. The evolution equation of the generating function of $P(N, t)$ is reminiscent of the Schrodinger equation:

$$\frac{d\Psi}{dt} = \hat{\mathcal{H}}\Psi, \qquad (2.47)$$

where $\Psi(X, t) = \sum_N P(N, t)X^N$. The evolution operator is

$$\hat{\mathcal{H}} = \frac{1}{2}\sum_{l,m} K(l, m)(x_{l+m} - x_l x_m)\frac{\partial^2}{\partial x_l \partial x_m}, \qquad (2.48)$$

where x_m and $\partial/\partial x_m$ are operators which create and annihilate a cluster of mass m respectively. Hence, the operators corresponding to number of clusters of mass m

and the total mass are

$$\hat{n}_m = x_m \frac{\partial}{\partial x_m}, \tag{2.49}$$

$$\hat{M} = \sum_m m x_m \frac{\partial}{\partial x_m}. \tag{2.50}$$

At $t = 0$, there are M monomers. A formal solution for $\Psi(t)$, which is consistent with the initial condition and the mass conservation, is constructed. The mean mass distribution $n_m(t)$ is obtained using the solution of $\Psi(t)$ and Eq (2.49), using the expression

$$n_m(t) = \hat{n}_m \Psi(X, t)|_{X=1}. \tag{2.51}$$

This remarkable solution for $n_m(t)$ captures the mean mass distribution including the behaviour of the gel, as shown in Fig. 2.2. The final solution is given as follows:

$$n_m(t) = \binom{M}{m} e^{(m^2 - 2Mm + m)t} (e^{t/M} - 1)^{m-1} F_{m-1}(e^{t/M}) \tag{2.52}$$

$$F_m(x) = \sum_{l=1}^{m} \binom{m-1}{l-1} \sum_{i=0}^{l-1} x^i F_{l-1}(x) F_{m-l}(x), \tag{2.53}$$

where $F_m(x)$ are Mallows-Riordan polynomials. Lushnikov's solution for $n_m(t)$ of the product kernel is obtained from an exact master equation for a finite collection of clusters, and hence solves the issues associated with the Smoluchowski solution.

Both the Lushnikov solution and the Smoluchowski solution describe the mean or typical mass distribution. In this thesis, we are interested in studying atypical or rare trajectories of aggregating clusters, and their distribution. The mathematical framework for the analytical study of rare events is provided by large deviation theory.
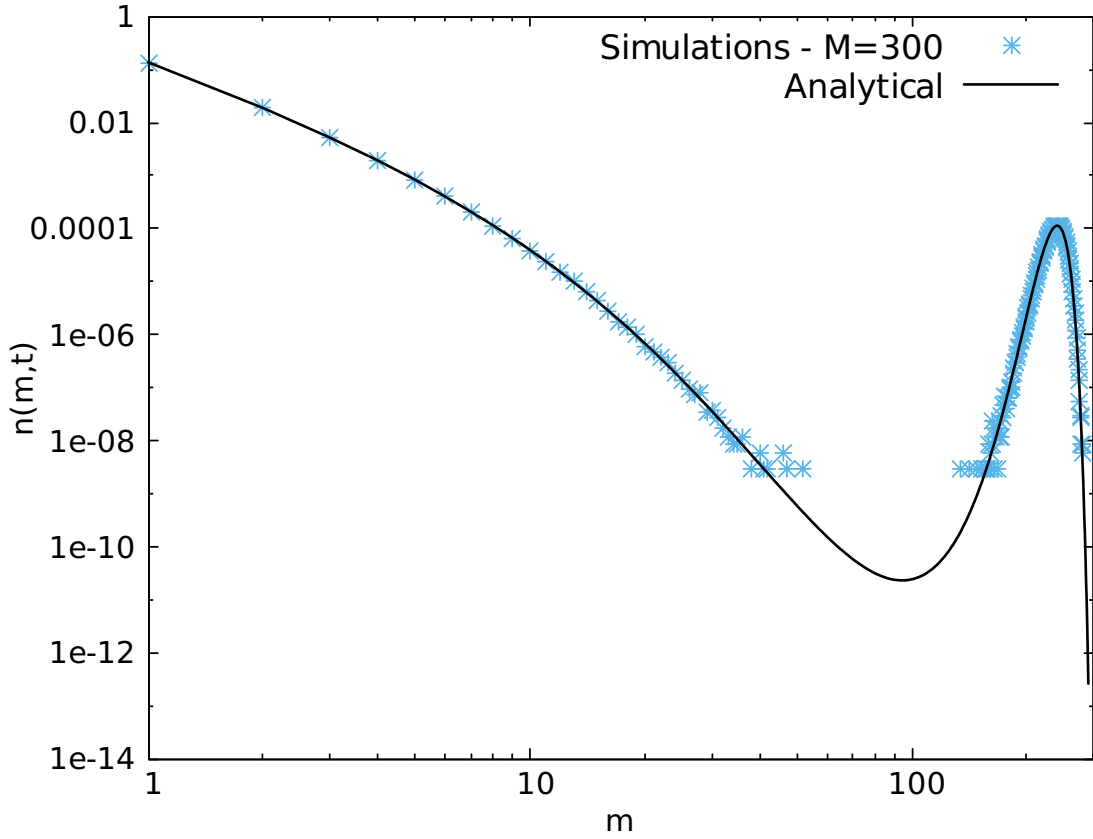
Figure 2.2: Lushnikov's solution for the mean mass distribution, $n(m,t)$ captures the behaviour of the gel perfectly.

2.7 Review of large deviation theory

Large deviation theory deals with probability distributions whose tails decay exponentially fast, with respect to a large parameter called the rate,

$$P(x) \sim e^{-NI(x')}, \tag{2.54}$$

where N is the large parameter, x' is a scaled random variable and $I(x')$ is the rate function or large deviation function. $P(x)$ satisfies a large deviation principle if the limit

$$-\lim_{N\to\infty} \frac{\ln P(x)}{N} = I(x') \tag{2.55}$$

exists.

The earliest known large deviation result was the Boltzmann's equation, *i.e.,* the relationship between entropy and the number of microstates corresponding to a macrostate in an ideal gas, discovered by Boltzmann in 1877. A rigorous large deviation result for the mean of random variables was derived by Cramer in the 1930s. There were also other important results such as the Gartner-Ellis theorem, Sanov's theorem etc. In 1966, the large deviation principle was defined by Varadhan, thus unifying all previous results.

In this section, we will illustrate the large deviation principle and obtain the rate function for the well-known random walk model. Let us consider a one dimensional random walk where the walker can move to the left or right with probability $p = 1/2$. Let the number of steps to the right and left be denoted by r and l respectively, the total displacement by x and the total number of steps by N. We are interested in the probability that the walker has travelled a displacement x in N steps. Then,

$$l + r = N, \tag{2.56}$$

$$r - l = x. \tag{2.57}$$

Solving for r and l,

$$r = \frac{N + x}{2}, \tag{2.58}$$

$$l = \frac{N - x}{2}. \tag{2.59}$$

The discrete probability that the walker has travelled a displacement x in N steps can be obtained from the binomial distribution

$$P(x, N) = \frac{1}{2^N} \binom{N}{r} = \frac{N!}{l! r!} \frac{1}{2^N}. \tag{2.60}$$

In order to find $P(x)$ in the continuum limit, we take the logarithm of the above
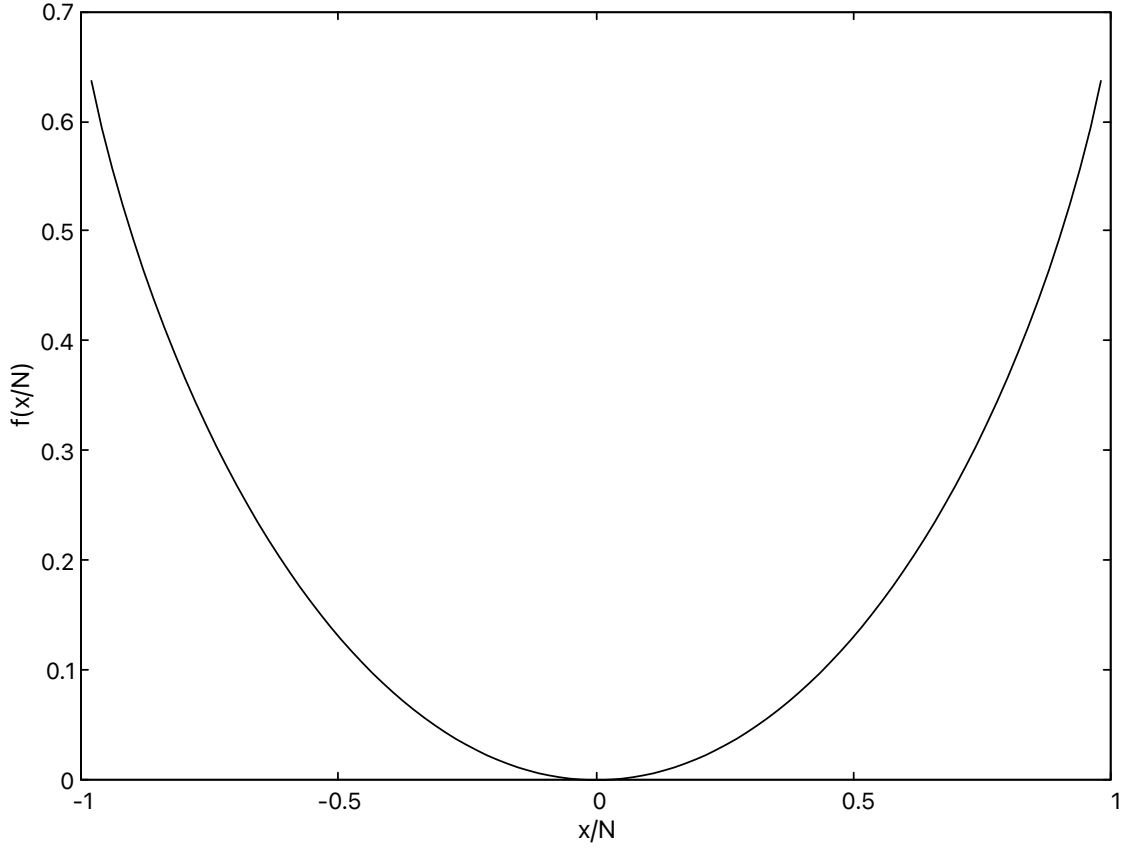
Figure 2.3: Large deviation rate function for a symmetric one-dimensional random walk, with rate N.

expression and expanding the factorials using the Stirling approximation,

$$\ln x! \approx x \ln x - x + \frac{1}{2} \ln 2\pi x, \tag{2.61}$$

we obtain

$$P(x, N) = -\ln \frac{2\pi N}{2} - \frac{N}{2} \left[\ln \left(1 + \frac{x}{N} \right) + \ln \left(1 - \frac{x}{N} \right) \right]$$
$$+ \frac{x-1}{2} \ln \left(1 - \frac{x}{N} \right) - \frac{x+1}{2} \ln \left(1 + \frac{x}{N} \right). \tag{2.62}$$

According to the central limit theorem, the distribution of the mean of a set of independent, identically distributed random variables approaches the normal distribution, for a sufficiently large sample size. The limit which will give the result obtained by the central limit theorem in the case of the random walk is $N \to \infty$ and

29

x^2/N is finite. In other words, the displacement is much smaller than the total number of steps travelled. Applying this limit to Eq. (2.62), we obtain the well-known normal distribution:

$$P(x, N) \approx \frac{1}{\sqrt{2\pi N}} e^{-x^2/2N}, \quad x, N \to \infty, x^2/N \ finite. \quad (2.63)$$

From this distribution, we understand that the walker is most likely to be found around $x = \sqrt{N}$. This distribution captures the most probable or mean outcome of the random walk, and the surrounding regions, very well. However, it cannot describe the tails of the distribution effectively, as it is accurate only upto order of the standard deviation, or $\sqrt{N}$. To understand the behaviour of the distribution at the tails, we consider the limit of finite x/N, while $N \to \infty$. That is, the walker is far from the mean. In this limit, we obtain a large deviation principle:

$$P(x, N) \sim e^{-Nf(x/N)}, \quad x, N \to \infty, x/N \ finite, \quad (2.64)$$

with the large deviation rate function

$$f\left(\frac{x}{N}\right) = -\lim_{N \to \infty} \frac{\ln P}{N} = \frac{1}{2}\left[(1 + \frac{x}{N})\ln(1 + \frac{x}{N}) + (1 - \frac{x}{N})\ln(1 - \frac{x}{N})\right], \quad (2.65)$$

as shown in Fig. 2.3. The rate function in this case, is a strictly convex function. The minimum of $f(x/N)$, which approaches zero, corresponds to the most probable displacement. This result holds true when the probability of moving to the right is not equal to the probability of moving to the left, as well.

In general, it is not a straightforward task to compute the large deviation rate functions for a given problem. Depending on the nature of the problem at hand, techniques such as variational methods, macroscopic field theory, and other field-theoretic methods are used to establish a large deviation principle and obtain the rate function.

Chapter 3

Monte Carlo algorithm

3.1 Introduction

Computing the probability of rare events numerically is, in general, a challenging and computationally expensive exercise, because of the sparsity of data contributing to these events. Often, sophisticated techniques and algorithms are required to obtain data of reasonable robustness. Some popular techniques are importance sampling, splitting and cloning.

In this chapter, we develop a Monte Carlo algorithm to measure probabilities of rare events in CCA for arbitrary collision kernels. The algorithm is based on importance sampling. The key contribution of the algorithm is to identify local modifications to a trajectory consistent with the collision rules, as well as the probabilities arising from collision rates and waiting times. We show that the algorithm is ergodic by giving a protocol that transforms any given trajectory to a standard trajectory using reversible moves. The algorithm's effectiveness in sampling low-probability events is established by numerically reproducing the exact large deviation function for the constant-kernel aggregation. Further, it is shown that the algorithm can obtain the rate functions for gelling kernels, as well as the instanton trajectories for both typical

and atypical times. The dependence of the autocorrelation times, both temporal and configurational, on the different parameters of the algorithm is also characterized. The content of this chapter is published in [51].

3.2   Marcus-Lushnikov model

The model has previously been described in Sec. 2.2, and is reproduced here for ease of reference.

Consider a collection of particles which are labeled by their masses. Given a configuration, the system evolves in time through mass-conserving binary aggregation:

$$A_i + A_j \xrightarrow{K(i,j)} A_{i+j}, \tag{3.1}$$

where A_k denotes a particle of mass k, and the collision kernel $K(i,j)$ is the rate at which two particles of masses i and j aggregate. In an infinitesimal time dt, the probability of collision of two particles having masses i and j is given by $K(i,j)dt$. Since each aggregation event reduces the number of particles, $N(t)$, by 1, $N(t)$ decreases monotonically with time. Initially, there are $N(0) = M$ particles with equal mass m_0. We set $m_0 = 1$, so that all masses are measured in units of m_0.

We are interested in the probability distribution $P(M, N, t)$, defined as the probability of t being the minimum time at which exactly N particles are remaining, or equivalently the probability that the $(M-N)^{th}$ collision occurs at time t, given that there are M particles of mass 1 initially. Here, we consider t as the random variable with $\int_0^\infty dt P(M, N, t) = 1$. Also, we would like to know what the most probable trajectory is for a given M, N, t.

When t is the typical time for given M and N, then we expect that the most probable

trajectory is described by the Smoluchowski equation:

$$\frac{dN_i(t)}{dt} = \frac{1}{2} \sum_{m_1} \sum_{m_2} K(m_1, m_2) N_{m_1} N_{m_2} \delta(m_1 + m_2 - i) - N_i \sum_{m_1} K(i, m_1) N_{m_1}, \quad (3.2)$$

where $N_i(t)$ is the number of particles of mass i at time t. This equation is solvable for the typical trajectory for only few collision kernels: constant, sum and product [27, 28, 29]. We note that the Smoluchowski equation ignores correlations among the particles, and also does not give any information about atypical times, the focus of this thesis.

3.3   Monte Carlo Algorithm

We now describe a Monte Carlo algorithm to numerically determine $P(M, N, t)$ for any given aggregation kernel. This includes times which are atypical for a given M, N, and hence are dominated by rare events. A trajectory that contributes to $P(M, N, t)$ consists of $C = M - N$ collisions. As C increases, the number of trajectories increases rapidly. Figure (3.1) shows all the possible configurations for 6 collisions. Any path from the top row to the bottom row along the directed edges constitutes a trajectory.

To compute $P(M, N, t)$ for atypical times t, we use a method known as importance sampling [52]. The simulations are performed at constant M and N, and t is considered as the random variable. In addition to weights arising from the aggregation kernel, each trajectory is weighted by e^{wt}, where w is a biasing parameter which can be positive or negative. Thus, the biased distribution is

$$P_w(M, N, t) = \frac{1}{Z} P(M, N, t) e^{wt}, \quad (3.3)$$

where Z is a normalizing factor. Positive w biases the system towards larger times
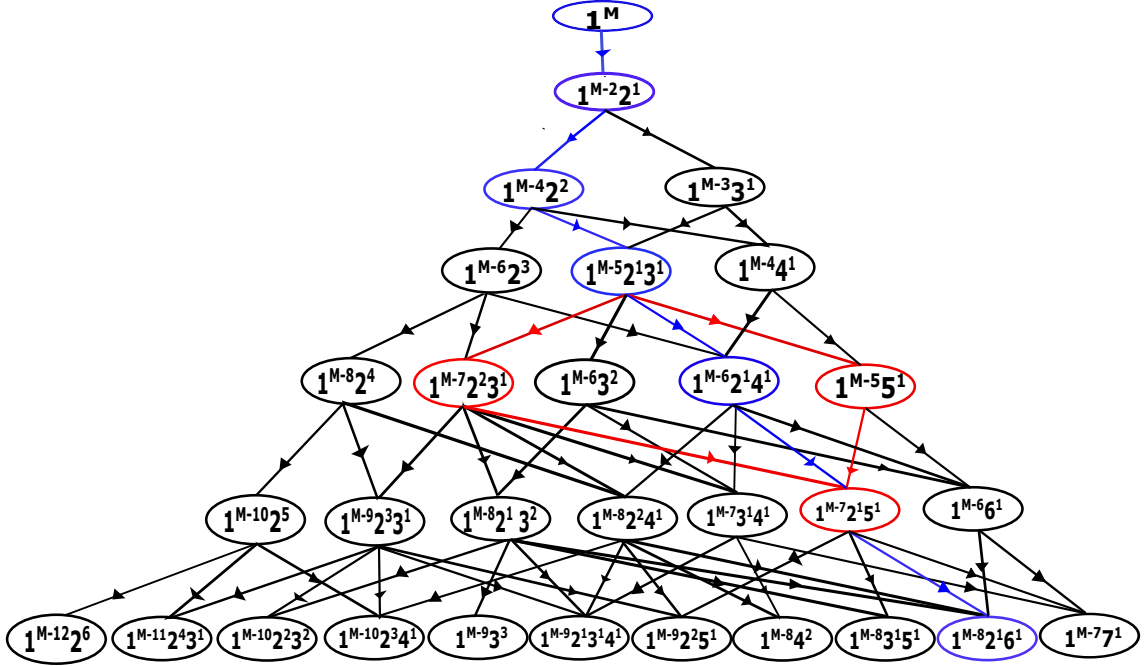
Figure 3.1: All possible configurations and trajectories for 6 collisions. The configurations after each collision are shown inside the bubbles. The bubbles at a certain level are arranged from left to right according to the order relation described in text (see Sec. 3.3.1). For the trajectory shown in blue, the red lines denote possible alternate paths that alter only the 4-th configuration.

and negative w towards smaller times, resulting in robust sampling of atypical trajectories. We first determine $P(M, N, t)$ without bias, *i.e.*, for $w = 0$. Then, we obtain $P_w(M, N, t)$ for $w \neq 0$ and unbias the distribution using Eq. (3.3), i.e., multiplying by e^{-wt}. To combine the data obtained from different choices of w, we proceed as follows. The base normalized distribution is the unbiased distribution of $P(M, N, t)$ obtained for $w = 0$. The values of w are chosen such that between two successive choices of w, there is some overlap in the sampled times. The biased distribution is glued on by minimizing the error in the data for the overlapping times.

The probability distribution $P(M, N, t)$ is a sum over the probabilities of each trajectory with C collisions. A trajectory is characterized both by the sequence of collisions as well as the waiting times between consecutive collisions. In the Monte Carlo algorithm, we introduce local modifications to the trajectory by changing both of the above, as described below.

To characterize a trajectory, we introduce the following notation. We will refer to the configuration after the i-th collision as the i-th configuration. Its mass distribution, the number of particles of mass m, will be denoted by $N_i(m)$. Note that it suffices to give either the sequence of collisions or the configurations to specify the trajectory. The waiting time between the i-th and the $(i+1)$-th collisions, or equivalently the waiting time for the i-th configuration, will be denoted by Δt_i. Also, (m_i, m_i') will refer to the pair of masses aggregating in the i-th collision.

At each micro-step, a configuration is chosen uniformly at random, say the i-th configuration. With probability p, the waiting time, Δt_i, associated with the i-th configuration, is modified, keeping all the configurations fixed. With probability $(1-p)$, the i-th configuration is modified, keeping all other configurations as well as all waiting times fixed. We will treat p as a parameter of the algorithm.

We first describe the change in waiting times. Let the current waiting time for the i-th configuration be denoted by Δt_i^{old}. A new waiting time Δt_i^{new} is drawn from an exponential distribution [53]

$$P(\Delta t_i) = \mathcal{R}_i e^{-\mathcal{R}_i \Delta t_i}, \tag{3.4}$$

where $\mathcal{R}_i$ is the total rate of collision of the i-th configuration. In terms of the collision kernel,

$$\mathcal{R}_i = \sum_{m_1=1}^{M} \sum_{m_2 \geq m_1}^{M} K(m_1, m_2) \mathcal{C}_i(m_1, m_2), \tag{3.5}$$

where

$$\mathcal{C}_i(m_1, m_2) = N_i(m_1) N_i(m_2) - \frac{N_i(m_1) [N_i(m_2) + 1]}{2} \delta_{m_1, m_2}, \tag{3.6}$$

is the combinatorial factor associated with the number of ways of choosing particles of masses m_1 and m_2. For ensuring detailed balance, we first note that when the waiting times are changed the sequence of collisions remains the same for both the old and new trajectories. Since the waiting times are biased with weight e^{-wt}, it

is easy to see that detailed balance is satisfied if the new waiting time Δt_i^{new} is accepted with a probability $\min[1, e^{w(\Delta t_i^{new} - \Delta t_i^{old})}]$.

Second, we describe the moves to modify the trajectory through changes in the configurations. There are multiple ways of choosing a different pair of successive collisions such that only the i-th configuration is changed. An example of possible options is shown in Fig. 3.1. Consider the trajectory shown in blue. To change the 4-th configuration, keeping other configurations fixed, the paths that are marked in red are also allowed, but each with different weights. We now formulate the general rules to obtain the set of collisions which will preserve all configurations except the i-th configuration.

If $1 < i < C$, then the i-th and $(i + 1)$-th collisions have to be modified, while if $i = C$, only the C-th collision has to be modified. We first discuss the case $1 < i < C$. For convenience of notation, let the pair of successive collisions be denoted as (m_1, m_2),(m_3, m_4) respectively. The most obvious way that the collisions can be modified is to reverse the sequence of collisions such that the collision (m_3, m_4) occurs first, and then (m_1, m_2) occurs, provided the masses m_3 and m_4 exist independent of the (m_1, m_2) collisions. The collisions can also occur such that the product from the ith collision, $i.e.$, $m_1 + m_2$, is one of the colliding masses of the next collision, say m_3. This possibility leads to the classification of the pair of collisions into three types. A pair of collisions where $m_1 + m_2 \neq m_3$ or m_4 can undergo only reversal of the sequence of collisions. This type of collision will be denoted as α. A pair of collisions where $m_1 + m_2 = m_3$ falls into two types, β and γ. All the three types are described below. The rules pertaining to all three types are given in Table 3.1.

Type α: $m_1 + m_2 \neq m_3$ or m_4. Here the only possibility is to reverse the sequence of collisions and thus there are only two pairs of collisions to choose from.

Type β : $m_1 + m_2 = m_3$, and there is at least one particle of mass m_3 in the $(i-1)$-th configuration. In this case, there are 6 possible pairs of collisions to choose from.

Table 3.1: Given a pair of successive collisions (m_1, m_2) and (m_3, m_4), all allowed alternate pairs of collisions that alter only the intermediate configuration i are tabulated. If the product of the first collision takes part in the second, we denote the product as m_3 without loss of generality.

Type	Description	i-th collision	$(i+1)$-th collision
α	$m_1 + m_2 \neq m_3$	(m_1, m_2)	(m_3, m_4)
		(m_3, m_4)	(m_1, m_2)
β	$m_1 + m_2 = m_3,$ $N_i(m_3) > 0$	(m_1, m_2)	(m_3, m_4)
		(m_3, m_4)	(m_1, m_2)
		(m_1, m_4)	$(m_1 + m_4, m_2)$
		$(m_1 + m_4, m_2)$	(m_1, m_4)
		(m_2, m_4)	$(m_2 + m_4, m_1)$
		$(m_2 + m_4, m_1)$	(m_2, m_4)
γ	$m_1 + m_2 = m_3,$ $N_i(m_3) = 0$	(m_1, m_2)	(m_3, m_4)
		(m_1, m_4)	$(m_1 + m_4, m_2)$
		$(m_1 + m_4, m_2)$	(m_1, m_4)
		(m_2, m_4)	$(m_2 + m_4, m_1)$
		$(m_2 + m_4, m_1)$	(m_2, m_4)

Type γ: $m_1 + m_2 = m_3$, but there are no particles of type m_3 in the $(i-1)$-th configuration. Compared to type β, the pair of reversed collisions $(m_3, m_4), (m_1, m_2)$ would not occur. Thus, there are 5 possible pairs of collisions to choose from.

Each of the possibilities in Table 3.1 occurs with weight,

$$W(m_1, m_2; m_3, m_4) = K(m_1, m_2)\mathcal{C}_{i-1}(m_1, m_2)\mathcal{R}_{i-1}e^{-\mathcal{R}_{i-1}\Delta t_{i-1}}$$
$$K(m_3, m_4)\mathcal{C}_i(m_3, m_4)\mathcal{R}_i e^{-\mathcal{R}_i \Delta t_i}. \tag{3.7}$$

If $i = C$, i.e., the C-th configuration is chosen, then any two masses from the $(C-1)$-th configuration may aggregate. For the final collision, the weight of choosing a pair is

$$W(m_C, m_C') = K(m_C, m_C')\mathcal{C}_{C-1}(m_C, m_C')\mathcal{R}_{C-1}e^{-\mathcal{R}_{C-1}\Delta t_{C-1}}. \tag{3.8}$$

From all the allowed possibilities, we choose a particular configuration with probability proportional to its weight, thus making the choice rejection-free. A Monte
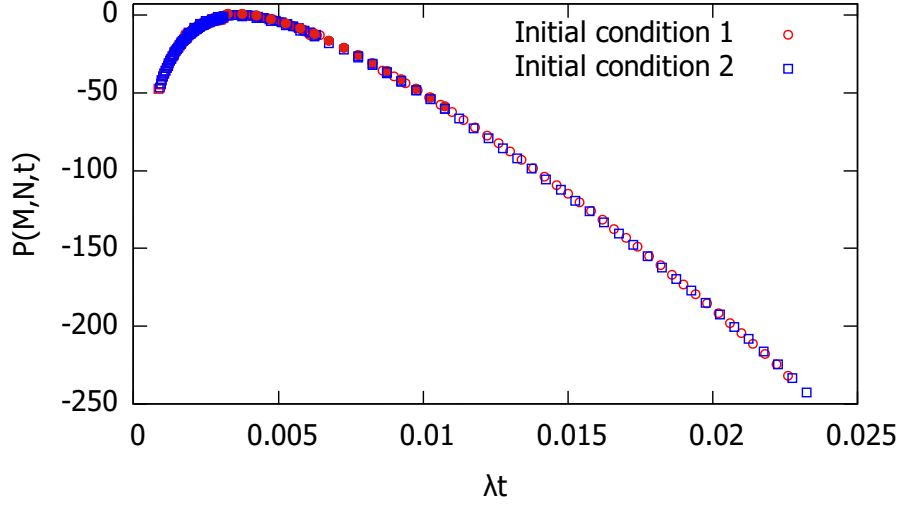
Figure 3.2: Comparison of $P(M, N, t)$ for $M = 240$, $N = 168$, obtained for two different initial conditions. Initial condition 1 corresponds to the initial trajectory consisting of $C = M - N$ random collisions. Initial condition 2 corresponds to the trajectory $(\mathbf{1})^{M-i}(\mathbf{i})^1$, formed by the collision of a particle of mass 1 with a particle of mass $M - i$. The data are for the constant kernel.

Carlo move consists of $2C$ micro-steps.

The algorithm obeys detailed balance. Once the set of new configurations is determined, based on the current configuration, the probability of choosing a particular configuration is only proportional to its weight, and independent of the current configuration. Hence, the configurational moves satisfy detailed balance trivially. The assignment of waiting times follows the usual Metropolis rule and hence satisfies detailed balance.

The initial configuration is chosen by colliding a randomly chosen pair of particles at each collision. The initial waiting times are drawn from the exponential distribution Eq. (3.4). To confirm convergence, we check that the results do not depend on the initial trajectory, by choosing other initial trajectories such as $(\mathbf{1})^{M-i}(\mathbf{i})^1$. As an example, in Fig. 3.2 we compare $P(M, N, t)$ for the constant kernel, obtained for the two initial conditions discussed above. The data are indistinguishable from each other, confirming equilibration.

3.3.1 Ergodicity of the Monte Carlo Algorithm

The Monte Carlo algorithm modifies trajectories using local moves which are reversible and obey detailed balance. We now show that the algorithm is ergodic, *i.e.,* it allows all trajectories to be accessed. To do so, it is enough to prove that an arbitrary trajectory, A, can transform to a standard trajectory, S, through a given protocol. Then, to transform A to any given trajectory B, we follow the protocol from A to S and reverse the moves from B to S.

We choose the standard trajectory S to be one where after every collision, only one mass different from 1 is allowed at all times. That is, after i collisions, the configuration is $(\mathbf{1})^{M-i-1}(\mathbf{i+1})^1$. In this trajectory, at each collision, the largest mass collides with a particle of mass 1.

To describe the protocol of transforming an arbitrary trajectory to S, it is convenient to introduce an ordering among configurations that have undergone the same number of collisions. We will say that $(\mathbf{1})^{N_1}(\mathbf{2})^{N_2}\cdots < (\mathbf{1})^{N_1'}(\mathbf{2})^{N_2'}\ldots$ if $N_1 = N_1', N_2 = N_2',\ldots,N_{k-1} = N_{k-1}', N_k < N_k'$, where k is the smallest mass for which $N_k \neq N_k'$. The configurations are then arranged in increasing order, as shown in Fig. (3.1). In this representation, the standard trajectory S is the rightmost trajectory.

Consider any arbitrary trajectory A. The following transformations are applied till no more transformation is possible :

- The lower most edge is moved to the rightmost allowed node.

- For the bottom most configuration that can be modified such that the trajectory moves rightward, we choose the rightmost path.

We give an example of the above protocol for a trajectory with 4 collisions. Consider the leftmost trajectory shown in blue, in Fig. 3.3(a) where the configuration after i collisions is $(\mathbf{1})^{M-2i}(\mathbf{2})^i$. The protocol transforms the trajectory as follows.
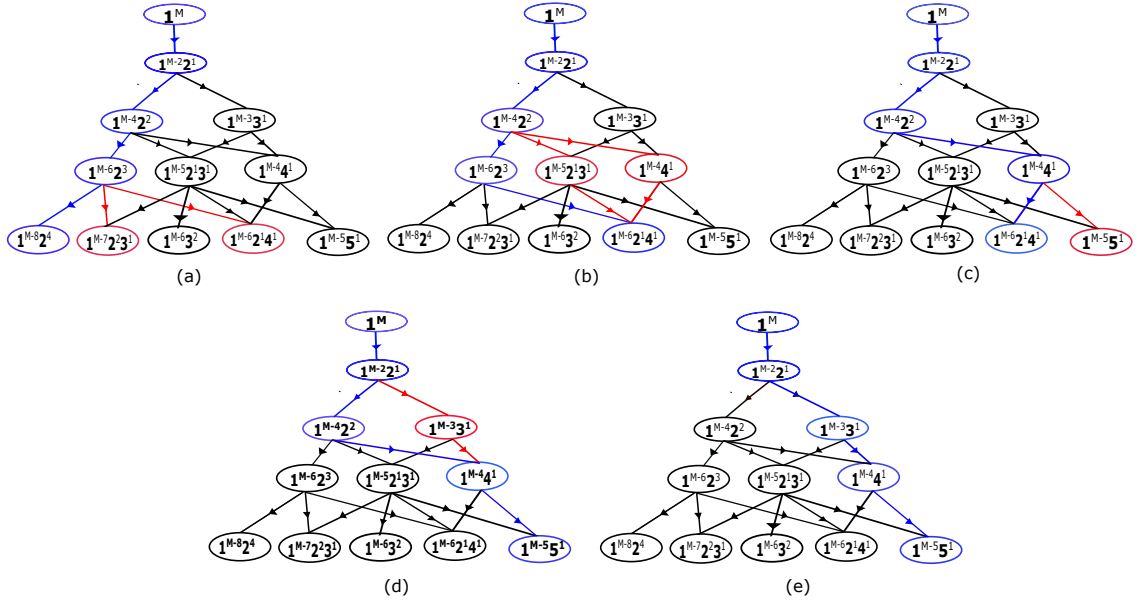
Figure 3.3: The transformation from the leftmost trajectory [blue path in (a)] where all the configurations result from the collision $(1, 1)$, to the rightmost trajectory, S, using the protocol described in the text. The current path is depicted in blue, and the possible transformations in the next collision, as prescribed by the protocol, are denoted in red.

The lowest-most edge has two other valid choices as shown in red in Fig. 3.3(a). We choose the rightmost of these to obtain the blue trajectory in Fig. 3.3(b). The third configuration now can be moved rightwards along the paths shown in red in Fig. 3.3(b). We choose the right-most configuration to obtain the blue trajectory in Fig. 3.3(c). The bottom-most edge is now moved to the edge shown in red in Fig. 3.3(c) to obtain the blue trajectory in Fig. 3.3(d). Finally, the second configuration is moved to the right along the red path shown in Fig. 3.3(d) to obtain the standard trajectory shown in blue in Fig. 3.3(e).

We now show that the protocol transforms an arbitrary trajectory A to the standard trajectory S. Suppose, on application of the protocol, A is transformed to S'. We will now show that $S' = S$. Let the sequence of collisions in S' be denoted by (m_i, m_i'), *i.e.*, in the i-th collision, masses m_i and m_i' aggregates. We derive the constraints that two consecutive collisions in S', $\left[(m_i, m_i'), (m_{i+1}, m_{i+1}') \right]$ should

obey. A pair of collisions falls under one of the three types, α, β and γ as described in Sec. 3.3.

The argument is based on the following observation. Suppose, given a configuration, we consider two possible collisions: (m_1, m_2) or (m_3, m_4). If the trajectory due to (m_3, m_4) colliding is to the right of the trajectory due to (m_1, m_2) colliding, then based on the order relation, it is easy to see that $\min(m_1, m_2) \leq \min(m_3, m_4)$.

For collisions of the type α, there are two possibilities (see Table 3.1) for the sequence of collision. The reversed sequence of collisions (m_{i+1}, m'_{i+1}), (m_i, m'_i) would lead to a trajectory to the right of S' if $\min(m_{i+1}, m'_{i+1}) > \min(m_i, m'_i)$. Since we cannot have a trajectory that is to the right of S', we obtain the condition, based on the argument in the previous paragraph, $\min(m_{i+1}, m'_{i+1}) \leq \min(m_i, m'_i)$.

Now consider collisions of types β and γ. The pair of collisions are (m_i, m'_i) and $(m_i + m'_i, m'_{i+1})$. Suppose $m'_{i+1} > \min(m_i, m'_i)$. Then the pair of collisions $(m'_{i+1}, \max(m_i, m'_i))$, $(\min(m_i, m'_i), m'_{i+1} + \max(m_i, m'_i))$ creates a trajectory to the right of S' that is allowed by the protocol. But since S' is the rightmost trajectory, there is a contradiction and hence

$$m'_{i+1} = \min(m_{i+1}, m'_{i+1}) \leq \min(m_i, m'_i), \tag{3.9}$$

that holds for all collision types α, β and γ.

The first collision is $(1, 1)$. To satisfy the condition in Eq. (3.9), it is clear that at least one of the colliding masses in the second collision should be 1, as the minimum possible mass is 1. It follows that in order to satisfy the condition in Eq. 3.9 for every sequence of consecutive collisions in the trajectory, at least one of the colliding masses in all the subsequent collisions should be 1.

Now consider the C-th collision. For the rightmost trajectory, the two largest masses have to be collided. But we have already shown that one of the masses should be

41

1, *i.e.*, the second largest mass is 1. This implies that the C-th configuration is $\mathbf{1}^{M-1}\mathbf{C}^1$. Using the property that mass 1 is used in each step, it follows that the i-th configuration is $\mathbf{1}^{M-i}i^1$, which is the standard configuration. This implies that $S' = S$, and hence proves that the algorithm is ergodic.

3.3.2 Large Deviation Function

To show the efficacy of the algorithm, we compare the numerical results with the exact solution of the model of constant kernel where collision rates are independent of the masses. The collision kernel $K(m_1, m_2) = \lambda$.

Exact result for constant kernel

When the collision rates are independent of masses, $P(M, N, t)$ can be analytically computed. After i collisions, $M - i$ particles remain, and the total rate of collision is given by

$$\mathcal{R}_i = \frac{\lambda(M - i)(M - i - 1)}{2}. \tag{3.10}$$

Using the exponential time distribution Eq.(3.4),

$$P(M, N, t) = \int_0^\infty d\Delta t_0 \int_0^\infty d\Delta t_1 ... \int_{t=0}^\infty d\Delta t_{C-1} \ \mathcal{R}_0 e^{-\mathcal{R}_0 \Delta t_0}$$
$$\mathcal{R}_1 e^{-\mathcal{R}_1 \Delta t_2} ... \mathcal{R}_{C-1} e^{-\mathcal{R}_{C-1}\Delta t_{C-1}} \delta\left(\sum_{i=0}^{C-1} \Delta t_i - t\right). \tag{3.11}$$

The δ-function constrains the sum of waiting times to the total time t. The Laplace transform of $\widetilde{P}(M, N, s)$, defined as

$$\widetilde{P}(M, N, s) = \int_0^\infty dt e^{-st} P(M, N, t), \tag{3.12}$$
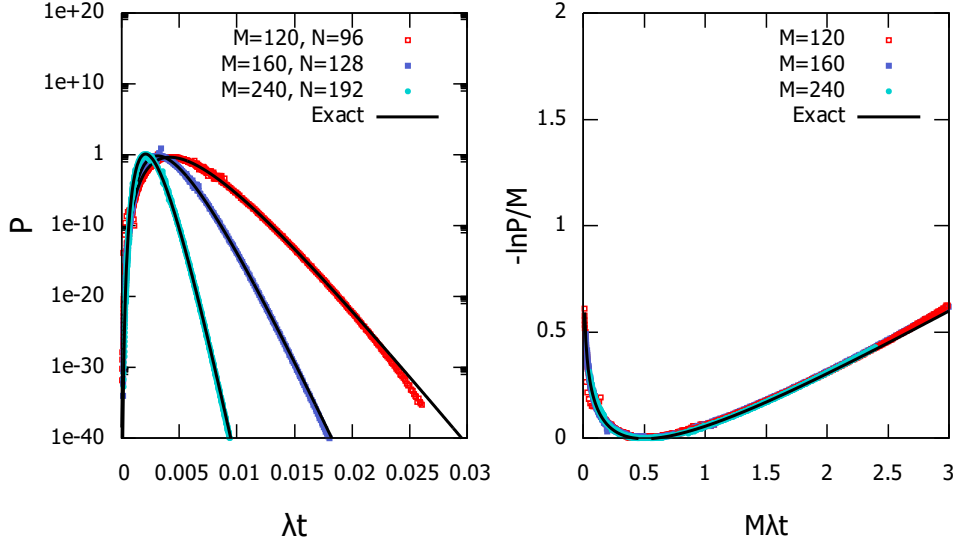
Figure 3.4: (a) $P(M, N, t)$ for the constant kernel for different M, keeping $\Phi = N/M = 0.8$ fixed are compared with the exact solution, Eq. (13). (b) The data in (a) for different M collapse onto one curve when scaled as in Eq. (14), to give the rate function.

is then

$$\widetilde{P}(M, N, s) = \prod_{i=0}^{C-1} \frac{\mathcal{R}_i}{\mathcal{R}_i + s}. \tag{3.13}$$

Doing the inverse Laplace transform, we obtain

$$P(M, N, t) = \left(\prod_{k=0}^{C-1} \mathcal{R}_k\right) \sum_{i=0}^{C-1} e^{-\mathcal{R}_i t} \prod_{j \neq i, j=0}^{C-1} \frac{1}{\mathcal{R}_j - \mathcal{R}_i}. \tag{3.14}$$

We compare the results from the Monte Carlo simulations for the constant kernel with the exact results. Plotting the unbiased $P(M, N, t)$ (with $w = 0$) as the reference, $P(M, N, t)$ obtained from non-zero values of w are merged with the reference distribution by appropriate normalization. In Fig. 3.4(a), the results for $P(M, N, t)$ from Monte Carlo simulations are compared with the exact solution for a fixed $\Phi = N/M = 0.8$ and $M = 120, 160, 240$. It is clear that the data are in good agreement with the exact results, thus providing a benchmark for correctness. Also, we are able to measure very low probabilities, of the order of 10^{-35}, and even lower, at times much larger and much smaller than the typical time.
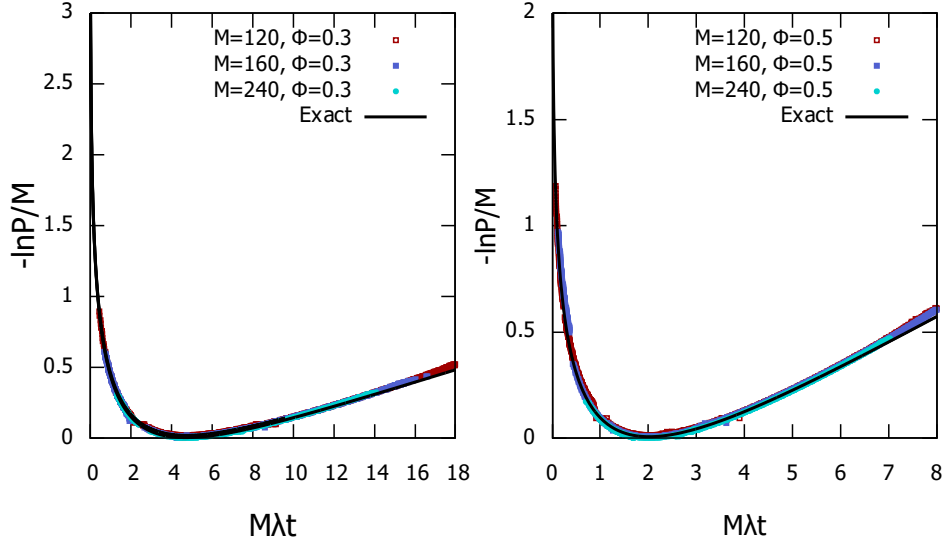
Figure 3.5: (a) $P(M, N, t)$ for the constant kernel for different M, and keeping $\Phi = N/M = 0.3$ fixed collapse onto one curve when scaled as in Eq. (3.15), to give the rate function. (b) $P(M, N, t)$ for the constant kernel for different M, and keeping $\Phi = N/M = 0.5$ fixed collapse onto one curve when scaled as in Eq. (3.15), to give the rate function.

For large M, $P(M, N, t)$ for different M, N, t collapse onto one curve when scaled as in

$$- \ln P(M, N, t) = M f\left(\frac{N}{M}, M\lambda t\right), \quad M, N, t^{-1} \to \infty, \quad (3.15)$$

as shown in Figure 3.4(b). We then identify M with the rate and f with the large deviation function [41]. $-\ln P$ has a minimum value of zero. We will identify the corresponding value of time as the typical time, t_{typ} for $M - N$ collisions, *i.e.*, $f(\Phi, M\lambda t_{typ}) = 0$.

To show that the algorithm works for the full range of Φ, we compare the results from simulations of the constant kernel with the exact results for $\Phi = 0.3, 0.5$ in Fig. 3.5. Excellent agreement is seen.

We note that there is an upper bound for the value of the bias w. To see this, we observe that $P(M, N, t)$ in Eq. (13) is a sum over $(C + 1)$ terms, each one of which decreases exponentially with t as $e^{-R_i t}$. Thus, for large t, the term with the smallest
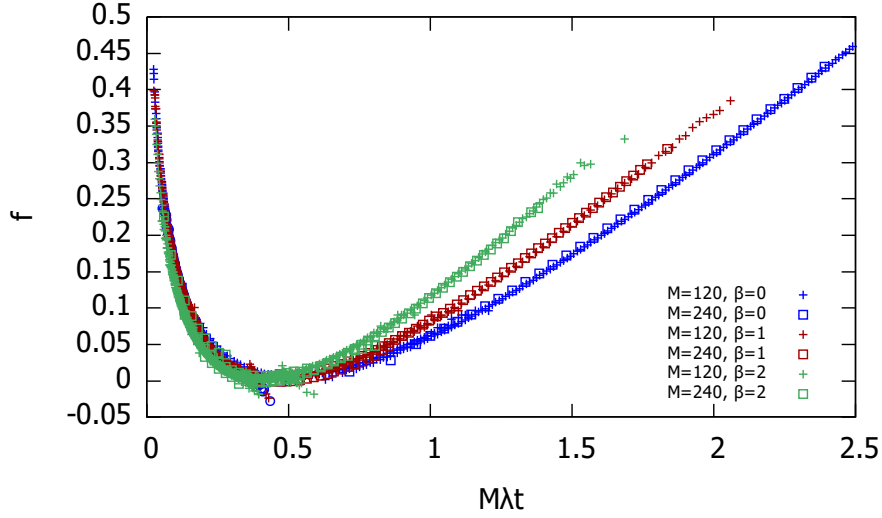
Figure 3.6: The large deviation rate function $f(\Phi, M\lambda t)$ [see Eq. (3.15)] for fixed $\Phi = N/M = 0.8$ and different kernels, $K(m_1, m_2) = (m_1 m_2)^{\frac{\beta}{2}}$ where $\beta = 0, 1, 2$. The data are for $M = 120$ and $M = 240$.

R_i will dominate. Since the smallest rate is R_C, we expect that

$$P(M, N, t) \approx \mathcal{R}_{C-1} e^{-\mathcal{R}_{C-1}t} \prod_{j=0}^{C-2} \frac{\mathcal{R}_j}{\mathcal{R}_j - \mathcal{R}_C - 1}, \quad t \to \infty. \qquad (3.16)$$

This implies that a bias $w > \frac{1}{2}N(N+1)$ cannot be applied since the biased distribution $P_w(M, N, t)$ would diverge, making it not normalisable. For small times, there is no such cutoff for the bias.

The large deviation functions of kernels other than the constant kernel can also be obtained using the algorithm. Depending on the form of the collision kernel $K(m_1, m_2)$, a phenomenon known as gelation occurs in aggregating systems, where there is a non-trivial fraction of the total mass, $(1 - \Phi)M$, and the rest are masses which are much smaller than $(1 - \Phi)M$. In gelling kernels, collisions between large masses are dominant. After gelation occurs, the smaller masses are consumed by the large mass. For a collision kernel of the form $K(m_1, m_2) \approx \lambda(m_1 m_2)^{\frac{\beta}{2}}$, the criteria for gelation has been established as $\beta > \frac{1}{2}$ [54, 55], where $\beta = \nu + \mu$. Here, ν and μ are the kernel parameters corresponding to the generalised homogeneous
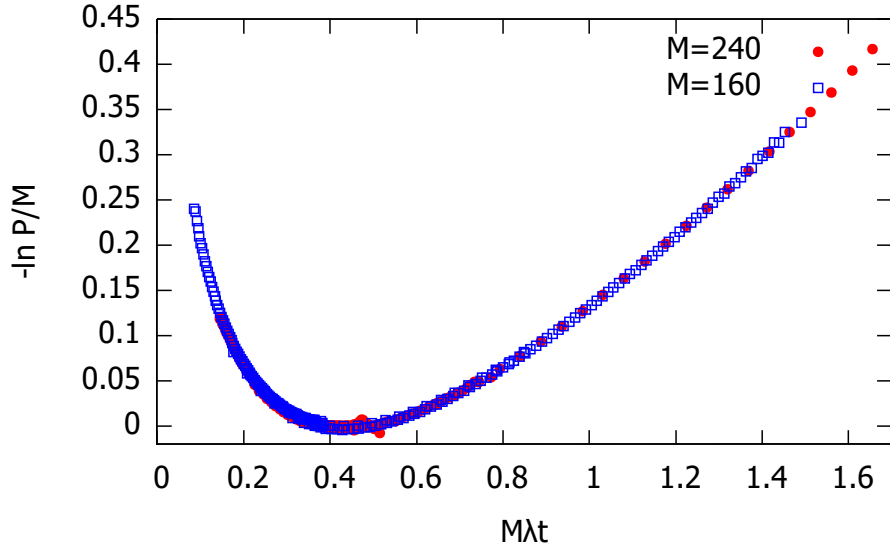
Figure 3.7: The large deviation rate function $f(\Phi, M\lambda t)$ [see Eq. (3.15)] for the Brownian kernel, $K(m_1, m_2) = (\frac{m_1}{m_2})^{1/3} + (\frac{m_2}{m_1})^{1/3} + 2$, for $\Phi = N/M = 0.7$. The data are for $M = 160$ and $M = 240$.

collision kernel, $K(m_1, m_2) = \frac{\lambda}{2}(i^\mu j\nu + i^\nu j^\mu)$. Figure 3.6 shows the rate function for the collision kernels with $\beta = 0, 1, 2$. The algorithm is able to obtain the rate function for small and large arguments, showing that a numerical analysis similar to the constant kernel can be done for any arbitrary kernel.

In addition to obtaining the large deviation function for the well-known constant, sum and product kernels, we also demonstrate the usefulness of the algorithm by determining the large deviation function for a collision kernel for which the mean field Smoluchowski equation cannot be solved for. Figure 3.7 shows the rate function for the Brownian kernel, $K(m_1, m_2) = (m_1/m_2)^{1/3} + (m_2/m_1)^{1/3} + 2$, which is widely used in aerosol physics [56].

3.3.3 Typical trajectories

In the algorithm for determining $P(M, N, t)$, the initial condition was fixed as $N(0) = M$, but the final time was varying. Now, we fix the final time to be T, i.e., $N(T) = N$, and determine the most probable trajectory under these condi-

tions. We will refer to this trajectory as the instanton trajectory.

To determine the instanton trajectory, we modify the algorithm as follows. The rules to alter the configurations remain the same as before. The rules for assignment of waiting times are modified as follows. A configuration $1 \leq i \leq C$ is chosen. Let the current waiting times associated with the $(i-1)$-th and i-th configurations be $\Delta t'_{i-1}$ and $\Delta t'_i$. These waiting times are reassigned, keeping their sum fixed, thus ensuring that the total time taken for C collisions to occur does not change. Let the new waiting times be Δt_{i-1} and Δt_i. Then, Δt_{i-1} is drawn from the distribution

$$P(\Delta t_{i-1}) = \mathcal{N} \mathcal{R}_{i-1} e^{-\mathcal{R}_{i-1}\Delta t_{i-1}} \mathcal{R}_i e^{-\mathcal{R}_i \Delta t_i}, \qquad (3.17)$$

where $\mathcal{N}$ is the normalizing factor, and Δt_i is fixed by

$$\Delta t_i = \Delta t'_{i-1} + \Delta t'_i - \Delta t_{i-1}. \qquad (3.18)$$

Integrating over Δt_{i-1} from $\Delta t_{i-1} = 0$ to $\Delta t_{i-1} = \Delta t'_{i-1} + \Delta t'_i$, we obtain

$$\mathcal{N} = \frac{(\mathcal{R}_{i-1} - \mathcal{R}_i) e^{\mathcal{R}_i(\Delta t'_{i-1} + \Delta t'_i)}}{\mathcal{R}_{i-1}\mathcal{R}_i (1 - e^{-(\mathcal{R}_{i-1} - \mathcal{R}_i)(\Delta t'_{i-1} + \Delta t'_i)})}. \qquad (3.19)$$

Hence, the final distribution is

$$P(\Delta t_{i-1}) = \frac{(\mathcal{R}_{i-1} - \mathcal{R}_i) e^{-(\mathcal{R}_{i-1} - \mathcal{R}_i)\Delta t_{i-1}}}{1 - e^{-(\mathcal{R}_{i-1} - \mathcal{R}_i)(\Delta t'_{i-1} + \Delta t'_i)}}. \qquad (3.20)$$

To benchmark our simulations, we first ask how the typical trajectories look. The trajectory obtained for a given M and Φ, without any constraints on the final time and in the absence of bias, is the typical trajectory. We expect that this typical trajectory is described by the Smoluchowski equation (see Sec 3.2). Summing over i and dividing by M in Eq. (3.2), gives the rate of decay of the fraction of particles, $n(t) = N(t)/M$ with time.

For the constant kernel $K(m_1, m_2) = \lambda$,

$$\frac{dn}{dt} = -\frac{M\lambda n^2}{2}. \tag{3.21}$$

The solution of this equation, with the initial condition $n(0) = 1$ is

$$n(t) = \frac{1}{1 + \frac{M\lambda t}{2}}, \quad \text{constant kernel.} \tag{3.22}$$

This solution describes a typical trajectory provided the number of particles are not of order 1, which is when the Smoluchowski equation breaks down. For the sum kernel, $K(m_1, m_2) = \frac{\lambda}{2}(m_1 + m_2)$ and the product kernel, $K(m_1, m_2) = \lambda m_1 m_2$, the solution for the Smoluchowski equation is easily obtained, and are given by [27]

$$n(t) = e^{-\frac{M\lambda t}{2}}, \quad \text{sum kernel,} \tag{3.23}$$

$$n(t) = 1 - \frac{\lambda M t}{2}, \quad \text{product kernel.} \tag{3.24}$$

We note that these solutions are valid before gelation, where an infinite mass forms in finite time. Given $\Phi = N/M$, the typical times t_{typ} for the different kernels are obtained by equating $n(T)$ in Eqs. (3.22), (3.23) and (3.24) to Φ. To check that the simulations reproduce the typical trajectories, we set $T = t_{typ}$, and then ask whether the numerically obtained instanton solution matches with the solution to the Smoluchowski equation.

Figure 3.8 shows the numerically obtained instanton trajectories for the constant, sum, and product kernels, for typical as well as atypical final times T, for $\Phi = 0.8$. For $T = t_{typ}$, the data are in excellent agreement with the solution of the Smoluchowski equation for all the three kernels, thus providing a check for the correctness of the implementation of the algorithm. The algorithm is also able to obtain the instanton trajectories for atypical trajectories for times which are both much smaller than as well as much larger than the typical times. The exact answers
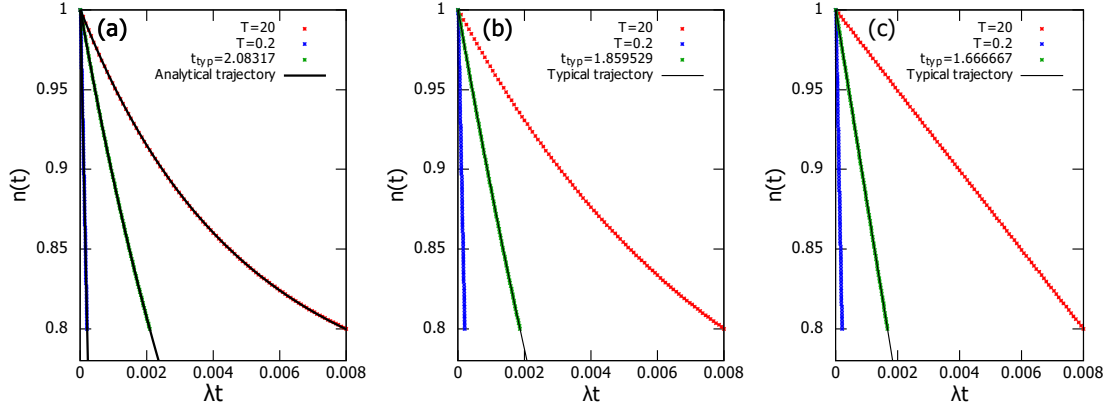
Figure 3.8: Instanton trajectories for different final times T are shown for (a) constant kernel and $\Phi = 0.3$, (b) sum kernel and $\Phi = 0.5$, and (c) product kernel and $\Phi = 0.8$. The three times shown are for $T = t_{typ}$, $t_{typ}/10$ and $4t_{typ}$. The data for the typical times are compared with the exact solution of the Smoluchowski equation [see Eqs. (3.22), (3.23) and (3.24)]. For the constant kernel, the data for atypical times are also compared with the exact result [see Eqs. (3.25), (3.26). The data are for $M = 240$.

for the atypical trajectories of the constant kernel are [57]

$$n(t) = -p \tan \frac{M\lambda p(t - t_0)}{2} \qquad T < t_{typ}, \tag{3.25}$$

$$n(t) = q \coth \frac{M\lambda q(t - t_1)}{2} \qquad T > t_{typ}, \tag{3.26}$$

where p, t_0, q and t_1 are determined from the boundary conditions $n(0) = 1$ and $n(T) = \Phi$. The simulation results are in excellent agreement with the exact results for the instanton trajectories for atypical events, as shown in Fig. 3.8.

We also check that the minimum of the large deviation rate function for the constant, sum, and product kernels for $\Phi = 0.8$, shown in Fig. 3.6, occurs at the typical times as calculated by the Smoluchowski equation in Eqs. (3.22), (3.23), and (3.24).

3.3.4 Addition and deletion of collisions

We also compute $\tilde{P}(M, N, t)$, the probability that N particles remain at a given time t. Here, N is the random variable of interest. A trajectory that contributes

to $\tilde{P}(M, N, t)$ consists of $C = M - N$ collisions, and in addition to the waiting times between collisions and sequence of collisions, is also defined by the number of collisions. No collision occurs after the final waiting time. At $t = 0$, there are M particles of mass 1. A trajectory is evolved by reassigning a waiting time with probability p_1, reassigning a collision with probability p_2, or modifying the number of collisions with probability p_3, such that $p_1 + p_2 + p_3 = 1$. Each of these moves is described below.

Reassign waiting times: Keeping the number of collisions C, total time for C collisions, and sequence of collisions fixed, a configuration i is chosen. Δt_i is the waiting time before the $i-$th configuration, and λ_i is the total rate of collision of the $i-$th configuration. The new waiting time $\Delta t'_{i-1}$ is drawn from the distribution Eq. (3.20). The next waiting time $\Delta t'_i$ is automatically fixed by the condition that the sum of the old waiting times, $\Delta t_{i-1} + \Delta t_i$ is constant.

Reassign a collision: Keeping the number of collisions and the total time for C collisions fixed, a collision i is chosen at random, and reassigned according to the rules listed in Sec 3.3.

Add/delete collision: With equal probability, a collision is added or deleted.

In order to add a collision, two masses m_1 and m_2 are selected at random from the configuration resulting from the final collision. The collision rate for these masses are calculated, and used to generate the waiting time for the $(C + 1)$-th collision, Δt_{C+1}.

In order to delete a collision, the final configuration is deleted, and the waiting times are modified such that the new final waiting time $\Delta t'_{C-1} = \Delta t_C + \Delta t_{C-1}$.

Addition and deletion of a collision are performed in such a way that the principle of

detailed balance is satisfied. Suppose the old trajectory consists of C collisions, and the new trajectory consists of $C + 1$ collisions. The probability of the old and new trajectories are $P(C)$ and $P(C + 1)$ respectively, and the weights associated with adding a collision, and deleting a collision, are $Wt(C \to C+1)$ and $Wt(C+1 \to C)$ respectively. The condition for detailed balance is:

$$P(C)Wt(C \to C + 1) = P(C + 1)Wt(C + 1 \to C). \tag{3.27}$$

The old trajectory has the probability

$$P(C) = \frac{1}{\mathcal{R}_C} \left[\prod_{i=0}^{C} \mathcal{R}_i e^{-\mathcal{R}_i \Delta t_i} \prod_{i=1}^{C} P(\xi_i) \right] e^{WC}, \tag{3.28}$$

where ξ_i denote the possible configurations and W is a bias parameter. The new trajectory has the probability

$$P(C + 1) = \frac{1}{\mathcal{R}_{C+1}} \left[\prod_{i=0}^{C+1} \mathcal{R}_i e^{-\mathcal{R}_i \Delta t_i} \prod_{i=1}^{C+1} P(\xi_i) \right] e^{W(C+1)}. \tag{3.29}$$

The protocol for adding the $(C + 1)-$th collision is the following:

- Let there be L possible mass pairs which can collide, *i.e.,* $p = 1, 2, \dots L$. The $p-$ th mass pair, (m_1, m_2), is chosen with probability

$$\frac{K(m_1, m_2)n_{m_1}n_{m_2}}{\sum_{i,j} K(m_i, m_j)n_{m_i}n_{m_j}}. \tag{3.30}$$

- Choosing the mass pair fixes the collision rate as $\mathcal{R}_{C+1}^{(p)}$. Using this rate, we choose $\Delta t_C'^p$ such that $\Delta t_C'^p + \Delta t_{C+1}' = \Delta t_C$, from the distribution

$$P(\Delta t_C'^p) = \frac{(\mathcal{R}_{C+1}'^p - \mathcal{R}_C)e^{(\mathcal{R}_{C+1}'^p - \mathcal{R}_C)\Delta t_C'^p}}{e^{(\mathcal{R}_{C+1}'^p - \mathcal{R}_C)\Delta t_C} - 1}. \tag{3.31}$$

- Now, the weight of adding a collision is

$$Wt(C \to C + 1) = P(\xi_j)P(\Delta t_C'^p). \tag{3.32}$$

The protocol for deleting a collision just involves deleting the final configuration and setting $\Delta t_C = \Delta t_C' + \Delta t_{C+1}'$. That is,

$$Wt(C + 1 \to C) = 1/\kappa, \tag{3.33}$$

where κ is a constant.

Substituting Eqs. (3.28), (3.29), (3.32) and (3.33) into Eq. (3.27), we obtain

$$\kappa = \frac{\mathcal{R}_C e^W (1 - e^{-(\mathcal{R}_{C+1} - \mathcal{R}_C)\Delta t_C})}{\mathcal{R}_{C+1} - \mathcal{R}_C}. \tag{3.34}$$

That is, addition of a collision is accepted with probability $\min(\kappa, 1)$, and deletion of a collision with probability $\min(1/\kappa, 1)$.

Implementing the algorithm described, we see that the numerical results are in excellent agreement with the analytical LDF, as seen in Fig 3.9.

3.3.5   Autocorrelation times

To characterize the algorithm, we determine the dependence of the autocorrelation time on bias w, fraction $\Phi = N/M$ and the parameter p. We recall that p is probability that in a given micro-step the sequence of collisions is modified, while $(1 - p)$ is the probability that the waiting times are modified. The autocorrelation function, $ACF(\tau)$, for a stationary variable X is defined as

$$ACF(\tau) = \frac{1}{T'} \int_0^{T'} dt[X(t + \tau) - \langle X \rangle][(X(t) - \langle X \rangle)], \tag{3.35}$$
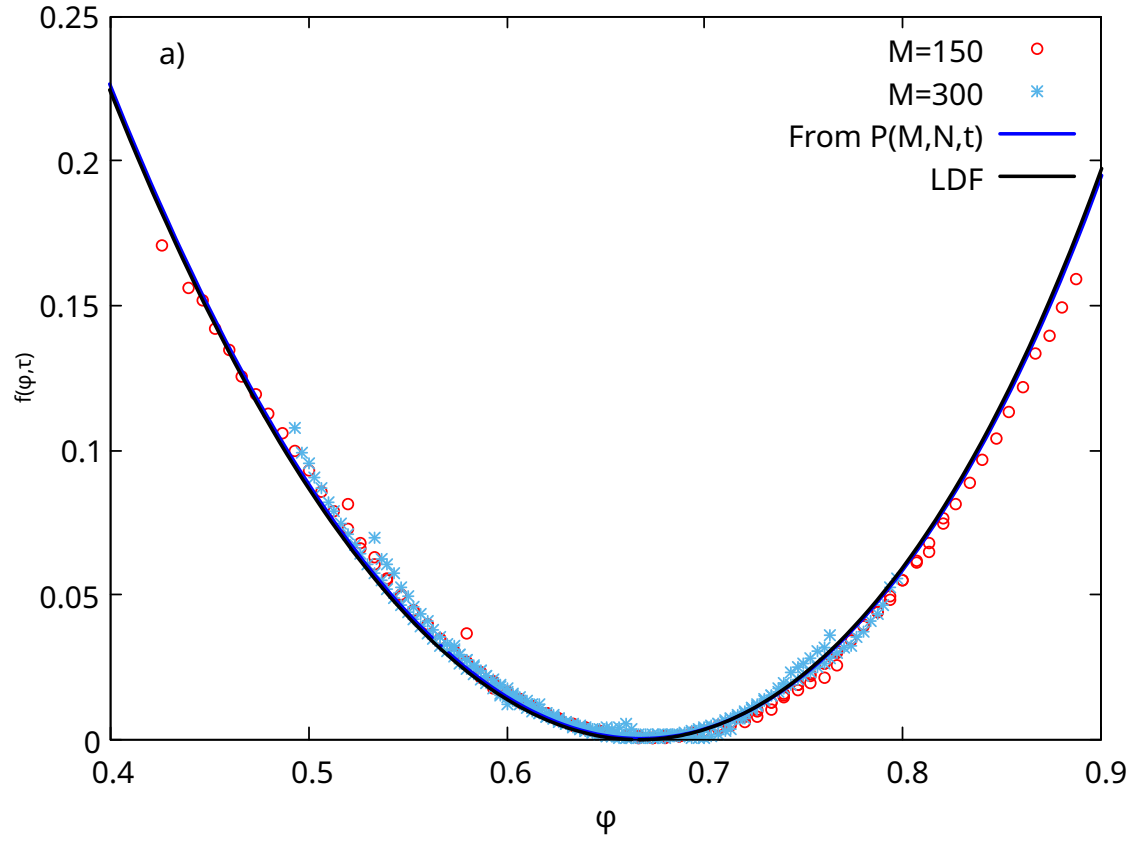
Figure 3.9: Comparison of $f(\phi, \tau)$ keeping $\tau = 1$ fixed, for the constant kernel, with the exact answer.

where T' is the total time over which X is measured, and τ is the delay.

The Monte Carlo algorithm involves introducing local modifications to the trajectory by changing either the waiting time associated with a collision or the sequence of collisions. To measure the autocorrelation in time as well as in configuration space, we define

$$t = \sum_{i=0}^{C} \Delta t_i, \qquad (3.36)$$

$$Q_i = \sum_{m=1}^{M} m^2 N_i(m), \quad i = 2, \ldots, C. \qquad (3.37)$$

Q_i is a measure of the mass distribution after the i-th collision. We choose the second moment of mass, as it is the lowest moment that changes when the mass distribution is modified, the zeroth and first moments being constants.

The autocorrelation functions $ACF_t(\tau)$ and $ACF_Q(\tau)$, corresponding to t and Q decay exponentially with time, as shown in Fig. 3.10. To decide which configuration we should use for the Q autocorrelation, we compare the autocorrelation functions for the C-th, $C/2$-th, and $C/4$-th collisions in Fig. 3.10 (b). We find that the correlation time, determined by the slope of the curve on the semi-log plot, is nearly the same for all the three data. For convenience, we choose the C-th configuration, henceforth, to measure the autocorrelation time τ_Q, and will drop the subscript i from the second moment Q in Eq. (3.37). We define autocorrelation times, τ_t and τ_Q via

$$\frac{ACF_t(\tau)}{ACF_t(0)} \approx e^{-\tau/\tau_t}, \tag{3.38}$$

$$\frac{ACF_Q(\tau)}{ACF_Q(0)} \approx e^{-\tau/\tau_Q}. \tag{3.39}$$

The autocorrelation times τ_t and τ_Q are obtained by fitting these exponential functions to the exponentially decaying regions of $ACF_t(\tau)$ and $ACF_Q(\tau)$, respectively. We now characterize the dependence of τ_t, τ_Q on the fraction of particles remaining, Φ, bias w, and the parameter p. All the simulations have been performed for the constant kernel.

Figure 8 shows the dependence of τ_t and τ_Q on the bias, w for fixed $\Phi = 0.8$ and $p = 0.5$. For $w > 0$, τ_t increases sharply with w and diverges at the cutoff bias [see Fig. 3.11 (a)]. For $w < 0$, τ_t increases much more slowly. We find that τ_t decreases with M, however, we cannot find a scaling behaviour. For the unbiased case, $w = 0$, we find that τ_t is independent of M. In contrast, we find that τ_Q shows at most a very weak dependence on w. It increases with M, but the data for different M collapse onto one curve when τ_Q is scaled by M^2 [see Fig. 3.11(b)].

The variation of τ_t and τ_Q with the parameter p is shown in Fig. 3.12 for fixed $\Phi = 0.8$ and $w = 0$. τ_t diverges as $p \to 1$. This is expected since, in this limit,
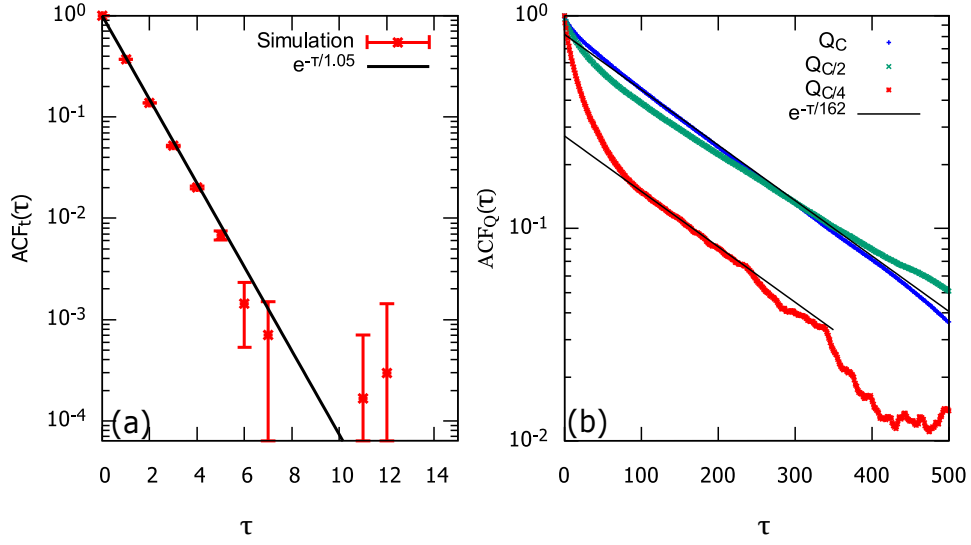
Figure 3.10: Autocorrelation functions for (a) total time t and $C = 60$, and (b) Q_i, for $i = C, C/2, C/4$, where $C = 24$, with delay τ, for the constant kernel, for $M = 120, w = 0, p = 0.5$.
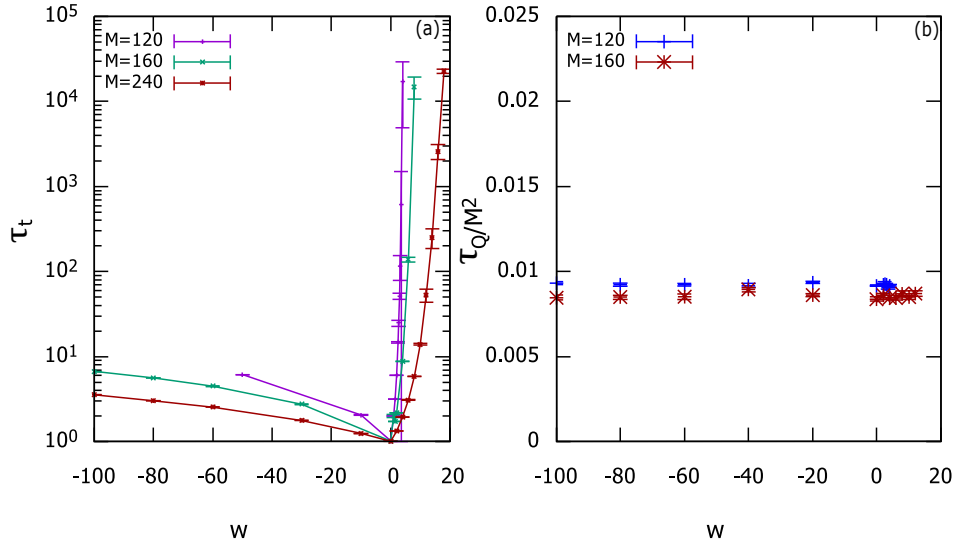
Figure 3.11: The variation of the autocorrelation times (a) τ_t and (b) τ_Q/M^2 with w for different M. The data are for the constant kernel for $p = 0.5$ and $\Phi = 0.8$.
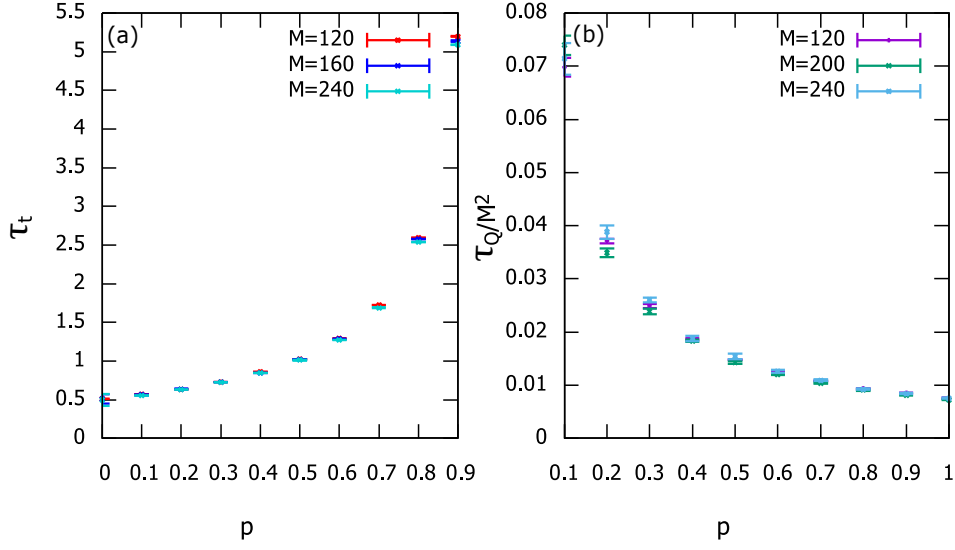
Figure 3.12: The variation of the autocorrelation times (a) τ_t and (b) τ_Q/M^2 with p for different M. The data are for the constant kernel for $\Phi = 0.8$ and $w = 0$.

the probability of modifying waiting times tends to zero. We also find that τ_t is independent of M. τ_Q, on the other hand, increases with M. However, the data for different M collapse onto one curve when τ_Q is scaled by M^2. As expected, τ_Q diverges for small p because the probability of updating configurations tends to zero in this limit.

We also checked the variation of τ_t and τ_Q with the parameter p for non-zero values of w. We again find that the data for τ_Q collapse when scaled by M^2. However, we do not find a scaling for τ_t.

The variation of τ_t and τ_Q with Φ is shown in Fig. 3.13 for fixed $p = 0.5$ and $w = 0$. τ_t is order 1 and very weakly dependent on both Φ as well as M. For τ_Q, like before, the data for different M collapse onto one curve when τ_Q is scaled by M^2. We also find that τ_Q is larger for smaller Φ.

From Figs. 3.11-3.13, we see that τ_t remains small unless $p \to 1$, or if the positive bias is close to the cutoff bias. On the other hand, τ_Q is order of $M^2/100$ times larger than τ_t. Choosing a value of p close to 1 will optimize the implementation of the algorithm, keeping both autocorrelation times finite.

56
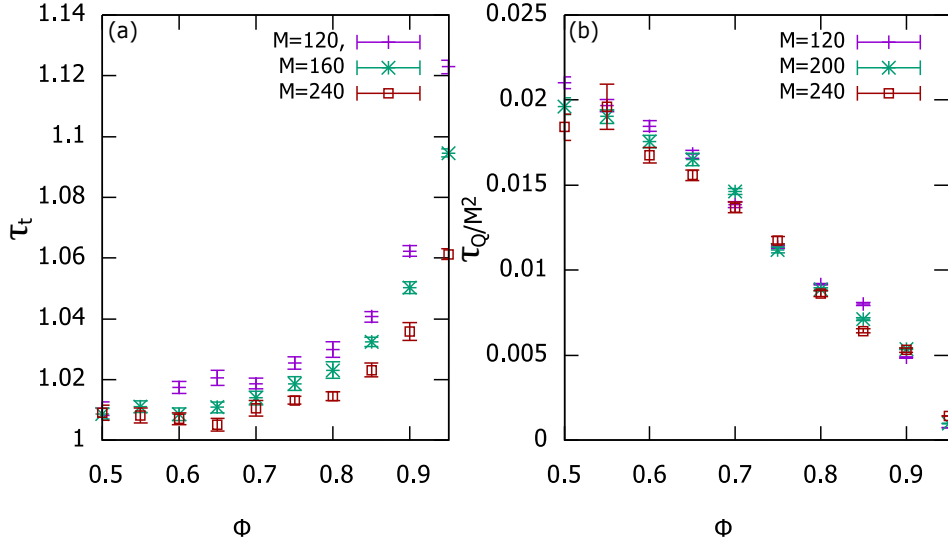
Figure 3.13: The variation of the autocorrelation times (a) τ_t and (b)τ_Q/M^2 with Φ for different M. The data are for the constant kernel for $p = 0.5$ and $w = 0$.

3.4 Summary

To summarize, we developed a biased Monte Carlo algorithm to compute probabilities of rare events in irreversible cluster-cluster aggregation for an arbitrary collision kernel. In particular, the algorithm measures $P(M, N, t)$, the probability of N particles remaining at time t when there are M particles initially, as well as the most probable trajectories for fixed M, N, and t. By choosing appropriate biases, the algorithm can efficiently sample the tails of the distribution with low computational effort. We prove that the algorithm is ergodic by specifying a protocol that transforms any given trajectory to a standard trajectory using valid Monte Carlo moves. The algorithm is benchmarked against the exact solution for the constant kernel.

To characterize the algorithm, we define autocorrelation times τ_t and τ_Q, corresponding to the waiting times as well as the configurations. We find that τ_t is much smaller than τ_Q for almost the entire range of parameters. From simulations for different M, we find that τ_t is at most only weakly dependent on M, while τ_Q is proportional to M^2. Based on the dependence of τ_t and τ_Q on the bias w, the fraction

of particles remaining $\Phi = N/M$, and the parameter p which decides what fraction of the Monte Carlo moves are changes to configurations, we conclude that it is best to choose a value of p as close to 1 as possible.

Generalizing the numerical results for constant, sum, and product kernels, we conclude that there exists a large deviation principle for arbitrary kernels, where the total mass M is the rate. This provides hints for a more rigorous treatment of the large deviation function for the problem of aggregation. In the next chapter, we provide a derivation of the large deviation function for some kernels.

Although this chapter deals with binary aggregation, the algorithm that we have developed can also be easily generalized to the numerical study of the non-binary processes $kA \to \ell A$, with suitably modified rates. Adding spatial degrees of freedom, and transport, like diffusion, is a problem of interest. However, generalizing the algorithm to such systems is a challenging problem. Adding a competing process such as fragmentation is another problem of interest [12, 13, 58, 59].Competing processes like these can lead to phase transitions and oscillations, at least in the mean field limit [60]. These are promising areas for future study.

Chapter 4

Large deviation function for $P(M, N, t)$

In the previous chapter, a biased Monte Carlo algorithm was developed to access the tails of the probability distribution $P(M, N, t)$. In this, and the next chapter, we study the probability $P(M, N, t)$ that exactly N particles remain at time t, or equivalently $M - N$ collisions occur up to time t, given that there are M particles of mass 1 initially. Here, the number of remaining particles N, is the random variable. We develop an analytical formalism using the Doi-Peliti-Zeldovich (DPZ) path integral method [61, 62, 63, 64, 65, 66], and establish the existence of a large deviation principle for an arbitrary collision kernel, and obtain the corresponding large deviation function. We calculate the exact large deviation functions and optimal evolution trajectories for the constant, sum and product kernels. The content of this chapter is published in [57].

4.1 Marcus-Lushnikov model

The model has been detailed in Sec. 2.2. We reproduce it here for ease of reference.

Consider a collection of particles which are labeled by their masses. Given a configuration, the system evolves in time through mass-conserving binary aggregation (also known as Marcus-Lushnikov model [6, 7, 49, 50]):

$$A_i + A_j \xrightarrow{\lambda K(i,j)} A_{i+j}, \tag{4.1}$$

where A_k denotes a particle of mass k, and $\lambda K(i,j)$ is the rate at which two particles of masses i and j aggregate. In an infinitesimal time dt, the probability of collision of two particles having masses i and j is given by $\lambda K(i,j)dt$. The collision kernel, $K(i,j)$, is dependent on the transport properties of the clusters and their collisional area of cross-section. We note that all the spatial information has been encoded into the collision kernel. Since each aggregation event reduces the number of particles, $N(t)$, by 1, $N(t)$ decreases monotonically with time. Initially, there are $N(0) = M$ particles with equal mass m_0. We set $m_0 = 1$, so that all masses are measured in units of m_0.

4.2   Analytical formalism

Let $\widetilde{P}(\vec{N}, t)$ denote the probability of a system being in a configuration $\vec{N}$ at time t, where $\vec{N}(t) = \{N_1(t), N_2(t), \ldots N_M(t)\}^\mathsf{T}$, and $N_i(t)$ is the number of particles of mass i at time t. Initially, there are $N(0) = M$ particles of equal mass (set equal to 1). Our quantity of interest is the probability density function $P(M, N, t_f)$, of having exactly N particles remain at time t_f. Additionally, we ask what the most probable trajectory is for a given M, N, t_f.

4.2.1 Master equation to action

We first express $P(M, N, t_f)$ in terms of an effective action [67, 68]. Then,

$$P(M, N, t_f) = \sum_{\vec{N}} \widetilde{P}(\vec{N}, t_f) \delta \left(\sum_{i=1}^{M} N_i(t_f) - N \right).$$ (4.2)

The time evolution of $\widetilde{P}(\vec{N}, t)$ is described by the master equation:

$$\frac{d\widetilde{P}(\vec{N})}{dt} = \sum_{i,j} \frac{\lambda K(i,j)}{2} \Big[(N_i + 1 + \delta_{i,j})(N_j + 1)$$

$$\widetilde{P}(\vec{N} + \mathcal{I}_i + \mathcal{I}_j - \mathcal{I}_{i+j}) - N_i(N_j - \delta_{i,j})\widetilde{P}(\vec{N}) \Big],$$ (4.3)

where $\mathcal{I}_k$ is the M-dimensional column vector whose j-th component equals δ_{jk}. The first term in the right hand side of Eq. (6.14) enumerates all possible collisions that lead to the configuration $\vec{N}$ while the second term enumerates all possible collisions that lead to the system exiting $\vec{N}$.

The DPZ formalism allows one to rewrite the master equation in the form of a Schroedinger equation in imaginary time. The number of clusters of mass i, N_i, is denoted as the eigenvalue of a number operator $\widehat{N}_i$ acting on a state $|\vec{N}\rangle = |N_1, N_2, \ldots N_M\rangle$,

$$\widehat{N}_i |\vec{N}\rangle = N_i |\vec{N}\rangle.$$ (4.4)

The operator $\hat{N}_i$ is expressed in terms of annihilation and creation operators a_i and $a_i^\dagger$, as

$$\hat{N}_i = a_i^\dagger a_i.$$ (4.5)

The annihilation and creation operators have the following properties,

$$a_i \ket{\vec{N}} = N_i \ket{\vec{N} - \mathcal{I}_i}, \tag{4.6}$$

$$a_i^\dagger \ket{\vec{N}} = \ket{\vec{N} + \mathcal{I}_i}, \tag{4.7}$$

$$a_i^\dagger a_i \ket{\vec{N}} = N_i \ket{\vec{N}}, \tag{4.8}$$

where $\mathcal{I}_i$ denotes the change in $\ket{\vec{N}}$ through the increase or decrease of the number of clusters of mass i by 1. The creation and annihilation operators obey the canonical commutation relations,

$$[a_i, a_j^\dagger] = \delta_{ij}. \tag{4.9}$$

We now define a state $\ket{\psi(t)}$, as a linear combination of $\ket{\vec{N}}$:

$$\ket{\psi(t)} = \sum_{\vec{N}} \tilde{P}(\vec{N}, t) \ket{\vec{N}}. \tag{4.10}$$

By multiplying both sides of the master equation by $\ket{\vec{N}}$ and summing over the configurations, we obtain a differential equation for $\ket{\psi(t)}$. Further, using Eq. (4.8), we obtain the master equation in the form of a Schroedinger equation in imaginary time:

$$\frac{d\ket{\psi(t)}}{dt} = -H(\{a_i^\dagger, a_i\}), \ket{\psi(t)}, \tag{4.11}$$

where the corresponding effective Hamiltonian $\widehat{H}(\{a^\dagger\}, \{a\})$ is obtained as a polynomial in the creation and annihilation operators:

$$H(\{a_i^\dagger, a_i\}) = -\frac{1}{2} \sum_i \sum_j \lambda K(i,j)(a_{i+j}^\dagger - a_i^\dagger a_j^\dagger)a_i a_j. \tag{4.12}$$

The dimensions of the rate λ are the inverse of time. In the following analysis, we make the transformation $\lambda t \to t$. The solution of Eq. (4.11) is

$$\ket{\psi(t)} = e^{-Ht} \ket{\psi(0)}, \tag{4.13}$$

where $|\psi(0)\rangle = \sum_{\vec{N}} \delta_{\vec{N},\{M,0,0...0\}} |\vec{N}\rangle$, *i.e.*, at $t = 0$, there are M particles of mass 1.

Multiplying both sides of the equation on the left by an arbitrary state $\langle \vec{L}|$ and using the relation $\langle \vec{L}|\vec{N}\rangle = \frac{1}{\vec{N}!}\delta_{\vec{L},\vec{N}}$, we obtain,

$$\tilde{P}(\vec{N},t) = \frac{\langle \vec{N}|\psi(t)\rangle}{\vec{N}!}, \tag{4.14}$$

where $\vec{N}! = N_1!N_2!\ldots N_M!$. Substituting the expression for $\tilde{P}(\vec{N},t)$ in Eq. (4.2), and multiplying and dividing by $N!$, we obtain,

$$P(M,N,t) = \frac{1}{N!} \langle \vec{0}| \sum_{k_1} a_{k_1} \sum_{k_2} a_{k_2} \cdots \sum_{k_N} a_{k_N} e^{-H(a^\dagger,a)t} |\psi(0)\rangle. \tag{4.15}$$

We ensure mass conservation by introducing a constrained sum:

$$P(M,N,t_f) = \frac{1}{N!} \langle \vec{0}| \sideset{}{'}\sum_{k_i=1}^{k^*} \prod_{i=1}^{N} a_{k_i} e^{-H(a^\dagger,a)t_f} |\psi(0)\rangle. \tag{4.16}$$

where $k^* = M - N + 1$, and ′ on the summation denotes the constraint $\sum_i k_i = M$.

In order to write Eq. (4.16) as a path integral, the evolution operator $e^{-\widehat{H}(a^\dagger,a)t_f}$ is split into a product of the evolution operators $e^{-H\epsilon}$ for infinitesimal times ϵ, in the limit $\epsilon \to 0$:

$$P(M,N,t_f) = \frac{1}{N!} \lim_{\epsilon \to 0} \langle \vec{0}| \sideset{}{'}\sum_{k_i=1}^{k^*} \prod_{i=1}^{N} a_{k_i} \prod_{n=1}^{t/\epsilon} e^{-H(a^\dagger,a)\epsilon} |\psi(0)\rangle \tag{4.17}$$

Using the Trotter formula and complete sets of coherent states for every infinitesimal evolution $e^{-H\epsilon}$, a solution to the master equation can be constructed in terms of in terms of coherent states, $|\mathbf{z}\rangle$ and their complex conjugates. The coherent state $|\mathbf{z}\rangle$

and the corresponding identity operator $\hat{I}$ are defined as follows:

$$a_i \left| \mathbf{z} \right\rangle = z_i \left| \mathbf{z} \right\rangle, \tag{4.18}$$

$$\left\langle \mathbf{z} \right| a_i^\dagger = \left\langle \mathbf{z} \right| \tilde{z}_i, \tag{4.19}$$

$$\hat{I} = \int \prod_i \frac{dz_i d\tilde{z}_i}{\pi} e^{-\sum_i z_i \tilde{z}_i} \left| \mathbf{z} \right\rangle \left\langle \mathbf{z} \right|, \tag{4.20}$$

where $\tilde{z}_i$ is the complex conjugate of z_i ($|z_i|^2 = z_i \tilde{z}_i$), and $\left| \mathbf{z} \right\rangle$ is written in terms of creation operators as

$$\left| \mathbf{z} \right\rangle = e^{-\frac{1}{2} \sum_m |z_m|^2} e^{\sum_m z_m a_m^\dagger} \left| \mathbf{0} \right\rangle. \tag{4.21}$$

Inserting the identity Eq. (4.20) for every infinitesimal evolution, we obtain

$$P(M, N, t_f) = \frac{1}{N!} \sum_{k_i=1}^{k^*} {}' \lim_{\epsilon \to 0} \left\langle \mathbf{0} \right| \prod_{i=1}^{N} a_{k_i} e^{-\sum_i z_i \tilde{z}_i |_{t_f}} \left| \mathbf{z}(t_f) \right\rangle \left\langle \mathbf{z}(t_f) \right| e^{-H(a^\dagger, a)\epsilon} e^{-\sum_i z_i \tilde{z}_i |_{t_f - \epsilon}}$$

$$\left| \mathbf{z}(t_f - \epsilon) \right\rangle \left\langle \mathbf{z}(t_f - \epsilon) \right| e^{-H\epsilon} e^{-\sum_i z_i \tilde{z}_i |_{t_f - 2\epsilon}} \left| \mathbf{z}(t_f - 2\epsilon) \right\rangle \left\langle \mathbf{z}(t_f - 2\epsilon) \right| \ldots$$

$$e^{-\sum_i z_i \tilde{z}_i |_{t=0}} \left| \mathbf{z}(0) \right\rangle \left\langle \mathbf{z}(0) | \psi(0) \right\rangle. \tag{4.22}$$

We write the coherent states $\left| \mathbf{z} \right\rangle$ in terms of the number operators using Eq. (4.21). We then evaluate the first bracket, which represents the system at the final time t_f, $\left\langle \mathbf{0} \right| \prod_{i=1}^{N} a_{k_i} \left| \mathbf{z}(t_f) \right\rangle$ and the last bracket, which represents the system at the initial time $t = 0$, $\left\langle \mathbf{z}(0) | \psi(0) \right\rangle$, using the following properties which arise from the commutation relations of the operators a and $a^\dagger$:

$$e^{ca} f(a^\dagger) = f(a^\dagger + c) e^{ca}, \tag{4.23}$$

$$f(a) e^{ca^\dagger} = e^{ca^\dagger} f(a + c), \tag{4.24}$$

and obtain for the first and the last brackets,

$$\langle \mathbf{0} | \prod_{i=1}^{N} a_{k_i} | \mathbf{z}(t_f) \rangle = \prod_{n=1}^{N} z_{k_n}(t_f), \tag{4.25}$$

$$\langle \mathbf{z}(0) | \psi(0) \rangle = \tilde{z}_1^M(0). \tag{4.26}$$

Using Eqs. (4.25) and (4.26) and evaluating the remaining terms, which are of the form $\langle \mathbf{z}(t) | e^{-H(a^\dagger, a)\epsilon} e^{-\sum_i z_i(t-\epsilon)\tilde{z}_i(t-\epsilon)} | \mathbf{z}(t-\epsilon) \rangle$, we obtain the probability $P(M, N, t_f)$:

$$P(M, N, t_f) = \sum_{k_i=1}^{k^*}{}' \int \mathcal{D}\tilde{z}_i \mathcal{D}z_i \prod_{n=1}^{N} \frac{z_{k_n}(t_f)}{N!}$$

$$\exp\left(\int_0^{t_f} dt \left[\sum_{m=1}^{M} \tilde{z}_m \dot{z}_m + H(\{z_i, \tilde{z}_i\}) \right] - M \ln \tilde{z}_1(0) + \sum_m z_m(0)\tilde{z}_m(0) \right), \tag{4.27}$$

Let $\tau = M^\alpha t$ and $z_i(\tau) \to M^\beta z_i(t)$. We observe that there is no scaling possible for $\tilde{z}_i$, as it is a dimensionless quantity. Scaling the integrand in the exponential in Eq. (4.27), we find that $\alpha = 1, \beta = -1$ and $H \to H/M^2$. Further, using the Stirling approximation,

$$\ln N! = N \ln N - N, \tag{4.28}$$

Eq. (5.7) simplifies to

$$P(M, \phi, \tau_f) \approx \int \{D\tilde{z}_i(\tau)\} \{Dz_i(\tau)\} \sum_{k_1, k_2, \dots k_N=1}^{k^*} \delta\left(\sum_m k_m - M \right) e^{-MS(\phi, \tau_f; \{z_i, \tilde{z}_i\})}, \tag{4.29}$$

where $\phi = N/M$, $\tau = Mt$, and the action S is given by

$$S(\phi, \tau_f; \{z_i, \tilde{z}_i\}) = \int_0^{\tau_f} d\tau \sum_i \tilde{z}_i \dot{z}_i + H + \left(\sum_i z_i(0)\tilde{z}_i(0) - \ln \tilde{z}_1(0) \right) \delta(\tau)$$

$$- \frac{\sum_{n=1}^{N} \ln z_{k_n}(\tau_f)}{M} \delta(\tau - \tau_f) + \phi \ln \phi - \phi, \tag{4.30}$$

where the scaled Hamiltonian is

$$H(\{\tilde{z}_i, z_i\}) = -\frac{1}{2} \sum_i \sum_j K(i,j)(\tilde{z}_{i+j} - \tilde{z}_i \tilde{z}_j) z_i z_j. \tag{4.31}$$

4.2.2 Euler-Lagrange equations

For large M, the integral Eq. (4.30) is dominated by the minimum of S. The Euler-Lagrange equations corresponding to the critical point of S are

$$\frac{dz_m}{d\tau} = \frac{1}{2} \sum_{j=1}^{m-1} K(m-j,j) z_j z_{m-j} - \sum_{j=1}^{M} K(m,j) \tilde{z}_j z_m z_j -$$

$$\left(z_m(0) - \frac{\delta_{m,1}}{\tilde{z}_1(0)} \right) \delta(\tau), \quad m = 1, \ldots M, \tag{4.32}$$

$$\frac{d\tilde{z}_m}{d\tau} = -\sum_{j=1}^{M-m} K(m,j) \tilde{z}_{m+j} z_j + \sum_{j=1}^{M} K(m,j) \tilde{z}_m \tilde{z}_j z_j - \frac{\sum_{n=1}^{N} \delta_{k_n,m}}{M z_m(\tau_f)} \delta(\tau - \tau_f) +$$

$$\tilde{z}_m(0) \delta(\tau), \quad m = 1, \ldots M. \tag{4.33}$$

Integrating Eq. (4.32) about $\tau = 0$, where the forward field $z_m(\tau) = 0$ for $\tau < 0$, we obtain the initial condition $\tilde{z}_1(0) z_m(0) = \delta_{m,1}, \quad 1 \leq m \leq M$, which is equivalent to

$$\tilde{z}_1(0) z_1(0) = 1, \tag{4.34}$$

$$z_m(0) = 0, \quad 1 < m \leq M, \tag{4.35}$$

where we use $\tilde{z}_1(0) \neq 0$. Integrating Eq. (4.33) about $\tau = \tau_f$, where the backward field $\tilde{z}_m(\tau) = 0$ for $\tau > \tau_f$, we obtain the final condition:

$$\tilde{z}_m(\tau_f) = \frac{\sum_{n=1}^{N} \delta_{k_n,m}}{M z_m(\tau_f)}. \tag{4.36}$$

In summary, $z_m(\tau)$ is integrated forward in time with the initial condition given at $\tau = 0$, while $\tilde{z}_m(\tau)$ is integrated backward in time with the final condition given at

$\tau = \tau_f$.

Notice that the action is invariant under the transformation $z_m \to c^m z_m$, $\tilde{z}_m \to c^{-m} \tilde{z}_m$, where c is a constant. Let us refer to such a transformation with parameter c as T_c. Both Eqs. (4.32), (4.33) as well as the the boundary conditions (4.34)–(4.36) are T_c-invariant for any $c \neq 0$: if $(z_m(\tau), \tilde{z}_m(\tau))_{0 \leq \tau \leq \tau_f, 1 \leq m \leq M}$ is a solution, then $T_c(z_m(\tau), \tilde{z}_m(\tau))_{0 \leq \tau \leq \tau_f, 1 \leq m \leq M}$ is also a solution. Therefore, the solution to Eqs. (4.32)–(4.36) is **not** unique, but rather there is a 1-parameter family of solutions labelled by c. Hence we are dealing with an example for which the naive counting ($2M$ ODE's for $2M$ variables with $2M$ boundary conditions have a unique solution) does not work. This non-uniqueness does not imply that there are issues with the formalism as the observables (the action functional, mass disitribution, the instanton energy, etc) are T_c-invariant. As a result, we can pick any solution from such a family, which simplifies the concrete analysis. This is exactly what we do: using $\bar{z}_1(0) \neq 0$, we choose the solution with $\bar{z}_1(0) = 1$. Uniqueness is then restored. The final action is

$$S(\phi, \tau_f; \{z_i, \tilde{z}_i\}) = -E\tau_f - \frac{\ln \prod_{n=1}^{N} z_{k_n}(\tau_f)}{M} + \phi \ln \phi, \qquad (4.37)$$

where the energy E is the value of the Hamiltonian. For the constant, sum, and product kernels, the term $\sum_{j=1}^{M} K(m,j) \bar{z}_j z_j$ in Eq. (4.32) can be expressed in terms of $N(t), M$ thus decoupling the dynamics for z from $\bar{z}$. This allows us to determine the rate function or action without requiring the full solution of $\tilde{z}_m(\tau)$. This observation does not extend to arbitrary kernels.

We now argue that the validity of the Euler Lagrange equations in Eqs. (4.32), (4.33) may be extended to all m. Given M and N, the maximum value that k_i in Eq. (4.29), and hence also in Eq. (4.36), can take is $k^* = M - N + 1$. Equation (4.36) immediately implies that $\tilde{z}_m(\tau_f) = 0$ for $m > k^*$. Also note that each term of $d\tilde{z}_m/d\tau$ in Eq. (4.33) is proportional to $\tilde{z}_i$, where $i \geq m$. Hence, it follows that $\tilde{z}_m(\tau) = 0$ for $m > k^*$, and all $\tau < \tau_f$. Given this result, we can extend the limits of the

summation to infinity, in the second term on the right hand side of Eq. (4.32), and the first and second terms on the right hand side of Eq. (4.33). We also note that the right hand side of Eq. (4.32) for $dz_m/d\tau$ depends only on z_i, where $i \leq m$. Hence, we can formally consider Eq. (4.32) to be valid for all $m = 1, \ldots \infty$.

From the Euler-Lagrange equations (4.32), (4.33), we find that the time evolution of $n = \sum_i z_i \tilde{z}_i$, the fraction of particles, is given by

$$\frac{dn}{d\tau} = \frac{-1}{2} \sum_{i,j} K(i,j) n_i n_j + E, n(0) = 1, n(\tau_f) = \phi. \tag{4.38}$$

We will call this equation as the instanton equation. For $\tilde{z}_i$, z_i satisfying the Euler Lagrange equations, it can be shown that H reduces to $2H = \sum_i z_i \frac{d\tilde{z}_i}{d\tau}$. Also, we have proved that H is a constant of motion.

We note that Eq. (4.33) is satisfied by $\tilde{z}_i(\tau) = 1$, in which case, $E = 0$ [see Eq. (4.31)]. For this special case, Eq. (4.32) for z_m, and hence n_m, is identical to the Smoluchowski equation for the mean mass distribution, and thus will correspond to the typical solution for a given time.

Equations (4.32), (4.33) and (4.37) describe the calculation of the LDF for an arbitrary kernel. Since $N = \phi M$, it is clear that in the limit $M \to \infty$, keeping ϕ and τ_f fixed, we can define a large deviation function

$$f(\phi, \tau_f) = \lim_{M \to \infty} \frac{-1}{M} \ln P(M, M\phi, \tau_f/M), \tag{4.39}$$

thus establishing a large deviation principle for any collision kernel.

4.2.3 Energy is a constant of motion

It follows from the Euler-Lagrange equations of motion Eqs. (4.32) and (4.33) that H is a constant of motion. For an arbitrary $K(i,j)$,

$$\frac{dH}{d\tau} = \sum_m \left(\frac{\partial H}{\partial z_m} \dot{z}_m + \frac{\partial H}{\partial \tilde{z}_m} \dot{\tilde{z}}_m \right). \tag{4.40}$$

Substituting the Euler-Lagrange equations in Eqs. (4.32) and (4.33), we prove that $\frac{dH}{d\tau} = 0$. The Hamiltonian H is constant along a particular trajectory where the fraction of particles remaining at time τ_f is ϕ. Hence, the value of the Hamiltonian, denoted by E, is uniquely determined for a given final condition.

We will now present an exact calculation of $f(\phi, \tau_f)$ for the constant, sum and product kernels.

4.3 Constant kernel $[K(i,j) = 1]$

The instanton equation, Eq. (4.38), reduces to $dn/d\tau = -n^2/2 + E$. Since $n(\tau)$ decreases with time, $E < n^2/2$. Integrating, the solution for $n(\tau)$ is

$$n(\tau) = \begin{cases} -\sqrt{-2E} \tan \frac{\sqrt{-2E}(\tau - \tau_0)}{2}, & E < 0, \\ \frac{1}{1 + \tau/2}, & E = 0, \\ \sqrt{2E} \coth \frac{\sqrt{2E}(\tau - \tau_1)}{2}, & E > 0, \end{cases} \tag{4.41}$$

where the constants E, τ_0, τ_1 are fixed by the initial and final conditions in Eq. (4.38). For determining the LDF, we also need to determine $z_m(\tau_f)$ and $\tilde{z}_1(0)$. Writing $z_m(\tau)$ in terms of its generating function, $Y(x, \tau) = \sum_m z_m(\tau) x^m - n(\tau)$, we obtain

$$\frac{\partial Y}{\partial \tau} = \frac{Y^2}{2} - E, \quad Y(x, 0) = z_1(0)x. \tag{4.42}$$

The right hand side of this equation is the negative of the instanton equation. Solving for Y and hence $z_m(\tau)$, we obtain

$$z_m(\tau) = \begin{cases} \dfrac{-2Ez_1(0)^m \sec^2 \sqrt{-E/2}\tau \left[\tan \sqrt{-E/2}\tau\right]^{m-1}}{\left[\sqrt{-2E}+\tan \sqrt{-E/2}\tau\right]^{m+1}}, & E < 0, \\[3ex] \dfrac{4\tau^{m-1}(z_1(0))^m}{(2+\tau)^{m+1}}, & E = 0, \\[3ex] \dfrac{2Ez_1(0)^m \sinh^{m-1}\sqrt{E/2}\tau}{\left[\sinh \sqrt{E/2}\tau+\sqrt{2E}\cosh \sqrt{E/2}\tau\right]^{m+1}}, & E > 0. \end{cases} \qquad (4.43)$$

The combinatorial prefactor in Eq. (4.29) is easily solved to be

$$\sum_{k_i=1}^{k^*}{}' 1 = \binom{M-1}{N-1}. \qquad (4.44)$$

Using Stirling's approximation and substituting for $z_m(\tau)$ in Eq. (4.30), the LDF is

$$f(\phi,\tau_f) = \begin{cases} \phi \ln \dfrac{\phi^2}{-2E+\phi^2} + \ln(1-2E) - E\tau_f, & E < 0, \\[3ex] 0, & E = 0, \\[3ex] -E\tau_f - \phi \ln \dfrac{2E}{\phi^2} - (1-\phi)\ln \dfrac{\sinh \tau_f \sqrt{E/2}}{1-\phi}+ \\[2ex] (1+\phi)\ln(\sqrt{2E}\cosh \tau_f \sqrt{E/2} + \sinh \tau_f \sqrt{E/2}), & E > 0, \end{cases} \qquad (4.45)$$

where $E < 0$, $E = 0$, $E > 0$ correspond to final times $\tau_f < \tau_{typ}$, $\tau_f = \tau_{typ}$ and $\tau_f > \tau_{typ}$ respectively, and τ_{typ} is the typical time for the fraction of particles to reach ϕ.

We demonstrate the correctness of the solution as well as the procedure by comparing $f(\phi,\tau_f)$ with results from both Monte Carlo simulations and the exact expression for $P(M,N,t_f)$. The simulations are based on the biased Monte Carlo scheme for fixed [51] as well as number of particles, described in the previous chapter, that accurately determines the probabilities of rare events and the instanton trajectory. For the constant kernel, the reaction rate does not explicitly depend on the mass dis-
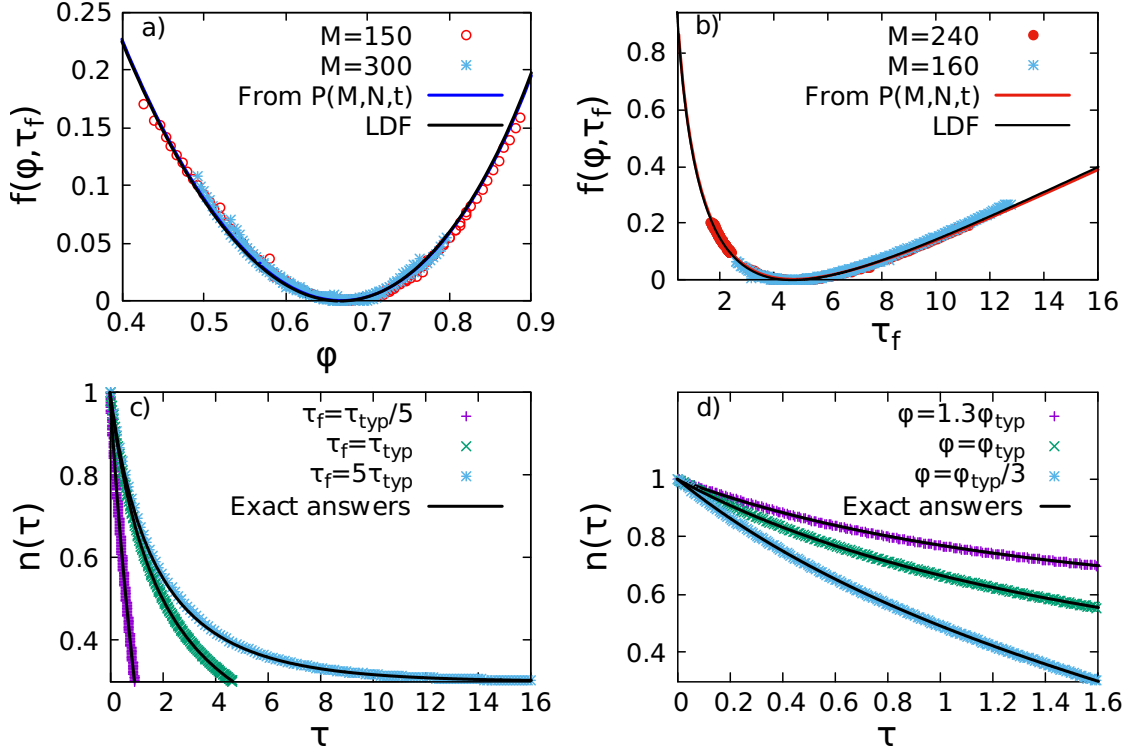
Figure 4.1: Constant kernel: Comparison of $f(\phi, \tau)$ with simulation data and exact expression for $P(M, N, t)$ for (a) varying ϕ for fixed $\tau_f = 1$, (b) varying τ_f for $\phi = 0.3$. The instanton trajectory in Eq. (4.41) is compared with simulation data for (c) $\phi = 0.3$ and different τ_f and (d) $\tau_f = 1.6$ and different ϕ.

tribution and hence it is possible to write $P(M, N, t)$ as a sum over exponentials [51]. We note that it is difficult to extract the LDF from this expression, however, it can be evaluated numerically. We find an excellent agreement of $f(\phi, \tau)$ with the simulations and exact answer both for fixed τ and varying ϕ [see Fig. 4.1(a)], and fixed ϕ and varying τ [see Fig. 4.1(b)]. The analytical results for the instanton solution [see Eq. (4.41)] are also in excellent agreement with the numerical results for short, typical and long times [see Fig. 4.1(c), (d)].
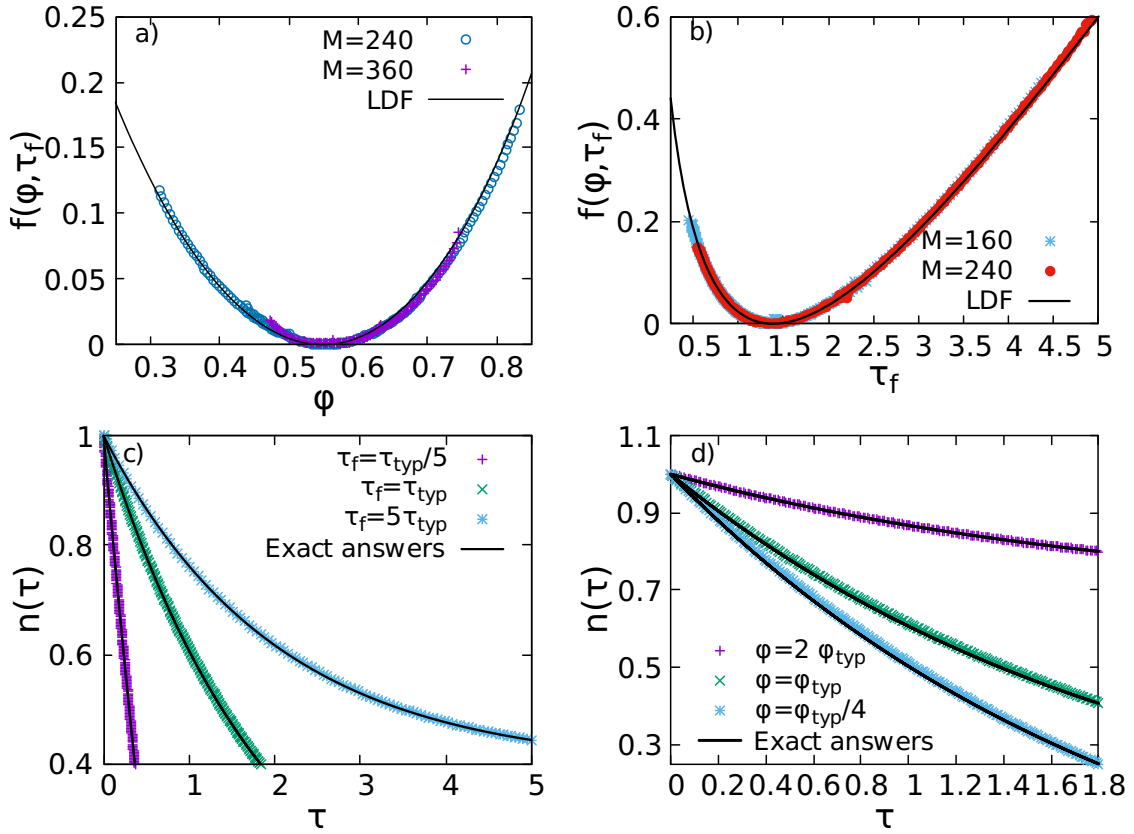
Figure 4.2: Sum kernel: Comparison of $f(\phi, \tau)$ with simulation data for (a) varying ϕ for fixed $\tau_f = 1.2$, (b) varying τ_f for $\phi = 0.5$. The instanton trajectory in Eq. (4.47) is compared with simulation data for (c) $\phi = 0.4$ and different τ_f and (d) $\tau_f = 1.8$ and different ϕ.

72

4.4   Sum kernel $[K(i,j) = (i+j)/2]$

The instanton equation, Eq. (4.38), reduces to

$$dn/d\tau = E - n/2. \tag{4.46}$$

Solving this equation and using the initial and final conditions,

$$n(\tau) = \frac{\phi - e^{-\tau_f/2}}{1 - e^{-\tau_f/2}} - \left(\frac{\phi - 1}{1 - e^{-\tau_f/2}}\right) e^{-\frac{\tau}{2}}. \tag{4.47}$$

The Euler-Lagrange equations for the sum kernel are:

$$\frac{dz_m}{d\tau} = \frac{1}{2}\sum_j K(m-j,j)z_j z_{m-j} - \sum_j K(m,j)\tilde{z}_j z_m z_j, \tag{4.48}$$

$$\frac{d\tilde{z}_m}{d\tau} = -\sum_j K(m,j)(\tilde{z}_{m+j} - \tilde{z}_m \tilde{z}_j)z_j, \tag{4.49}$$

Equation (4.48) has been solved in Chapter 2. We reproduce the main steps of the calculations here for ease of reference. In order to compute $z_m(\tau)$ for the sum kernel, we rewrite

$$z_m(\tau) = c_m(\tau) \exp\left(-\int_0^\tau d\tau_1 \frac{mn(\tau)+1}{2}\right). \tag{4.50}$$

Equation (4.48) now becomes

$$\frac{dc_m}{d\tau'} = \frac{1}{2}\sum_j mc_j c_{m-j}, \tag{4.51}$$

where $d\tau'/d\tau = \exp(-\tau/2)/2$. Further, using the ansatz

$$c_m(\tau') = a_m \tau'^{m-1}, \tag{4.52}$$

73

where a_m is a function of mass alone, and solving the resulting equation, we obtain

$$a_m = \frac{m}{m-1} \sum_i a_i a_{m-i}. \tag{4.53}$$

The generating function for a_m is written as

$$F(x) = \sum_m a_m x^m. \tag{4.54}$$

The equation for $F(x)$ is

$$x\frac{\partial F}{\partial x} - F(x) = 2F(x)x\frac{\partial F}{\partial x}. \tag{4.55}$$

Rearranging the terms and integrating,

$$\ln F - 2F = \ln\left(\frac{x}{x_0}\right), \tag{4.56}$$

and hence

$$Fe^{-2F} = \frac{x}{x_0}. \tag{4.57}$$

The left hand side can be rewritten in terms of the Lambert W function, $z = W(z)e^{W(z)}$ by multiplying both sides by -2,

$$-2Fe^{-2F} = \frac{-2x}{x_0}, \tag{4.58}$$

where $W(z) = -2F, z = \frac{-2x}{x_0}$. The Lambert function can be expanded as a series in z:

$$W(z) = \sum_{n=1}^{\infty} \frac{(-n)^{n-1}z^n}{n!}. \tag{4.59}$$

That is,

$$2F = \sum_{m=1}^{\infty} \frac{m^{m-1}}{m!}\left(\frac{2x}{x_0}\right)^m. \tag{4.60}$$

Hence,

$$a_m = \frac{(2m)^{m-1}a^m}{m!}, \tag{4.61}$$

where $a = 1/x_0$. Substituting this result in the ansatz Eq. (4.52), and the resulting answer in Eq. (4.50), we obtain the final mass distribution,

$$z_m(\tau) = \frac{m^{m-1}a_1^m}{m!}(1 - e^{-\tau/2})^{m-1}e^{-\int_0^\tau d\tau_1 \frac{mn+1}{2}}, \tag{4.62}$$

where $a_1 = 1$ from the initial condition, E. (4.34), and

$$\int_0^\tau d\tau_1 \left(\frac{mn(\tau_1) + 1}{2}\right) = m\left(E\tau - (2E - 1)(1 - e^{-\tau/2})\right) + \frac{\tau}{2}. \tag{4.63}$$

The combinatorial prefactor in Eq. (4.29) is then

$$\sum_{k_i=1}^{k^*}{}' \prod_{n=1}^{N} \frac{k_n^{k_n-1}}{k_n!} = e^{M(1-\phi)\left[1-\ln(1-\phi)\right]}. \tag{4.64}$$

Substituting $z_m(\tau)$ and the prefactor in Eq. (4.29), we obtain LDF for sum kernel to be

$$f(\phi, \tau) = -(1 - \phi)\ln\frac{1 - e^{-\frac{\tau}{2}}}{1 - \phi} + \frac{\tau\phi}{2} + \phi\ln\phi. \tag{4.65}$$

We find an excellent agreement of $f(\phi, \tau)$ with the simulations both for fixed τ and varying ϕ [see Fig. 4.2(a)], and fixed ϕ and varying τ [see Fig. 4.2(b)]. The analytical results for the instanton solution [see Eq. (4.47)] are also in excellent agreement with the numerical results for short, typical and long times [see Fig. 4.2(c), (d)].

4.5   Product Kernel

For the product kernel the Smoluchowski equation predicts that a gel that contains a finite fraction of the mass forms at gelling time $\tau_g = 1$ and gelling density $\phi_g = 0.5$.

In the discussion following Eq. (4.38), we showed that $E = 0$ corresponds to the solution to the Smoluchowski equation. However, this solution cannot be correct for $\tau \geq 1$ as mass is not conserved, violating the strict conservation of mass in the Marcus-Lushnikov model. We, therefore, modify the solution for product kernel as follows.

The probability distribution that we wish to calculate is [Eq. (4.16)]:

$$P(M, N, t_f) = \frac{1}{N!} \langle \vec{0}| \sum_{k_i=1}^{k^*}{}' \prod_{i=1}^{N} a_{k_i} e^{-H(a^\dagger, a)t_f} |\psi(0)\rangle .$$ (4.66)

We rewrite the unscaled Hamiltonian using number operator $\hat{n}_i$ and total mass operator $\hat{M}$, breaking normal ordering by using the commutation relation for a and $a^\dagger$:

$$H' = -\frac{1}{2} \sum_i \sum_j ij a_{i+j}^\dagger a_i a_j + \sum_j \frac{(j^2)\hat{n}_j}{2} + \frac{\hat{M}^2}{2}.$$ (4.67)

The last term in the above equation breaks normal ordering. To restore normal ordering, we use the relation $\hat{M}|\psi(0)\rangle = M|\psi(0)\rangle$, where $|\psi(0)\rangle = a_1^{\dagger M}|\vec{0}\rangle$, to rewrite $P(M, N, t_f)$ as

$$P(M, N, t_f) = \langle \vec{N}| \frac{(\sum_i a_i)^N}{N!} e^{-H'(\{a_i^\dagger\}, \{a_i\})t_f} |\psi(0)\rangle ,$$ (4.68)

$$H' = -\frac{1}{2} \sum_i \sum_j ij a_{i+j}^\dagger a_i a_j + \sum_j \frac{(Mj - j^2)a_j^\dagger a_j}{2}.$$ (4.69)

On introducing coherent states, we obtain the Euler-Lagrange equations to be

$$\dot{z}_k = \frac{1}{2} \sum_{l=1}^{k^*} l(k-l) z_l z_{k-l} - Mk z_k + \frac{k^2 z_k}{2},$$ (4.70)

$$\dot{\tilde{z}}_k = -\sum_{l=1}^{k^*} kl \tilde{z}_{l+k} z_l + kM\tilde{z}_k - \frac{k^2 \tilde{z}_k}{2}.$$ (4.71)

We note that we could have followed the same procedure of introducing the operators $\hat{M}$ and $\hat{n}_i$ for the constant and sum kernels. For these kernels, we find that the extra
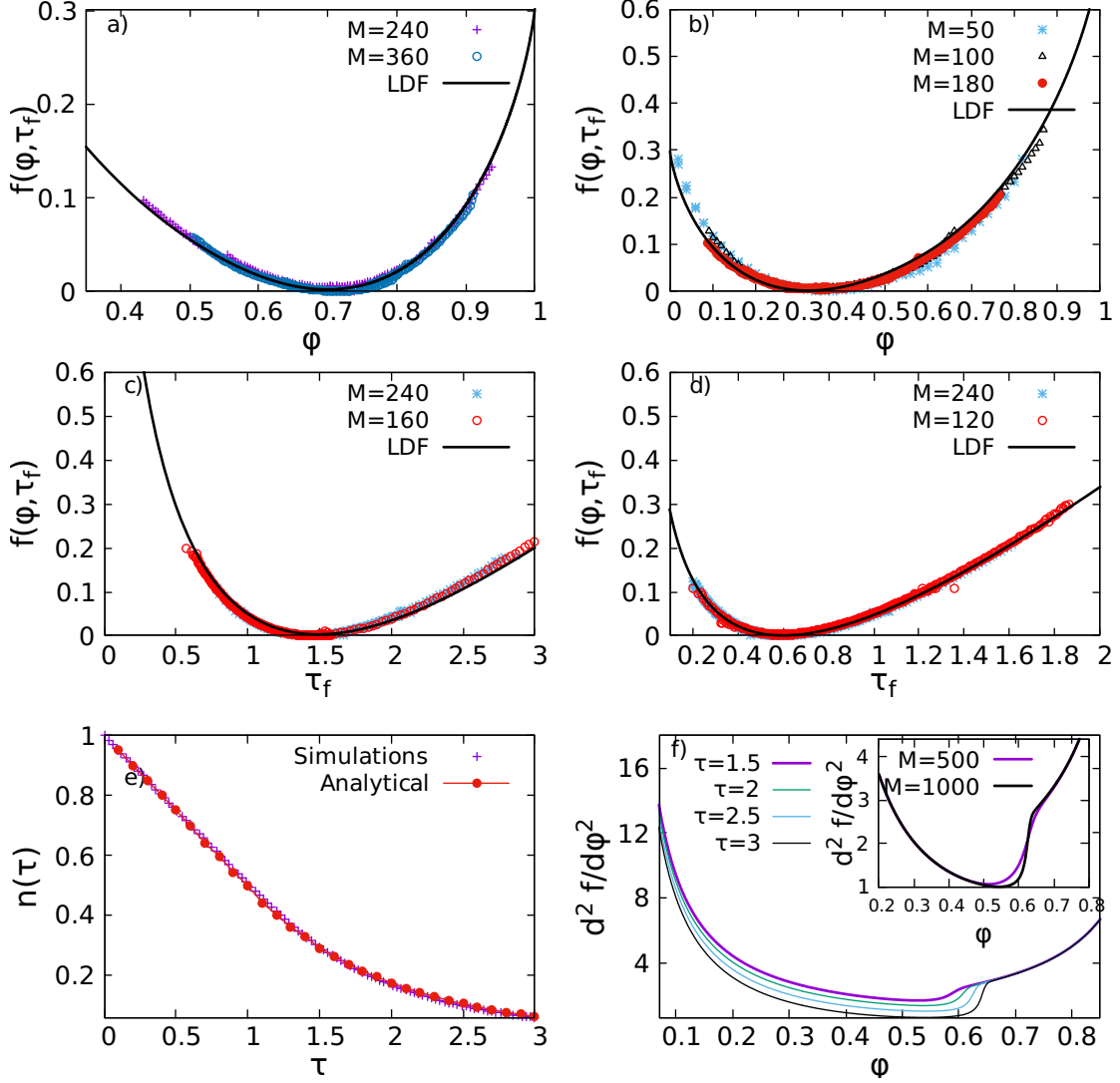
Figure 4.3: Product kernel: Comparison of $f(\phi, \tau)$ with simulation data for (a) fixed $\tau_f = 0.6 < \tau_g$, (b) fixed $\tau_f = 1.4 > \tau_g$ (c) fixed $\phi = 0.3 < \phi_g$ and (d) fixed $\phi = 0.7 > \phi_g$. (e) The value of ϕ at minimum of $f(\phi, \tau)$ is compared with Monte Carlo simulations of the typical trajectory. (f) $d^2 f/d\phi^2$ is discontinuous with ϕ. inset: $d^2 f/d\phi^2$ with ϕ for $\tau_f = 2.5$. The discontinuity becomes sharper with increasing M.

terms (second term on the right hand side of Eq. (4.67)) are always subleading in M, when $M \to \infty$. For the constant kernel, this term is $\sum_i \hat{n}_i$ and for the sum kernel, $\sum_i i \hat{n}_i$. Thus, these terms do not contribute to the LDF in the large deviation limit, $M \to \infty$. However, for the product kernel, the extra term becomes important when a gel is present, and hence cannot be neglected.

Equation (4.70) can be solved exactly. In order to compute $z_k(\tau)$, we solve the unscaled Euler-Lagrange equation for $z_k(t)$,

$$\dot{z}_k = \frac{1}{2} \sum_{l=1}^{k-1} l(k-l) z_l z_{k-l} - M k z_k + \frac{k^2 z_k}{2}, \quad k = 1 \ldots k^*, \qquad (4.72)$$

In the paragraph following Eq. (4.36), we argued that the equation for $\dot{z}_k$ for any kernel can be extended to all $k = 1 \ldots \infty$. In particular, the evolution of $\dot{z}_k$ depends only on z_i, where $i \leq k$. Let

$$G(x,t) = \sum_{k=1}^{\infty} z_k(t) x^k. \qquad (4.73)$$

Then, from Eq. (4.72), now considered valid for $k = 1 \ldots \infty$, we obtain

$$\frac{\partial G}{\partial t} = \frac{1}{2} \left(x \frac{\partial G}{\partial x} \right)^2 - M x \frac{\partial G}{\partial x} + \frac{1}{2} x \frac{\partial}{\partial x} \left(x \frac{\partial G}{\partial x} \right), \quad G(x,0) = z_1(0) x. \qquad (4.74)$$

Making the Cole-Hopf transformation $\ln D(p(x,t),t) = G(x,t)$, where $p(x,t) = x e^{-Mt}$, we obtain

$$\frac{\partial D}{\partial t} = \frac{1}{2} \frac{\partial}{\partial p} \left(p \frac{\partial D}{\partial p} \right), \qquad (4.75)$$

with the initial condition $D(x,0) = e^{z_1(0)x}$. Let

$$D(p,t) = \sum_m a_m(t) f(m) p^m. \qquad (4.76)$$

Then, substituting in Eq. (4.75) and matching the coefficients of p^m on both sides

of the equation,

$$\frac{da_m}{dt} = \frac{m^2 a_m}{2},$$ (4.77)

which can be solved to obtain

$$a_m(t) = c e^{\frac{m^2 t}{2}}.$$ (4.78)

We use the initial condition to obtain $f(m)$,

$$f(m) = \frac{z_1(0)^m}{m!}.$$ (4.79)

Combining Eqs. (4.78) and (4.79),

$$D(p, t) = \sum_m \frac{e^{\frac{m^2 t}{2}} (z_1(0) p)^m}{m!}.$$ (4.80)

In order to extract $G(x, t)$ from $D(p, t)$, we use Knuth identity [69]:

$$\ln \sum_{m=1}^{\infty} \frac{x^{m(m-1)/2} z^m}{m!} = \sum_{m=1}^{\infty} \frac{(x-1)^{m-1} F_{m-1}(x) z^m}{m!},$$ (4.81)

where $F_{m-1}(x)$ are known as Mallows-Riordan polynomials [69, 7], and obey the following recursion relation:

$$F_m(x) = \sum_{l=1}^{m} \binom{m-1}{l-1} \sum_{i=0}^{l-1} x^i F_{l-1}(x) F_{m-l}(x).$$ (4.82)

Converting $D(p, t)$ in terms of x, and equating the coefficients of x^m on both sides of the equation, we obtain

$$z_m(t) = \frac{(e^t - 1)^{m-1} F_{m-1}(e^t) M^m e^{m(-Mt + t/2)}}{m!},$$ (4.83)

Scaling $z_m(t) \to z_m(\tau)M$ and $t \to \tau/M$, we obtain

$$z_m(\tau) = \frac{(e^{\tau/M} - 1)^{m-1} F_{m-1}(e^{\tau/M}) M^{m-1} e^{m(-\tau+\tau/2M)}}{m!}. \qquad (4.84)$$

The term $e^{m\tau/2M}$ is subleading in M and can be neglected. We finally obtain

$$z_m(\tau) = \frac{(e^{\tau/M} - 1)^{m-1} F_{m-1}(e^{\tau/M}) M^{m-1} e^{-m\tau}}{m!}. \qquad (4.85)$$

From Eqs. (4.70) and (4.71), we find that $\sum_i \dot{z}_i \tilde{z}_i = -E' - M^2/2$, where E' is the value of H'. Substituting for z_i in Eq. (4.30), and computing the combinatorial prefactor, we obtain the LDF for the product kernel. We evaluate the combinatorial prefactor by writing the δ−function in Eq. (4.29) terms of an integral in x, and then obtain the minimum x in the limit $M \to \infty$ using saddle point approximation. Note that we denote $\min\{x\}$ by x. We thus obtain the critical ϕ in terms of x:

$$\phi = \frac{\sum_k \frac{x^k F_{k-1}}{k!}}{\sum_k \frac{x^{k-1} F_{k-1}}{(k-1)!}}. \qquad (4.86)$$

The final LDF for the product kernel is then

$$f(\phi, \tau) = \ln \frac{\phi^\phi e^{\tau/2 + 1 - \phi}}{\tau^{1-\phi}} + \min_x \{\ln x - \phi \, h(x)\}, \qquad (4.87)$$

$$h(x) = \sum_{k=1}^{k^*} \frac{x^k F_{k-1}(e^{\tau/M})}{k!}. \qquad (4.88)$$

It is difficult to evaluate the above expression exactly. In order to check the correctness of the LDF, we evaluate Eq. (4.87) numerically. We fix τ, and for every x, we calculate ϕ from Eq. (4.86). We find an excellent agreement of $f(\phi, \tau)$ with the simulations for both pre-gelling and post-gelling regimes [see Fig. 4.3(a)-(d)]. We also confirm that the minimum of the action corresponds to the typical solution [see Fig. 4.3(e)]. In particular, we find that this solution matches with simulation data for τ much larger than typical (see Fig. 4.5).
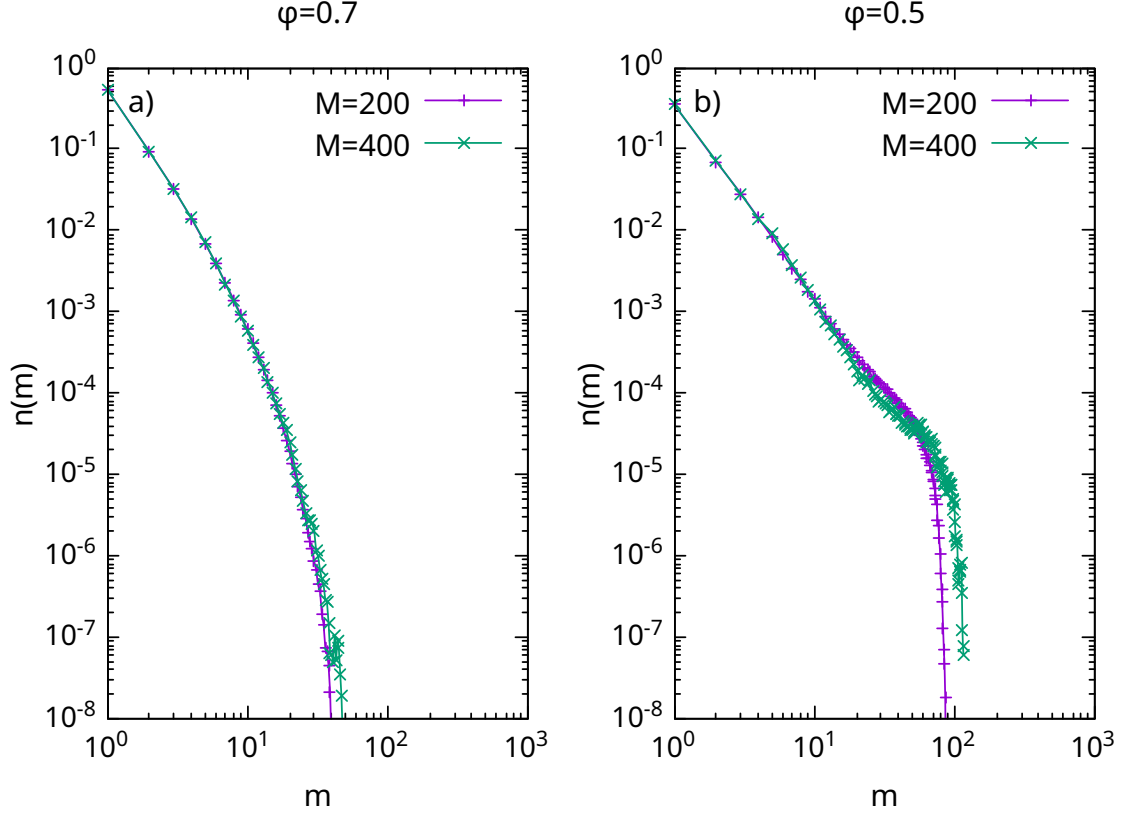
Figure 4.4: Product kernel: Mass distribution at final fixed time $\tau_f = 3$ for (a) $\phi = 0.7 > \phi_c$ and (b) $\phi = 0.5 < \phi_c$.

We find that the second derivative of the rate function, $\partial^2 f/\partial^2 \phi$ has a discontinuity at a critical ϕ [see Fig. 4.3(f)]. The discontinuity becomes sharper with M [see inset of Fig. 4.3(f)], suggesting the presence of a second order phase transition. We now argue that this transition is similar to the gelation transition seen in simulations of typical events: in particular, that for $\phi < \phi_c$, a gel is present for the optimal trajectories. To show this, we have considered a final time $\tau_f = 3$. For this final time, the transition occurs between $\phi = 0.63$ and $\phi = 0.65$ (see Fig. 4.3(f)). The numerically obtained mass distributions for $\phi = 0.5 < \phi_c$ and $\phi = 0.7 > \phi_c$ are shown in Fig. 4.4 for two different M. While the mass distribution is independent of M for $\phi = 0.7$, the cut-off for mass distribution for $\phi = 0.5$ is $M-$ dependent, as one would expect in the presence of a gel.
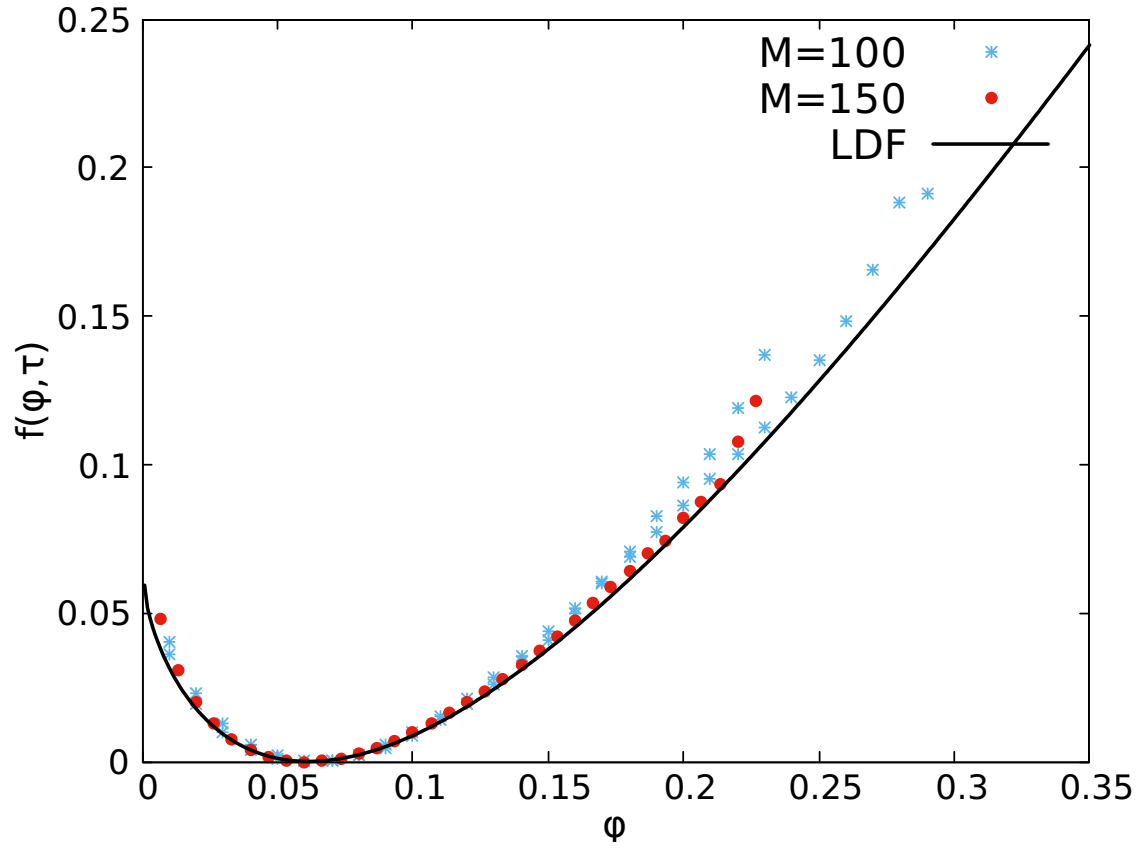
Figure 4.5: The large deviation function $f(\phi, \tau)$ with respect to ϕ for τ much larger than the typical time, $\tau = 3$, for $M = 100, 150$.

4.6 Summary

In summary, we developed a formalism to calculate the probabilities of rare events in cluster-cluster aggregation and demonstrated the existence of a large deviation principle for any collision kernel. The LDF is calculated exactly for the constant, sum, and product kernels. The known sol-gel transition for the product kernel is reflected as a singular behaviour in the LDF. Our general method allows us to obtain the optimal evolution trajectory corresponding to any rare event. These exact solutions will serve as a guideline for the numerical investigation of rare events in aggregation with collision kernels applicable to particular physical systems.

Chapter 5

Mass distribution for the constant and sum kernels

In the previous chapters, we have developed an analytical formalism and a Monte-Carlo algorithm to find the large deviation function for arbitrary collision kernels. Using the formalism, we could also calculate the exact large deviation functions for the constant, sum and product kernels. In this chapter, we derive the optimal mass distributions which contribute to typical and atypical events, for the constant and sum kernels. The manuscript containing the contents of this chapter is under preparation.

5.1 Large deviation function

The large deviation function derived in the previous chapter has the advantage that $\tilde{z}_1(0)$ can be set to 1 due to symmetry considerations. However, the full mass distribution can be obtained only by computing the solutions for both $z_m(\tau)$ and $\tilde{z}_m(\tau)$, as $n_m(\tau) = z_m \tilde{z}_m$ in the Doi-Peliti formalism. As explained in the previous chapter, the procedure for obtaining z and $\tilde{z}$ is to integrate $z(\tau)$ forward in time

with the initial condition given at $\tau = 0$, and $\tilde{z}_m$ backward in time with the final condition given at $\tau = \tau_f$.

In this chapter, we derive the large deviation function without introducing a constrained sum. This procedure gives the same Euler-Lagrange equations as the previous procedure, but we obtain an analytically tractable final condition for $\tilde{z}_m(\tau_f)$. The derivation detailed below retains both the terms $z_i(\tau)$ and $\tilde{z}_1(0)$. The procedure remains the same upto Eq. (4.16):

$$P(M, N, t) = \frac{1}{N!} \langle \vec{0} | \Big(\sum_k a_k \Big)^N e^{-H(a^\dagger, a)t} | \psi(0) \rangle. \tag{5.1}$$

In order to write Eq. (4.16) as a path integral, the evolution operator $e^{-\hat{H}(a^\dagger, a)t}$ is split into a product of the evolution operators $e^{-\hat{H}\epsilon}$ for infinitesimal times ϵ, in the limit $\epsilon \to 0$:

$$P(M, N, t) = \frac{1}{N!} \lim_{\epsilon \to 0} \langle \vec{0} | \Big(\sum_k a_k \Big)^N \prod_{n=1}^{t/\epsilon} e^{-H(a^\dagger, a)\epsilon} | \psi(0) \rangle \tag{5.2}$$

In the previous chapter, we introduce a constrained sum here, and this is the crucial step which leads to an action which remains invariant under the symmetry conditions $z_m \to c^m z_m, \tilde{z}_m \to c^{-m} \tilde{z}_m$. In Eq. (5.2), we insert identity operators $\mathbf{I}$ for every infinitesimal evolution $e^{-H\epsilon}$ in terms of coherent states, $|z\rangle$ and their complex conjugates. The coherent state $|z\rangle$ and $\mathbf{I}$ are defined as follows,

$$a_i | z \rangle = z_i | z \rangle, \tag{5.3}$$

$$\langle z | a_i^\dagger = \langle z | \tilde{z}_i, \tag{5.4}$$

$$\mathbf{I} = \int \prod_i \frac{dz_i d\tilde{z}_i}{\pi} e^{-\sum_i z_i \tilde{z}_i} | z \rangle \langle z |, \tag{5.5}$$

where $\tilde{z}_i$ is the complex conjugate of z_i ($|z_i|^2 = z_i \tilde{z}_i$), and $|z\rangle$ is written in terms of

creation operators as

$$|z\rangle = e^{-\frac{1}{2}\sum_m |z_m|^2} e^{\sum_m z_m a_m^\dagger} |0\rangle. \tag{5.6}$$

Using Eqs. (5.3), (5.4), and (5.5) in Eq. (5.2), $P(M, N, t)$ is written as follows,

$$P(M, N, t) = \frac{1}{N!} \sum_{k_i=1}^{k^*}{}' \int \{D\tilde{z}_i(t)\}\{Dz_i(t)\} e^{-S(M,N,t;\{z_i,\tilde{z}_i\})}, \tag{5.7}$$

where

$$S(M, N, t; \{z_i, \tilde{z}_i\}) = -\int_0^t dt' \left[\sum_i \tilde{z}_i \dot{z}_i + H\right]$$
$$+ M \ln \tilde{z}_1(0) + N \ln \sum_m z_m(t) - \sum_i z_i(0)\tilde{z}_i(0), \tag{5.8}$$

and the Hamiltonian is

$$H(\{z_i\}, \{\tilde{z}_i\}) = -\frac{1}{2} \sum_{i,j} K(i, j)\left(\tilde{z}_{i+j} - \tilde{z}_i\tilde{z}_j\right) z_i z_j. \tag{5.9}$$

5.1.1 Scaling the action

Let $\tau = M^\alpha t$ and $z_i(\tau) \to M^\beta z_i(t)$. We observe that no scaling is possible for $\tilde{z}_i$, as it is a dimensionless quantity. Scaling the integrand in the exponential in Eq. (5.7), we find that $\alpha = 1, \beta = -1$ and $H \to H/M^2$. Using the Stirling formula to write

$$\ln N! = N \ln N - N, \tag{5.10}$$

and using the Laplace method in the limit $M \to \infty$, Eq. (5.7) is

$$P(M, \phi, \tau_f) \approx e^{-MS(\phi,\tau_f;\{z_i,\tilde{z}_i\})}, \tag{5.11}$$

where $\phi = N/M$, $\tau = Mt$, and the scaled action can be written as

$$S(\phi, \tau; \{z_i, \tilde{z}_i\}) = \int_0^\tau d\tau' \left[\sum_i \tilde{z}_i \dot{z}_i + H \right] -$$

$$\ln \tilde{z}_1(0) - \phi \ln \sum_m z_m(\tau) + \sum_i z_i(0) \tilde{z}_i(0) + \phi \ln \phi - \phi. \qquad (5.12)$$

Note that the action Eq. (5.12) does not remain invariant under the symmetry conditions $z_m \to c^m z_m, \tilde{z}_m \to c^{-m} \tilde{z}_m$. We do not have the freedom to choose $\tilde{z}_1(0)$. Hence, we have to compute the full solution of z_m and $\tilde{z}_m$ in order to find the large deviation function. Such a computation yields the correct large deviation function, calculated in the previous chapter, for both the constant and sum kernels.

5.1.2   Euler-Lagrange equations

In the limit $M \to \infty$, keeping ϕ and τ fixed, the functional integral in Eq. (5.12) is dominated by the minimum of S, and hence can be calculated using Laplace method. The corresponding Euler-Lagrange equations for $z_m, \tilde{z}_m$, $m = 1 \ldots M$, are

$$\frac{dz_m}{d\tau'} = \frac{1}{2} \sum_j K(m-j, j) z_j z_{m-j} - \sum_j K(m, j) \tilde{z}_j z_m z_j$$

$$- \left(z_1(0) - \frac{1}{\tilde{z}_1(0)} \right) \delta(\tau'), \qquad (5.13)$$

$$\frac{d\tilde{z}_m}{d\tau'} = - \sum_j K(m, j)(\tilde{z}_{m+j} - \tilde{z}_m \tilde{z}_j) z_j +$$

$$\tilde{z}_1(0)\delta(\tau') - \frac{\phi}{\sum_i z_i(\tau)}\delta(\tau' - \tau). \qquad (5.14)$$

Integrating Eq. (5.13) about $\tau' = 0$ and Eq. (5.14) about $\tau' = \tau$, we obtain the boundary conditions $\tilde{z}_m(\tau) = \frac{\phi}{\sum_k z_k(\tau)}$ and $z_1(0)\tilde{z}_1(0) = 1$. Equation (5.13) is identical to the Smoluchowski equation, but differs in that the initial condition is $z_1(0) = a$, instead of $n_1(0) = 1$. However, we can use some of the techniques used to solve the Smoluchowski equation, as shown in Sec. (5.2) and (5.3.1).

Solving the integral in Eq. (5.12),

$$S(\phi, \tau; \{z_i, \tilde{z}_i\}) = -H\tau + \ln \tilde{z}_1(0) + \phi \ln \sum_m z_m(\tau) + \phi \ln \phi. \qquad (5.15)$$

By solving the Euler-Lagrange equations for $z_m(\tau)$ and $\tilde{z}_m(\tau)$, it is possible to compute the large deviation function for specific kernels such as the constant, sum and product kernels. For the constant and sum kernels, we have been able to verify that this method gives the same large deviation function as obtained in the previous chapter. In order to verify this for the product kernel, we would need to solve for $\tilde{z}_m(\tau)$. This is an open problem.

5.2   Constant kernel

The Euler Lagrange equations for the constant kernel are given by

$$\frac{dz_m}{d\tau} = \frac{1}{2} \sum_j z_j z_{m-j} - z_m n(\tau), \qquad (5.16)$$

$$\frac{d\tilde{z}_m}{d\tau} = -\sum_j \tilde{z}_{m+j} z_j + \tilde{z}_m n(\tau), \qquad (5.17)$$

where the fraction of particles $n(\tau) = \sum_m z_m(\tau)\tilde{z}_m(\tau)$, with the initial and final conditions

$$z_i(0) = a\delta_{i,1}, \qquad (5.18)$$

$$\tilde{z}_i(\tau_f) = \frac{\phi}{\sum_m z_m(\tau_f)}, \quad 1 \le i \le k^*, \qquad (5.19)$$

where $k^* = M - N + 1$ is the size of the largest cluster that can form for a given M, N. From the Euler Lagrange equations, the instanton evolution equation for $n(\tau)$ is

$$\frac{dn}{d\tau} = E - n^2/2. \qquad (5.20)$$

The solution for $n(\tau)$ is given by

$$n(\tau) = \sqrt{2E} \coth \frac{(\tau - \tau_0)}{2}, \tag{5.21}$$

where τ_0 is fixed using the initial condition, $n(0) = 1$. The energy E is fixed by the final condition, $n(\tau_f) = \phi$.

5.2.1 Solution for $z_m(\tau)$

In order to solve for $z_m(\tau)$, we define its generating function:

$$G(x, \tau) = \sum_m z_m(\tau) x^m. \tag{5.22}$$

Then,

$$\frac{\partial G}{\partial \tau} = \frac{1}{2}(G(x, \tau)^2 - 2n(\tau)G(x, \tau)), \tag{5.23}$$

with the initial condition

$$G(x, 0) = ax, \tag{5.24}$$

where $a = z_1(0)$. Defining $Y(x, \tau) = G(x, \tau) - n(\tau)$,

$$\frac{\partial Y(x, \tau)}{\partial \tau} + \frac{\partial n(\tau)}{\partial \tau} = -\frac{n^2}{2} + \frac{Y(x, \tau)^2}{2}. \tag{5.25}$$

Using Eq. (6.31),

$$\frac{\partial Y(x, \tau)}{\partial t} = -E + \frac{Y^2}{2}. \tag{5.26}$$

The equation for the evolution $Y(x, \tau)$ is very similar to Eq. (6.31), with the solution

$$Y(x, \tau) = -\sqrt{2E} \coth \frac{(\tau - \tau_1)}{2}, \tag{5.27}$$

89

where τ_1 is fixed using the initial condition for Y:

$$Y(x, 0) = z_1(0)x - 1. \tag{5.28}$$

Eliminating τ_1, we obtain

$$Y(x, \tau) = -\sqrt{2E}\left(\frac{\sqrt{2E} + (1 - ax)\coth\sqrt{2E}\tau/2}{(1 - ax) + \sqrt{2E}\coth\sqrt{2E}\tau/2}\right). \tag{5.29}$$

The coefficient of x^m gives $z_m(\tau)$:

$$z_m(\tau) = \frac{a^m 2E}{\sinh^2\sqrt{2E}\tau/2\left(1 + \sqrt{2E}\coth\sqrt{2E}\tau/2\right)^{m+1}}. \tag{5.30}$$

Rewriting the above equation,

$$z_m(\tau) = \frac{a^m 2E \sinh^{m-1}\sqrt{2E}\tau/2}{\left(\sinh\sqrt{2E}\tau/2 + \sqrt{2E}\cosh\sqrt{2E}\tau/2\right)^{m+1}}. \tag{5.31}$$

it can be seen that because $\sinh\sqrt{2E}\tau/2 = 0$, $z_m(0) = a\delta_{m,1}$.

5.2.2   Solution for $\tilde{z}_m(\tau)$

We solve Eq. (5.17),

$$\frac{d\tilde{z}_m}{d\tau} = -\sum_j \tilde{z}_{m+j}z_j + \tilde{z}_m n(\tau), \tag{5.32}$$

with $\tilde{z}_m(\tau_f)$ determined by Eq. (5.19). Define

$$\tilde{z}_m(\tau) = h_m(\tau)e^{\int_0^\tau d\tau' n(\tau')}. \tag{5.33}$$

Then, Eq. (5.17) is

$$\frac{dh_m}{d\tau} = -\sum_j h_{m+j}z_j. \tag{5.34}$$

Defining the genrating function of $h_m(\tau)$,

$$H(x,\tau) = \sum_{m=-\infty}^{\infty} h_m(\tau)x^{-m}, \tag{5.35}$$

we find that

$$\frac{\partial H}{\partial \tau} = -HG. \tag{5.36}$$

The solution to this equation is

$$H(x,\tau) = H_0 e^{-\int G d\tau}, \tag{5.37}$$

where H_0 is determined by the final condition derived from Eq. (5.19). Redefining $y = 1/x$, the final form of $H(y,\tau)$ is

$$H(y,\tau) = \frac{\phi}{\sum_m z_m(\tau_f)} e^{-\int_0^{\tau_f} d\tau' n(\tau')} \left(\frac{1 - yA_\tau}{1 - yA_{\tau_f}}\right)^2$$
$$\left(\frac{1 + \sqrt{2E}\coth\sqrt{2E}\tau_f/2}{1 + \sqrt{2E}\coth\sqrt{2E}\tau/2}\right) \sum_{m=-\infty}^{k^*} y^m, \tag{5.38}$$

where

$$A(\tau) = \frac{1 + \sqrt{2E}\coth\sqrt{2E}\tau/2}{a}, \tag{5.39}$$

and

$$\sum_m z_m(\tau_f) = \frac{2E(1-\phi)}{\phi\sinh\sqrt{2E}\tau_f/2(1 + \sqrt{2E}\coth\sqrt{2E}\tau_f/2)}. \tag{5.40}$$

Equating the coefficients of powers of y on both sides of Eq. (5.38),

$$h_k(\tau) = \frac{\phi}{\sum_m z_m(\tau_f)} \frac{2E}{(\sinh^2\sqrt{2E}\tau_f/2)a^2 A(\tau)^2}$$
$$\left[\sum_{m=-\infty}^{k}(k - m + 1)A(\tau)_f^{k-m} + A(\tau)^2\sum_{m=-\infty}^{k-1}(k - m - 1)A(\tau_f)^{k-m-2}\right.$$
$$\left. - A(\tau)\sum_{m=-\infty}^{k-1}(k - m)A(\tau_f)^{k-m-1}\right]. \tag{5.41}$$

91

Let $k' = k - m + 1$. Simplifying, we obtain

$$h_k(\tau) = \frac{\phi}{\sum_m z_m(\tau_f)} \frac{2E}{(\sinh^2 \sqrt{2E}\tau_f/2)a^2 A_\tau^2} \left(\frac{1 - A_\tau}{1 - A_{\tau_f}}\right)^2, \tag{5.42}$$

which is independent of index k. Using Eq. (5.33), we finally obtain

$$\tilde{z}_m(\tau) = \frac{\phi}{\sum_m z_m(\tau_f)} \left(\frac{\sinh \sqrt{2E}\tau/2}{\sinh \sqrt{2E}\tau_f/2}\right)^2 \left(\frac{1 - A_\tau}{1 - A_{\tau_f}}\right)^2. \tag{5.43}$$

In order to find a, we use the property of mass conservation:

$$\sum_m m z_m(\tau_f)\tilde{z}_m(\tau_f) = 1. \tag{5.44}$$

Using Eq. (5.19), we find that

$$\frac{\sum_m z_m(\tau_f)}{\sum_m m z_m(\tau_f)} = \phi. \tag{5.45}$$

Substituting Eq. (5.30) in the above equation, we obtain

$$a = (1 - \phi)(1 + \sqrt{2E} \coth \sqrt{2E}\tau_f/2). \tag{5.46}$$

Hence, the full mass distribution is

$$n_m(\tau) = \frac{\phi}{\sum_m z_m(\tau_f)} \left(\frac{\sinh \sqrt{2E}\tau/2}{\sinh \sqrt{2E}\tau_f/2}\right)^2 \left(\frac{1 - A_\tau}{1 - A_{\tau_f}}\right)^2$$
$$\frac{a^m 2E \sinh^{m-1} \sqrt{2E}\tau/2}{\left(\sinh \sqrt{2E}\tau/2 + \sqrt{2E} \cosh \sqrt{2E}\tau/2\right)^{m+1}} \tag{5.47}$$

We compare Eq. (5.47) with numerical simulations and find that they are in excellent agreement, as shown in Figs. 5.1(a) and (b).
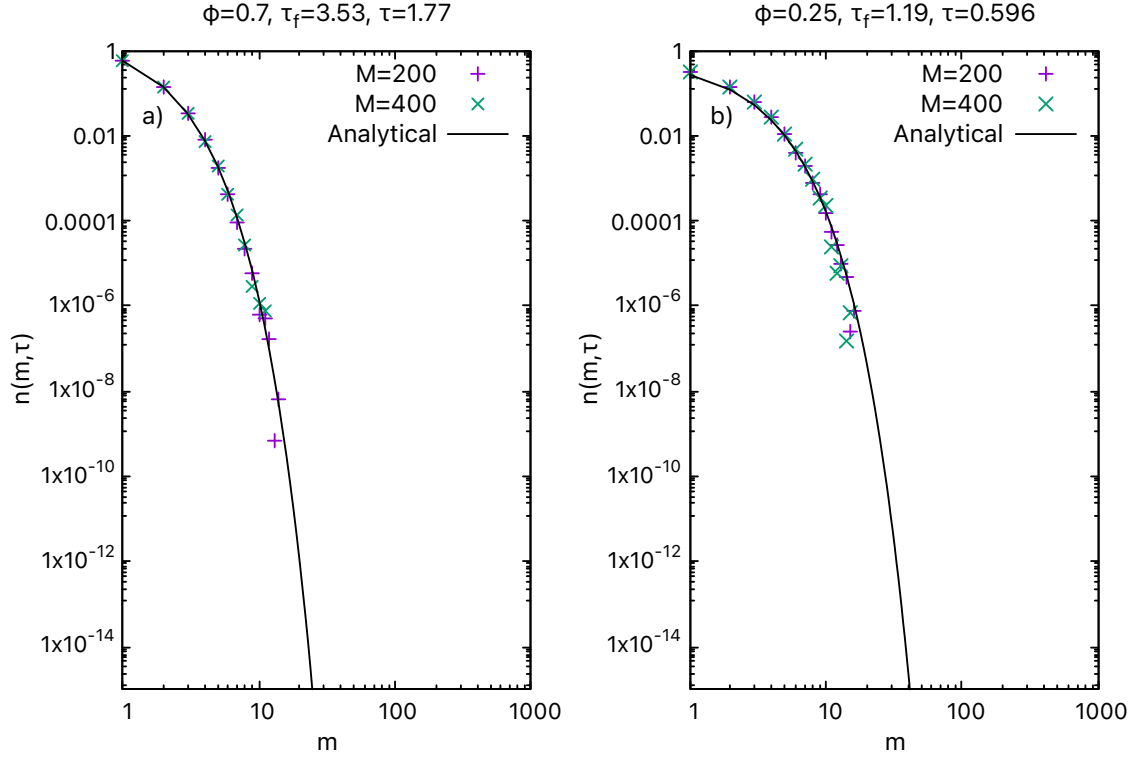
Figure 5.1: Constant kernel: Comparison of $n(m, \tau)$ with simulation data for (a) fixed $\phi = 0.7$, $\tau_f = 1.19$, (b) fixed $\phi = 0.25$, $\tau_f = 3.53$, where $\tau = \tau_f/2$.

5.3 Sum kernel

The Euler Lagrange equations for the sum kernel are given by

$$\frac{dz_m}{d\tau} = \frac{1}{4} \sum_j m z_j z_{m-j} - \frac{mn(\tau) + 1}{2} z_m, \tag{5.48}$$

$$\frac{d\tilde{z}_m}{d\tau} = -\frac{1}{2} \sum_j (m + j) \tilde{z}_{m+j} z_j + \frac{mn(\tau) + 1}{2} \tilde{z}_m, \tag{5.49}$$

with the same initial and final conditions given in Eqs. (5.18) and (5.19). The evolution of the optimal trajectory is

$$\frac{dn}{d\tau} = E - \frac{n}{2}. \tag{5.50}$$

Solving this equation and using the final condition to determine E, we obtain

$$2E = \frac{\phi - e^{-\tau_f/2}}{1 - e^{-\tau_f/2}}, \tag{5.51}$$

$$n(\tau) = 2E - (2E - 1)e^{-\tau/2}. \tag{5.52}$$

5.3.1 Equation for $z_m(\tau)$

Equation (5.48) is identical to the Smoluchowski equation for the mean mass distribution, and hence we can use techniques which have been described in Chapter 2 to obtain z_m. However, the initial condition Eq. (5.18) holds for typical and atypical times. We define

$$z_m(\tau) = c_m e^{-\int_0^\tau d\tau' \left(\frac{mn(\tau)+1}{2}\right)}, \tag{5.53}$$

$$\tilde{z}_m(\tau) = h_m e^{\int_0^\tau d\tau' \left(\frac{mn(\tau)+1}{2}\right)}. \tag{5.54}$$

Then,

$$\frac{dc_m(\tau)}{d\tau} = \frac{e^{-\tau/2}}{4} \sum_j mc_j c_{m-j}, \tag{5.55}$$

$$\frac{dh_m(\tau)}{d\tau} = -\frac{e^{\tau/2}}{2} \sum_j (m+j)h_{m+j}c_j. \tag{5.56}$$

We first obtain the solution for $z_m(\tau)$. Let $\tau_1 = \frac{1-e^{-\tau/2}}{2}$. Then,

$$\frac{dc_m}{d\tau_1} = \sum_j mc_j c_{m-j}. \tag{5.57}$$

Using the ansatz, $c_m(\tau_1) = a_m \tau_1^{m-1}$, where a_m is independent of τ_1, we obtain anequation for a_m,

$$a_m = \frac{m}{m-1} \sum_j a_j a_{m-j}. \tag{5.58}$$

94

The generating function for a_m is written as

$$F(x) = \sum_m a_m x^m. \tag{5.59}$$

The equation for $F(x)$ is

$$x\frac{\partial F}{\partial x} - F(x) = 2F(x)x\frac{\partial F}{\partial x}. \tag{5.60}$$

Rearranging the terms and integrating,

$$\ln F - 2F = \ln(\frac{x}{x_0}), \tag{5.61}$$

and hence

$$Fe^{-2F} = \frac{x}{x_0}. \tag{5.62}$$

The left hand side can be rewritten in terms of the Lambert W function, $z = W(z)e^{W(z)}$ by multiplying both sides by -2,

$$-2Fe^{-2F} = \frac{-2x}{x_0}, \tag{5.63}$$

where $W(z) = -2F, z = \frac{-2x}{x_0}$. The Lambert function can be expanded as a series in z:

$$W(z) = \sum_{n=1}^{\infty} \frac{(-n)^{n-1}z^n}{n!}. \tag{5.64}$$

That is,

$$2F = \sum_{m=1}^{\infty} \frac{m^{m-1}}{m!}(\frac{2x}{x_0})^m. \tag{5.65}$$

Hence,

$$a_m = \frac{(2m)^{m-1}a^m}{m!}, \tag{5.66}$$

where $a = 1/x_0$. We have now obtained the full form of $z_m(\tau)$:

$$z_m(\tau) = \frac{m^{m-1}a^m(1 - e^{-\tau/2})^{m-1}}{m!} e^{-\int_0^\tau d\tau' \left(\frac{mn(\tau')+1}{2}\right)}, \tag{5.67}$$

where the integral in the exponent is

$$\int_0^\tau d\tau' \left(\frac{mn(\tau') + 1}{2}\right) = m\left(E\tau - (2E - 1)(1 - e^{-\tau/2})\right) + \frac{\tau}{2}. \tag{5.68}$$

5.3.2 Equation for $\tilde{z}_m(\tau)$

In order to solve Eq. (5.56), using the fact that k' is the maximum mass that can form, given M, N, we set

$$\tilde{z}_m(\tau) = h_m(\tau) = 0, \forall m > k^*. \tag{5.69}$$

This implies that h_{k^*} is a constant, since k^* cannot form aggregates with any other mass, $i.e.,$

$$h_{k^*} = f_{k^*}. \tag{5.70}$$

The next lower mass, $k^* - 1$, can form aggregates only with mass 1. Writing the equation for h_{k^*-1},

$$\frac{dh_{k^*-1}}{d\tau} = -\frac{e^{\tau/2}}{2} k^* f_{k^*} a, \tag{5.71}$$

where $c_1 = a$. Integrating,

$$h_{k^*-1} = f_{k^*-1} - e^{-\tau/2} k^* f_{k^*} a. \tag{5.72}$$

96

Then, solving iteratively for h_m, where $m = k^* - 2, k^* - 3 \ldots 1$, we obtain that for an arbitrary mass m,

$$h_m(\tau) = \sum_{j=0}^{k^*-m} \frac{m^{j-1}(m+j)(-a)^j}{j!}(1 - e^{-\frac{\tau}{2}})^j f_{m+j}, \qquad (5.73)$$

where f_m can be computed from the final condition $\tilde{z}_m(\tau) = \frac{\phi}{\sum_i z_i(\tau_f)}$. Solving for f_m iteratively, we obtain:

$$f_m = \frac{\phi e^{-\tau_f/2}}{\sum_i z_i(\tau_f)} \sum_{j=0}^{k^*-m} \frac{(k^*-j)^{k^*-j-m}e^{-(k^*-j)\eta(\tau_f)}}{(k^*-m-j)!}(a(1-e^{-\tau_f/2}))^{k^*-j-m}, \qquad (5.74)$$

where

$$\eta(\tau_f) = \int_0^{\tau_f} d\tau' \frac{n(\tau')}{2} = E\tau_f - (2E-1)(1 - e^{-\tau_f/2}). \qquad (5.75)$$

Finally, the full solution for $n_m(\tau)$ is

$$n_m(\tau) = \frac{\phi e^{-\tau_f/2}}{m! \sum_i z_i(\tau_f)} \sum_{k=m}^{k^*} (-1)^{k-m} \sum_{j=0}^{k^*-k} \frac{m^{k-2}k a^{k^*-j}}{(k-m)!(k^*-k-j)!}$$

$$(k^*-j)^{k^*-k-j}(1 - e^{-\tau/2})^{k-1}(1 - e^{-\tau_f/2})^{k^*-k-j}e^{-(k^*-j)\eta(\tau_f)} \qquad (5.76)$$

It is difficult to evaluate this result mathematically. We have evaluated $n_m(\tau)$ numerically and find an excellent agreement with simulation results, as shown in Fig. 5.2.

5.4 Mass distribution at the final time

From the Monte Carlo simulations, we notice that the mass distribution at any final time τ corresponds to the typical or Smoluchowski solution, irrespective of τ. This can be explicitly proved in the case of the constant kernel. It follows from Eq. (5.39)

97
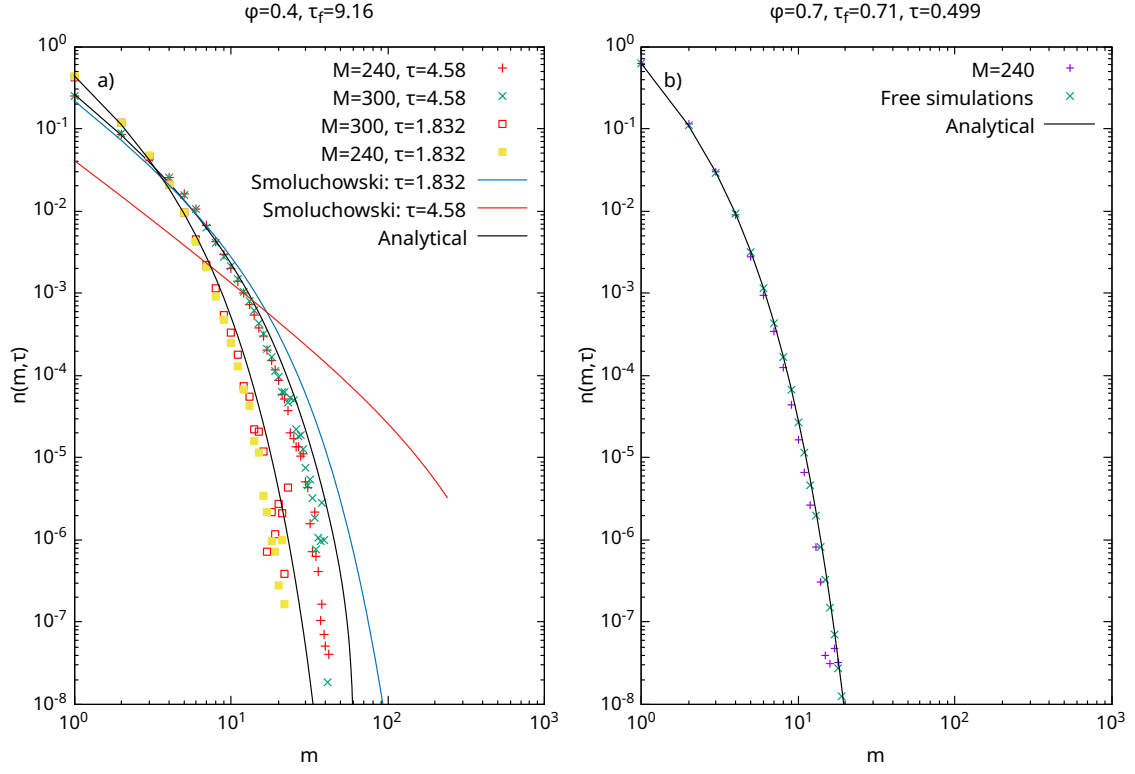
Figure 5.2: Sum kernel: Comparison of $n(m, \tau)$ with simulation data for (a) fixed $\phi = 0.4$, $\tau_f = 9.16 = 5\tau_{typ}$, where $\tau = \tau_f/2$, and $\tau = \tau_f/5$, and (c) fixed $\phi = 0.7$, $\tau_f = \tau_{typ}$, where $\tau = 0.7\tau_f$.

that

$$A_{\tau_f} = \frac{1}{1 - \phi}. \tag{5.77}$$

Hence, the final mass distribution for the constant kernel is

$$n_m(\tau_f) = z_m(\tau_f)\tilde{z}_m(\tau_f) = \frac{(1 - A_{\tau_f})^2}{A_{\tau_f}^{m+1}} \tag{5.78}$$

The solution is consistent with the initial and final conditions:

$$n_1(0) = 1, \tag{5.79}$$

$$\sum_m n_m(\tau_f) = \phi. \tag{5.80}$$
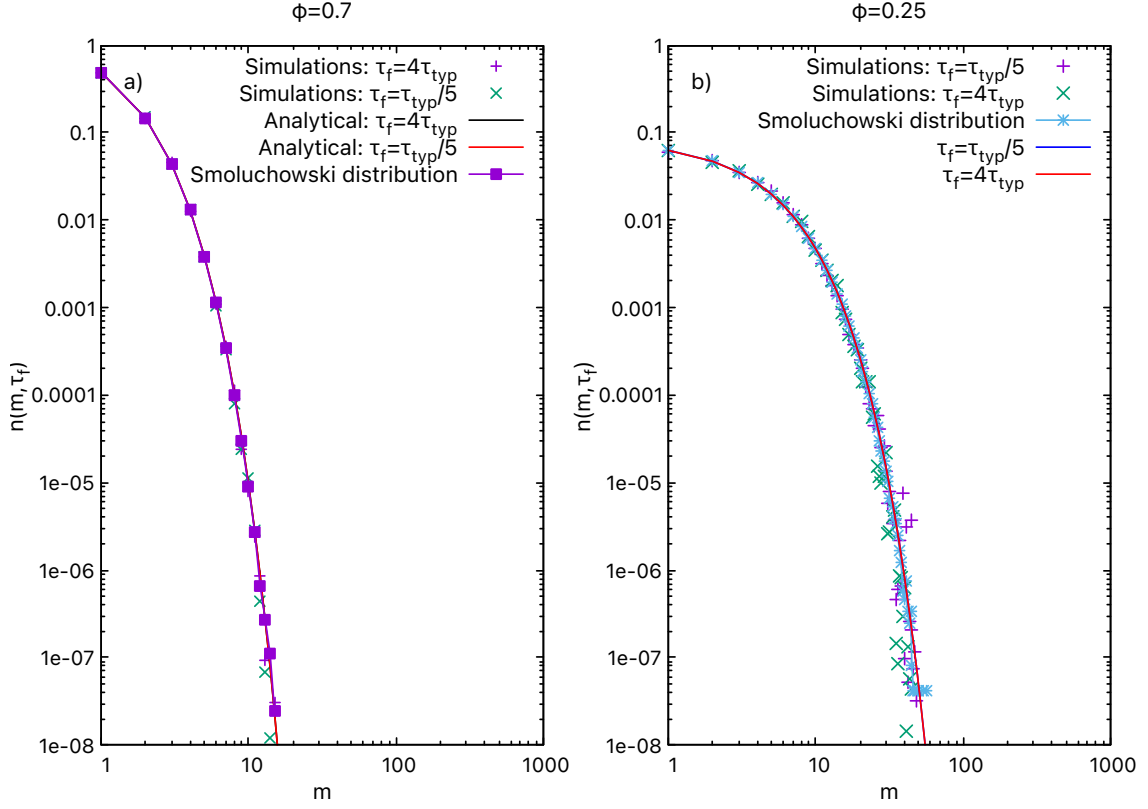
Figure 5.3: Constant kernel: Final mass distribution $n(m, \tau_f)$ at fixed $\phi = 0.7$ and various τ_f compared with the Smoluchowski distribution from simulations.

The final condition Eq. (5.80) can be verified by substituting Eq. (5.77) in Eq. (5.78) and solving. It can be seen that the final mass distribution

$$n_m(\tau_f) = \phi^2 (1 - \phi)^{m-1}, \qquad (5.81)$$

is independent of time. The typical evolution of the fraction of particles is

$$n(\tau_{typ}) = \phi = \frac{2}{2 + \tau_{typ}}. \qquad (5.82)$$

Substituting for ϕ in terms of τ_{typ} in Eq. (5.81), we obtain the final mass distribution to be

$$n_m(\tau_{typ}) = \frac{(\tau_{typ}/a)^{m-1}}{(1 + \tau_{typ}/2)^{m+1}}, \qquad (5.83)$$
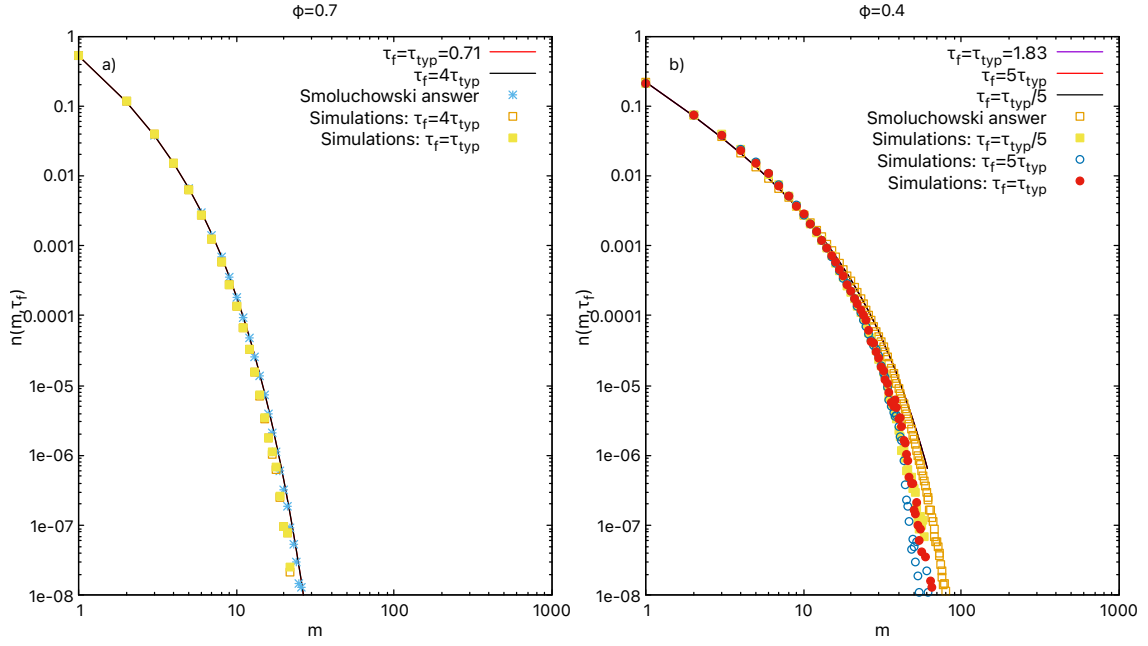
Figure 5.4: Sum kernel: Final mass distribution $n(m, \tau)$ at fixed ϕ and various τ_f compared with the Smoluchowski distribution from simulations.

which is the typical mass distribution which can be obtained by solving the solving the Smoluchowski equation, with collision rate $K(i, j) = 1$. This implies that at any value of the final time, the mass distribution $n_m(\tau_f)$ for a given ϕ corresponds to the typical mass distribution, as shown in Fig. 5.3.

5.5 Mass distribution as a function of number of collisions

The optimal trajectory for a rare event can differ from the optimal trajectory for typical events (typical trajectory) in two ways: the time between collisions can be different, and/or the sequence of collisions can be different. Figures 5.3 and 5.4 suggest that for the constant and sum kernels, the sequence of collisions remains the same while the waiting times differ between the optimal trajectory and typical trajectory.

Figure 5.5: Colouring of monomers according to the label of the cluster it belongs to for illustrating the argument for the product kernel provided in Sec. 5.5

This is definitely true for the constant kernel as we argue below. Initially, we have M monomers. After C collisions, the configuration consists of $M - C$ clusters of different masses. In the next collision, two clusters are chosen at random and collided, since the collision rates are independent of mass. Since the rules of collision are independent of the current mass distribution, it can only depend on the number of collisions, and not on the final time τ_f. This aspect can also be demonstrated by explicitly solving for the mass distribution as a function of collisions.

A similar argument can be constructed for the product kernel as follows. After C collisions, let the masses be $m_1, m_2, \ldots$. We visualise them as m_1 monomers of one colour, m_2 monomers of different colour and so on, so that the total number of monomers remain fixed at M. We pick two monomers of different colours at random and change the colour of all the monomers with the two colours to a new colour (see Fig. 5.5). With these rules, the probability of two clusters of masses m_1 and m_2 colliding is

$$P(m_1, m_2) = \frac{m_1}{M} \frac{m_2}{M - m_1} + \frac{m_2}{M} \frac{m_1}{M - m_2}. \tag{5.84}$$

In the limit $M \to \infty$,

$$P(m_1, m_2) \approx \frac{2m_1 m_2}{M^2}, \tag{5.85}$$

provided $m_1, m_2 \sim o(M)$. These collision rules are same as the product kernel, provided an aggregate is not present. The collision rules as stated above are independent of the current mass distribution, and hence will depend only on the number of collisions and not on the final time τ_f.
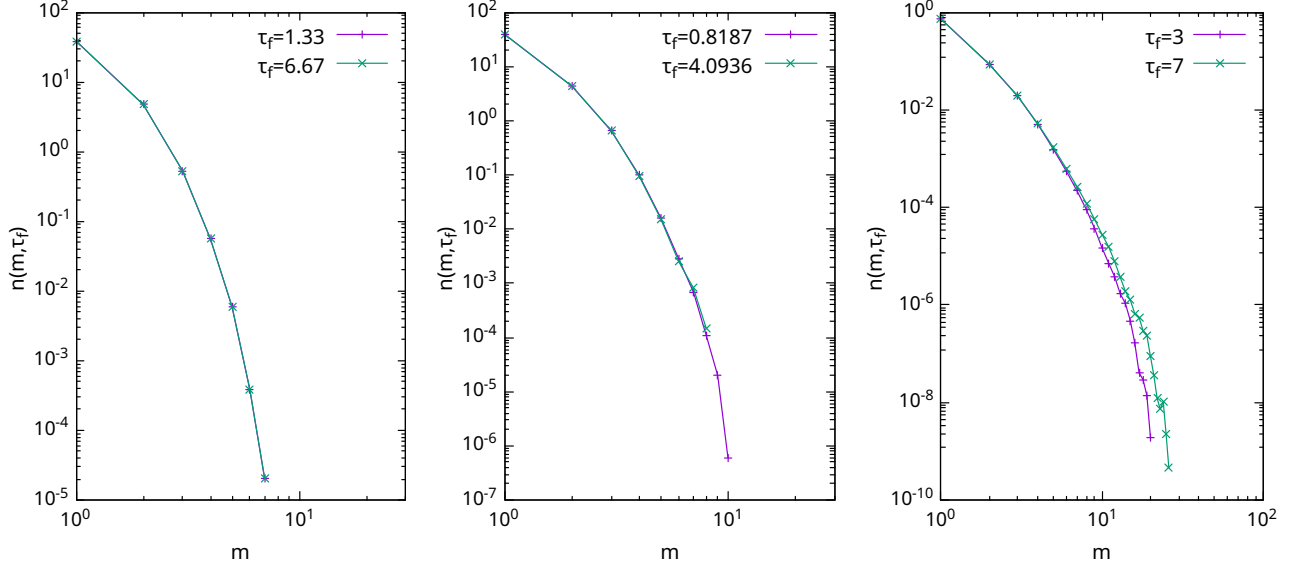
Figure 5.6: Mass distributions after $C = 25$ collisions for (a) Constant kernel and $\phi = 0.6$, (b)Sum kernel and $\phi = 0.6$, (c) Product kernel and $\phi = 0.7$.

For other kernels, we do not have a similar argument. But, the numerical results for sum kernel suggests that the optimal trajectory depends only on the number of collisions. In fact, we would conjecture that this aspect is true whenever gel is absent. To verify this, mass distributions after 25 collisions is shown to be the same for two different times, for constant, sum and product kernels (see Fig. 5.6).

5.6 Summary

We have calculated the full mass distributions for the constant and sum kernels, and compared the analytical answers with simulations. We have mathematically shown in the case of constant kernel that the final mass distribution is the same as the typical or Smoluchowski distribution, and benchmarked this result with simulations. We have shown numerically that the same result is true in the case of sum kernel also. We are trying to prove this result mathematically. For the product kernel, the equation for $\tilde{z}_i$ is unsolved. We observe from simulations that the mass distributions at any final time only collapse when $\tau_f < \tau_g$, where τ_g is the gelation time.

Chapter 6

$k-$nary Coalescence

6.1 Introduction

Physical phenomena in which aggregation or coalescence of constituents is a dominant dynamical process are ubiquitous in nature. Examples include cloud formation [9], aerosol dynamics [11, 70, 71], blood coagulation [8], dynamics of Saturn rings [12, 13, 72], neurodegenerative disorders such as Alzheimer's disease [73], dynamics of polyelectrolytes [20, 21], ductile fracture [74], etc. A model that isolates the effect of aggregation is the cluster-cluster aggregation model (CCA) in which the only dynamics is aggregation of clusters of particles to form larger clusters.

CCA has been studied using different approaches. Historically, it has been studied using the Smoluchowski equation, a deterministic mean-field, integro-differential equation for the rate of change of number of clusters of a particular size or mass (see Refs. [27, 28, 29, 30] for reviews). The information of the physical system being modelled such as shape of clusters [75] as well as the transport properties of the constituents are incorporated into a collision kernel that describes the rate of collision between clusters of different sizes. The Smoluchowski equation ignores fluctuations, both spatial and stochastic. In lower dimensions, when spatial density

fluctuations become dominant, the mass distribution in CCA has been studied using both analytical and numerical techniques [31, 32, 33, 34]. However, these approaches are limited to analysing the mean or typical mass distribution and its statistical low moments. They do not provide information about the probabilities of rare or atypical events, nor do they explain the pathways that lead to such events.

In Chapter 4, we developed a formalism to calculate the large deviation function (LDF), which describes the probabilities for rare events, in CCA [57]. This calculation was based on the Doi-Peliti-Zeldovich-Ochinnikov (DPZO) method [61, 62, 63, 64, 65, 66], a path integral approach that is based on writing the probabilities in terms of an effective action. An exact expression of the LDF of CCA was obtained for three standard collision kernels, the constant (rate is independent of mass), sum (rate is sum of masses) and product (rate is product of masses) kernels. The LDF has a singularity for the product kernel which is indicative of the sol-gel transition, wherein the Smoluchowski equation no longer conserves mass beyond a certain time. We could also determine the optimal evolution trajectories for a given rare event as solutions to the Euler-Lagrange equations that minimize the effective action [57]. Other studies of the LDF in CCA include the study of the gelation transition in the product kernel using large deviation theory in the probability literature (see [76] and references within), and a Monte Carlo algorithm for numerically determining the LDF for arbitrary collision kernels [51]. These results are for the case when the collisions were binary. In this chapter we extend these results to k-nary collisions where k particles aggregate in one event to form ℓ clusters, in particular the reaction $kA \xrightarrow{\lambda} \ell A$. We ignore the size of clusters, thus effectively studying the constant kernel problem.

We now briefly summarize what is known for the typical properties of the reaction $kA \xrightarrow{\lambda} \ell A$. Although the probability of more than two particles coalescing ($k > 2$ is significantly smaller than that of two particles coalescing ($k = 2$), higher order

collisions may become important in certain cases, for example, when a structure formed by three particles exhibits more stability. Ternary collisions as the primary collision mechanism can be observed in experiments that were motivated by drug delivery [77]. Moreover, the reaction $kA \xrightarrow{\lambda} \ell A$ is one of the simplest examples of interacting particle systems that are far from equilibrium, making it a useful model for testing conceptual ideas. In the presence of diffusion, the upper critical dimension of the model is known to be $d_c = 2/(k-1)$. Below d_c, the decay of mean density is dependent on the density fluctuations, and decays as $A_{k,\ell} t^{-d/2}$. Above d_c, the reaction is rate-limited and the mean density decays as $t^{-1/(k-1)}$. At d_c, mean density decays as $(t^{-1} \ln t)^{1/(k-1)}$. The prefactors for the power law decay can be computed as an ϵ-expansion for $d < d_c$, and exactly at $d = d_c$ [78]. For $k = 2$, using the empty interval method, the exact solution for the density can be found in one dimension [79, 80] and on the Bethe lattice [81]. Unlike density, the multi-particle correlations exhibit anomalous scaling in $d < d_c$. For $k = 2$, this anomalous scaling can be determined using renormalisation group methods in any dimension [82] and rigorously in one dimension [83]. The scaling exponents are independent of ℓ. This can be explicitly shown using field-theoretic methods [84, 85, 78, 86]. When mass is taken into account and for constant kernel, the exact result may be found in one dimension [31] and using renormalisation group in higher dimensions [33]. We also note that mass-dependent k-nary aggregation has been studied, starting from the Smoluchowski equation in Refs. [87, 88, 89].

In this chapter, we are interested in rare events in $k-$nary coalescence, *i.e.,* those events that occur at the tails of a probability distribution. The study of rare events is important because they could have significant impact despite their low likelihood of occurrence. Some common examples of rare events are natural disasters such as earthquakes and floods [35], financial black swan events [39], and epidemics [90]. The mathematical framework for the systematic study of rare events is provided by the large deviation theory [41]. The central focus of large deviation theory is the large

deviation principle, that is, the probabilities of rare events decrease exponentially fast. The large deviation function, or rate function, captures information about large fluctuations (deviations) from the most probable or typical states of a system. The rate function can also be interpreted as a non-equilibrium generalization of entropy or free energy.

In this chapter, we compute the LDF for $k-$nary coalescence. We also calculate the most probable trajectory for a given rare event. The contents of this chapter is published in [91].

6.2   Model

Consider a system of particles which evolves in time through the generalized coalescence process,

$$kA \xrightarrow{\lambda} \ell A, \quad \ell < k, \tag{6.1}$$

where A denotes a particle. Equation (6.1) describes the aggregation of k particles into ℓ particles at constant rate λ. In other words, we model the k-nary coalescence by a continuous time Markov chain on the state space $\mathbb{N}_0$ consisting of non-negative integers, defined by the transition $N \to N - (k - \ell)$ with the exponential rate $\lambda\binom{N}{k}$.

Each collision reduces the number of particles, $N(t)$, by $(k - \ell)$. The final absorbing state of this process contains $\ell, \ell + 1, \ldots k - 1$ particles, depending on the value of the initial number of particles, M.

In this chapter, we study $P(M, N, t)$, the probability that exactly N particles remain at time t, given that there are M particles initially. The number of collisions that have occurred, C, is related to N as

$$C = \frac{M - N}{k - \ell}. \tag{6.2}$$

6.3 Exact solution

It is possible to obtain the exact expression for $P(M, N, t)$ as a sum of exponentials for arbitrary k, ℓ [51]. Such an exact answer is possible because the collision rate after C collisions is known exactly, unlike the situation when masses are assigned to particles and the collision rates depend on the mass distribution. For a given k, ℓ, after i collisions, $M - (k - \ell)i$ particles remain, and the total rate of collision for the i-th collision, $\mathcal{R}_i$, is therefore given by

$$\mathcal{R}_i = \lambda \binom{M - (k - \ell)(i - 1)}{k}. \tag{6.3}$$

Using the exponential time distribution for waiting times, $P(\Delta t_i) = \mathcal{R}_i e^{-\mathcal{R}_i \Delta t_i}$,

$$P(M, N, t) = \int_0^\infty d\Delta t_1 \int_0^\infty d\Delta t_2 ... \int_0^\infty d\Delta t_{C+1} \ \mathcal{R}_1 e^{-\mathcal{R}_1 \Delta t_1}$$
$$\mathcal{R}_2 e^{-\mathcal{R}_2 \Delta t_2} \dots \mathcal{R}_C e^{-\mathcal{R}_C \Delta t_C} e^{-\mathcal{R}_{C+1} \Delta t_{C+1}} \delta \left(\sum_{i=1}^{C+1} \Delta t_i - t \right), \tag{6.4}$$

where C is as in Eq. (6.2). The final waiting time Δt_{C+1} denotes the waiting time during which no collision occurs. The δ-function constrains the sum of waiting times to the total time t. The Laplace transform of $\widetilde{P}(M, N, s)$, defined as

$$\widetilde{P}(M, N, s) = \int_0^\infty dt e^{-st} P(M, N, t), \tag{6.5}$$

is then

$$\widetilde{P}(M, N, s) = \prod_{i=1}^C \frac{\mathcal{R}_i}{\mathcal{R}_i + s} \frac{1}{\mathcal{R}_{C+1} + s}. \tag{6.6}$$

Doing the inverse Laplace transform, we obtain

$$P(M, N, t) = \left(\prod_{k=1}^C \mathcal{R}_k \right) \sum_{i=1}^{C+1} e^{-\mathcal{R}_i t} \prod_{j \neq i, j=1}^{C+1} \frac{1}{\mathcal{R}_j - \mathcal{R}_i}. \tag{6.7}$$

Though the exact expression for $P(M, N, t)$ can be obtained, it is not straightforward, either to derive the scaling for N and t with M in the large deviation limit, nor to derive the large deviation function directly from Eq. (3.14). Also, it is not possible to obtain the optimal trajectory for a given rare event. Instead, we will derive the large deviation function using the action formalism in Sec. 6.4, and use the numerical evaluation of Eq. (3.14) as a check for our results. In the process, we will also derive the optimal paths for rare events.

6.4   Results

6.4.1   Master equation and effective action

The time evolution of $P(M, N, t)$ is described by the master equation

$$\frac{dP(M, N, t)}{dt} = \lambda \left[\binom{N + k - \ell}{k} P(M, N + k - \ell, t) - \binom{N}{k} P(M, N, t) \right]. \quad (6.8)$$

The first term on the right hand side of Eq. (6.8) is a gain term, which describes the creation of a state with N particles, due to the aggregation of k particles from a state with $N + k - \ell$ particles. The second term is a loss term, which describes the aggregation of k particles from a state with N particles. We now rewrite the calculation of $P(M, N, t)$ in terms of an effective action using the DPZO procedure [57, 92, 63]. Let

$$|\psi(t)\rangle = \sum_{N'=0}^{M} P(M, N', t) |N'\rangle, \quad (6.9)$$

where $|N\rangle$ is the state with N particles which is acted upon by creation and annihilation operators a and $a^\dagger$, and the number-of-particles operator $\hat{N} := a^\dagger a$ as

follows:

$$a\,|N\rangle = N\,|N-1\rangle, \tag{6.10}$$

$$a^\dagger\,|N\rangle = |N+1\rangle, \tag{6.11}$$

$$\hat{N}\,|N\rangle = N\,|N\rangle, \tag{6.12}$$

$$[a, a^\dagger] = 1. \tag{6.13}$$

It is also useful to notice that $\langle N'|N\rangle = N!\delta_{N',N}$. In terms of $|\psi(t)\rangle$, the master equation Eq. (6.8) can be rewritten as

$$\frac{d\,|\psi(t)\rangle}{dt} = -\widehat{H}(a, a^\dagger)\,|\psi(t)\rangle, \tag{6.14}$$

where

$$\widehat{H}(a, a^\dagger) = -\frac{\lambda}{k!}(a^{\dagger\ell} - a^{\dagger k})a^k. \tag{6.15}$$

Equation (6.14) has the solution $|\psi(t_f)\rangle = e^{-\widehat{H}t_f}\,|\psi(0)\rangle$, where $|\psi(0)\rangle = |M\rangle$ and t_f is the final time. Multiplying Eq. (6.9) on the left with $\langle N|$, it is easy to see that

$$P(M, N, t) = \frac{\langle N|\psi(t)\rangle}{N!}. \tag{6.16}$$

Briefly, to find a path integral representation of Eq. (6.16), the evolution operator is first represented as an infinite product using Trotter's formula,

$$e^{-\widehat{H}(a^\dagger, a)t} = \lim_{n\to\infty}\left(1 - \widehat{H}(a^\dagger, a)\frac{t}{n}\right)^n.$$

Next the partition of the identity operator $\mathbf{I}$ in terms of the complete set of eigenfunctions of the annihilation operator a is inserted between every pair of factors of

$\left(1 - \widehat{H}(a^\dagger, a)\frac{t}{n}\right)$ entering the Trotter formula,

$$e^{-\widehat{H}(a^\dagger, a)t} = \lim_{n \to \infty} \left(1 - \widehat{H}(a^\dagger, a)\frac{t}{n}\right) \mathbf{I} \dots \mathbf{I} \left(1 - \widehat{H}(a^\dagger, a)\frac{t}{n}\right),$$

$$\text{where } \mathbf{I} = \int_{\mathbb{C}} \frac{dz d\tilde{z}}{\pi} e^{-|z|^2} |z\rangle \langle z|, \quad |z\rangle = e^{za^\dagger} |0\rangle.$$

Finally, the matrix elements $\langle z'| \left(1 - \widehat{H}(a^\dagger, a)\frac{t}{n}\right) |z\rangle$ are calculated using the representation of the operators $a, a^\dagger$ in the basis of $(|z\rangle)_{z \in \mathbb{Z}}$ (the so-called holomorphic representation):

$$|z\rangle = e^{zw}, \quad a^\dagger = w\cdot, \quad a = \frac{\partial}{\partial w}, \langle z|z'\rangle = e^{\bar{z}z'}, \quad w, z, z' \in \mathbb{C}$$

where the inner product is defined for a pair of holomorphic functions f, g as $\langle f|g\rangle = \int_{\mathbb{C}} \frac{dw d\bar{w}}{\pi} e^{-w\bar{w}} \overline{f(w)} g(w)$. The final answer is

$$P(M, N, t) = \int \mathcal{D}\tilde{z}(t) \mathcal{D}z(t) e^{-S(z, \tilde{z}, t)}, \tag{6.17}$$

where the action is given by

$$S(z, \tilde{z}, t) = \int_0^t dt \left[\tilde{z}\dot{z} + \lambda H(z, \tilde{z}) - N \ln z(t_f)\delta(t_f - t) - M \ln \tilde{z}(0)\delta(t)\right] + M + \ln N!, \tag{6.18}$$

and the effective Hamiltonian H is

$$H(z, \tilde{z}) = -\frac{\left(\tilde{z}^\ell - \tilde{z}^k\right)z^k}{k!}. \tag{6.19}$$

6.4.2   Existence of a large deviation principle

Defining $z \to zM^\alpha$, $\tilde{z} \to \tilde{z}M^\beta$ and $\tau = \lambda t M^\gamma$, and substituting in the action, we find that the choice $\alpha = 1$, $\beta = 0$ and $\gamma = k - 1$ keeps the form of the action unchanged.

The scaled action is then

$$S(z, \tilde{z}, \tau) = M \left[\int_0^\tau d\tau' \left[\tilde{z}\dot{z} + E(z, \tilde{z}) \right] - \phi \ln z(\tau) - \ln \tilde{z}(0) + z(0)\tilde{z}(0) + \phi \ln \frac{\phi}{e} \right],$$

(6.20)

where $\phi = N/M$. In the limit $M, N \to \infty$, keeping $\phi = N/M$ and $\tau = \lambda M^{k-1} t$ fixed, since the action in Eq. (6.20) is proportional to M, the functional integral Eq. (6.17) is dominated by the minimum of the action. Thus, there exists a large deviation principle

$$\lim_{M \to \infty} -\frac{\ln P(M, \phi M, \tau[\lambda M^{k-1}]^{-1})}{M} = f(\phi, \tau),$$

(6.21)

where $f(\phi, \tau) := \min_{z, \tilde{z}} S(z, \tilde{z}, \tau)$ is the rate function. We note that the number of particles formed after each collision, ℓ, does not appear in the scaling of time.

The Euler-Lagrange equations corresponding to the minimum of the action, Eq. (6.20) are given by

$$\dot{z} = \frac{1}{k!} \left(\ell \tilde{z}^{\ell-1} - k\tilde{z}^{k-1} \right) z^k + \left(\frac{1}{\tilde{z}(0)} - z(0) \right) \delta(\tau),$$

(6.22)

$$\dot{\tilde{z}} = -\frac{k}{k!} \left(\tilde{z}^\ell - \tilde{z}^k \right) z^{k-1} - \frac{\phi \delta(\tau - \tau_f)}{z(\tau_f)} = \frac{kE}{z} - \frac{\phi \delta(\tau - \tau_f)}{z(\tau_f)}.$$

(6.23)

By integrating Eqs. (6.22) and (6.23) about $\tau = 0$ and $\tau = \tau_f$, we obtain the boundary conditions to be

$$z(0)\tilde{z}(0) = n(0) = 1,$$

(6.24)

$$z(\tau_f)\tilde{z}(\tau_f) = n(\tau_f) = \phi,$$

(6.25)

where $n(\tau) = z(\tau)\tilde{z}(\tau)$ is the fraction of particles at time τ. Note that the Euler-Lagrange equations conserve energy $E := H(z(\tau), \tilde{z}(\tau))$, i.e., $dE/d\tau = 0$. Using
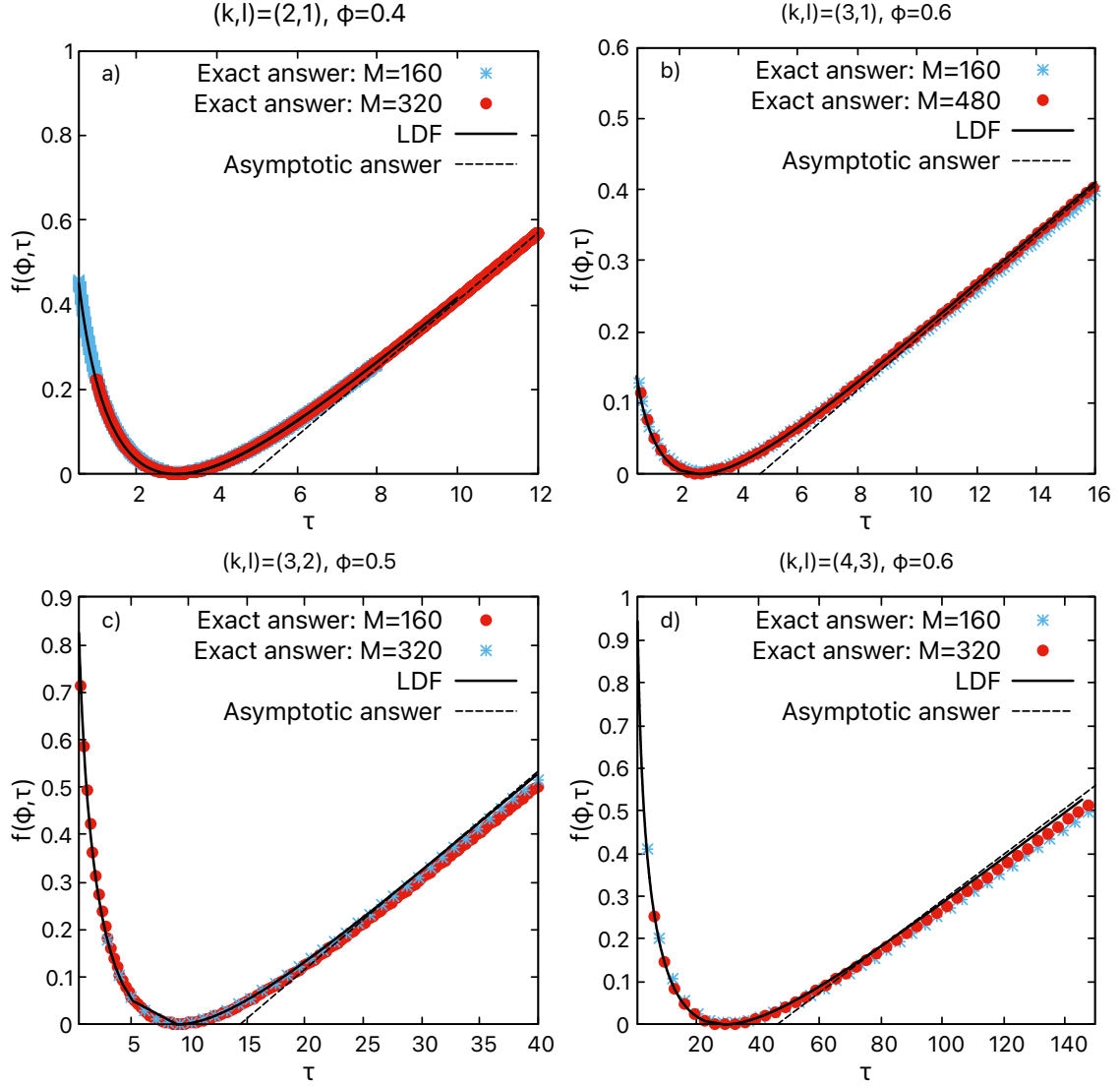
Figure 6.1: Large deviation functions $f(\phi,\tau)$ respect to τ are compared with the exact answer, Eq. (6.7), for a) $(k,\ell) = (2,1), \phi = 0.4$, b) $(k,\ell) = (3,1), \phi = 0.6$, c) $(k,\ell) = (3,2), \phi = 0.5$, d) $(k,\ell) = (4,3), \phi = 0.6$. The agreement of the exact solution with the large deviation function is better for larger values of the total mass M. The asymptotic answers for $\tau \to \infty$ are shown (broken black lines).
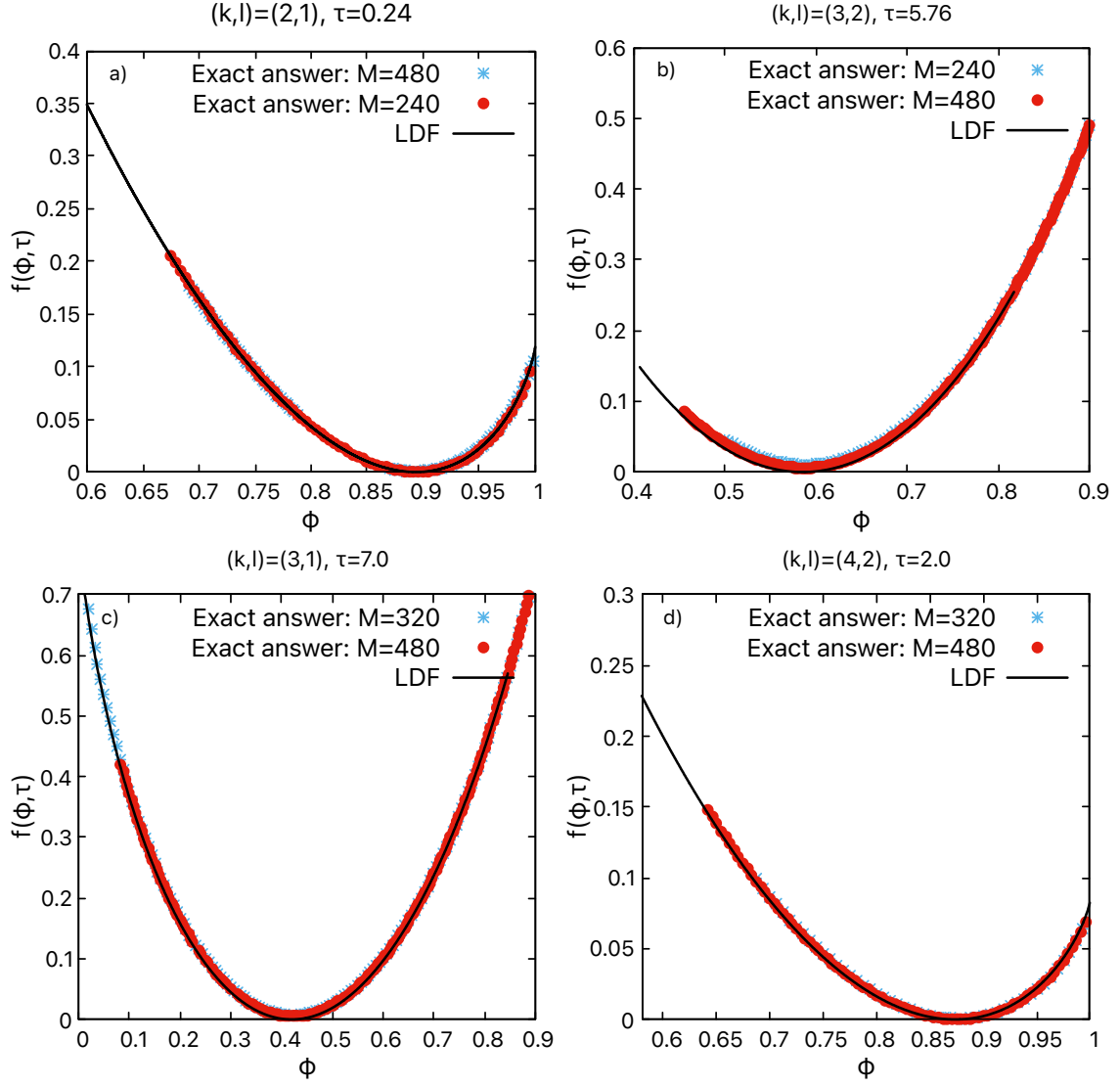
Figure 6.2: Large deviation functions $f(\phi, \tau)$ with respect to ϕ are compared with the exact answer Eq. (6.7) plotted with respect to ϕ for a) $(k, \ell) = (2, 1), \tau = 0.24$, b) $(k, \ell) = (3, 2), \tau = 5.76$, c) $(k, \ell) = (3, 1), \tau = 7.0$, d) $(k, \ell) = (4, 2), \tau = 2.0$.

Eq. (6.19), one can rewrite the energy in terms of $n(\tau)$ to be

$$E = \frac{n(\tau)^k - n(\tau)^\ell z(\tau)^{k-\ell}}{k!}. \tag{6.26}$$

Knowing the values of the boundary conditions $n(0)$ and $n(\tau_f)$, Eqs. (6.24) and (6.25) allows us to write $z(0)$ and $z(\tau_f)$, and consequently $\tilde{z}(0)$ and $\tilde{z}(\tau_f)$ in terms of E and ϕ. Additionally, integrating the first term in Eq. (6.20) by parts, and using Eq. (6.23), the rate function for general k, ℓ is

$$f(\phi, \tau) = -(k-1)E\tau - \frac{\phi}{k-\ell} \ln \frac{\phi^k - k!E}{\phi^l} + \frac{1}{k-\ell} \ln\left(1 - k!E\right) + \phi \ln \phi, \tag{6.27}$$

where E is a function of ϕ and τ. It is determined by the equation for the fraction of surviving particles n which follows from the Euler-Lagrange equations (6.22), (6.23). The corresponding initial and final conditions follow from Eqs. (6.24), (6.25). We will refer to the this equation as the *instanton equation* and analyse it below.

6.4.3   The instanton equation

The instanton trajectory for $n(\tau) = z(\tau)\tilde{z}(\tau)$ that minimizes the action is is derived from Eqs. (6.22) and (6.23) to be

$$\frac{dn}{d\tau} = (k-\ell)\left[E - \frac{n^k}{k!}\right], \tag{6.28}$$

which needs to be solved subject to the initial condition $n(0) = 1$ and the final condition $n(\tau_f) = \phi$. As the equation is of the first order, the final condition yields an equation for the 'instanton energy' E. Equation (6.28) implies that if $\tau \to (k-\ell)\tau$, then the instanton trajectory for fixed k and different ℓ should be identical. When $E = 0$, Eq. (6.28) for $n(\tau)$ reduces to the mean field equation for the mean number of particles. This corresponds to the mean field or the 'typical'
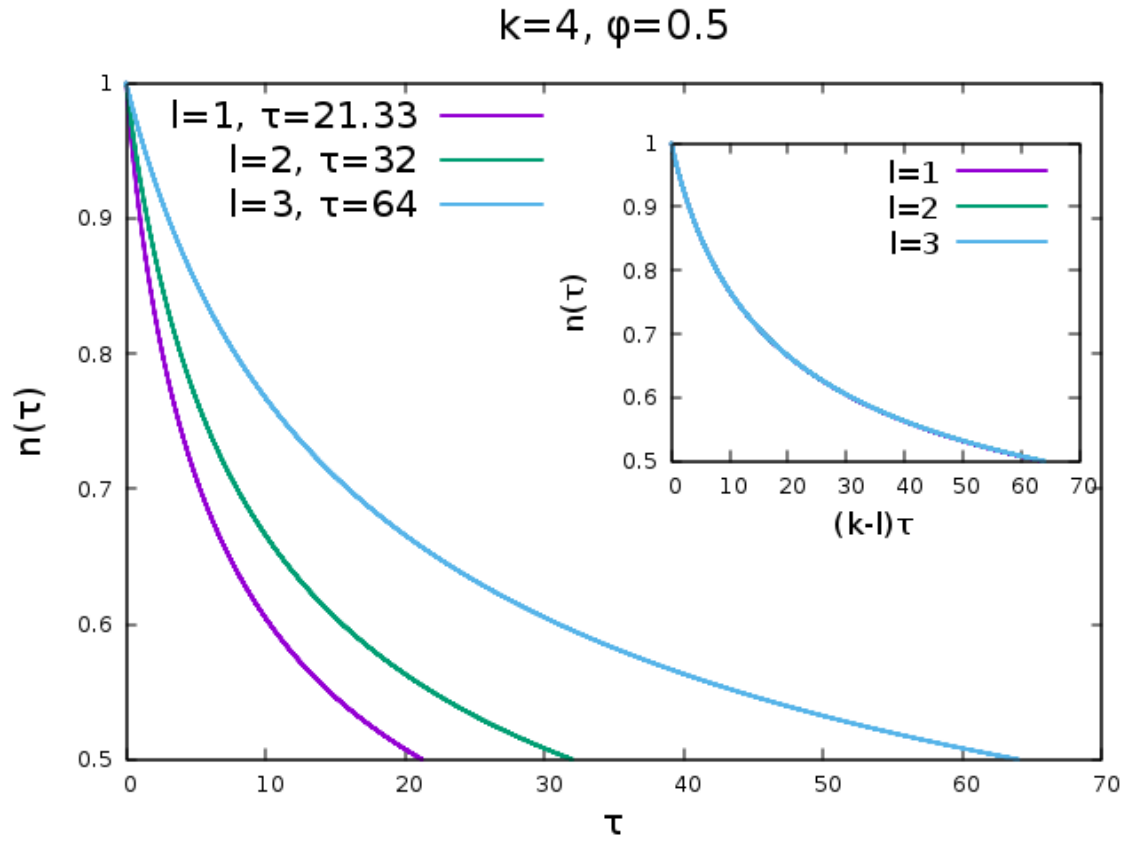
Figure 6.3: The instanton trajectories for $k = 3, \phi = 0.3$ and $\ell = 1, 2$, plotted with respect to $(k - l)\tau$ collapse.

solution which is followed by the system with the probability close to 1:

$$n(\tau) = \left[1 + \frac{(k-\ell)(k-1)\tau}{k!}\right]^{1/1-k}, \tag{6.29}$$

It is seen that the typical trajectory achieves the fraction ϕ of the surviving particles at the time

$$\tau_{typ} = \frac{k!}{(k-\ell)(k-1)} \left(\phi^{1-k} - 1\right).$$

It follows from (6.28) that $E > 0$ corresponds to rare events such that the time of reaching ϕ is smaller than τ_{typ}, $E < 0$ - rare events reaching ϕ at the time larger than τ_{typ}. The atypical trajectories corresponding to $E \neq 0$ can be obtained by solving Eq. (6.28). Rewriting it as

$$\frac{dx}{d\tau} = -\frac{(k-\ell)e_0^{k-1}}{k!}\left[x^k - 1\right], \tag{6.30}$$

where $x = n/e_0$ and $e_0^k = k!E$, factorising $1/(x^k - 1)$ in terms of the k-th roots of unity, $(\omega_i)_{i=1}^k$, and then using the partial fraction decomposition, we obtain

$$\frac{1}{x^k(\tau) - 1} = \frac{1}{\prod_{j=1}^k (x(\tau) - \omega_j)} = \sum_{m=1}^k \frac{A_m}{x(\tau) - \omega_m}, \tag{6.31}$$

where $\omega_j = e^{\frac{2\pi i j}{k}}$ and the coefficients A_m are complex. Solving for A_m, we obtain

$$A_m = \oint_{\Gamma_m} \frac{dz}{2\pi i} \frac{1}{z^k - 1} = \frac{\omega_m}{k}. \tag{6.32}$$

Here Γ_m is a small contour around the ω_m.

Substituting Eq. (6.32) into Eq. (6.31), one obtains the following implicit solution to Eq. (6.30):

$$\sum_{m=1}^k \omega_m \ln(x(\tau) - \omega_m) = -\frac{(k-\ell)(k!E)^{k-1}\tau}{(k-1)!} + c, \tag{6.33}$$

116

where the constants c and E are fixed using the initial condition, $n(0) = 1$ and the final condition $n(\tau_f) = \phi$. Solving for c, we obtain

$$\sum_{i=1}^{k} \Omega_i \ln \frac{n(\tau) - \Omega_i}{1 - \Omega_i} = -k(k - \ell)E\tau, \qquad (6.34)$$

where

$$\Omega_i = \omega_i (k!E)^{1/k}. \qquad (6.35)$$

The instanton energy E can be found by solving the equation

$$\sum_{i=1}^{k} \Omega_i \ln \frac{\phi - \Omega_i}{1 - \Omega_i} = -k(k - \ell)E\tau_f, \qquad (6.36)$$

which can be analysed either numerically or analytically in the limit of $\tau_f \gg \tau_{typ}$ or $\tau_f \ll \tau_{typ}$ (see Sec. 6.6 below).

It can be checked that for the constant kernel, $k = 2$, $\ell = 1$, we obtain

$$n(\tau) = \sqrt{2E} \coth[\sqrt{E/2}\,\tau + \tanh^{-1}\sqrt{2E}],$$

as derived in [57]. The trajectories for various values of (k, ℓ) are shown in Fig. 6.4.

6.5 Comparison with exact answer

In order to test the correctness of the rate function derived in Eq. (6.27), it is compared with the exact answer, Eq. (6.7). The rate function is plotted with respect to both τ and ϕ, as shown in Figs 6.1 and 6.2 , and shows an excellent agreement with the exact answer. Figures 6.1(a) and 6.2(a) show the rate function for binary coalescence.
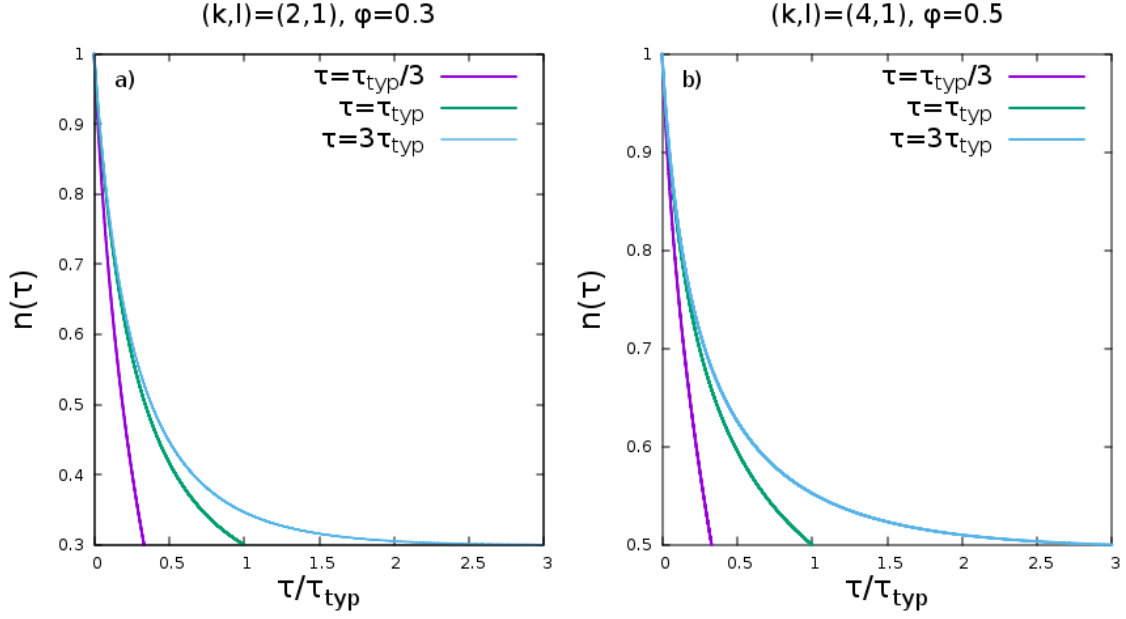
Figure 6.4: The instanton trajectories for a) Constant kernel, $(k, \ell) = (2, 1), \phi = 0.3$ and b) $(k, \ell = (3, 2), \phi = 0.7)$ are plotted for typical final time τ_{typ}, which corresponds to $E = 0$, as well as final times $\tau > \tau_{typ}$ and $\tau < \tau_{typ}$, which correspond to $E > 0$ and $E < 0$ respectively.

6.6 Asymptotic analysis

It is possible to calculate exact asymptotics for the large deviation in the limits $\tau_f >> \tau_{typ}$ (anomalously slow evolution) and $\tau_f << \tau_{typ}$ (anomalously fast evolution). Let us first consider the case $\tau_f >> \tau_{typ}$. In this limit, let us seek the solution to (6.36) in the form

$$E = \frac{\phi^k}{k!}(1 - \epsilon(\tau_f)), \tag{6.37}$$

where $\epsilon(\tau_f) << 1$. Substituting this Ansatz into (6.36) one finds

$$\epsilon(\tau_f) = \exp\left(-\frac{k(k - \ell)\phi^{k-1}}{k!}\tau_f + O(1)\right). \tag{6.38}$$

Substituting (6.37) in Eq. (6.27) and taking the limit $\tau_f \to \infty$, we obtain

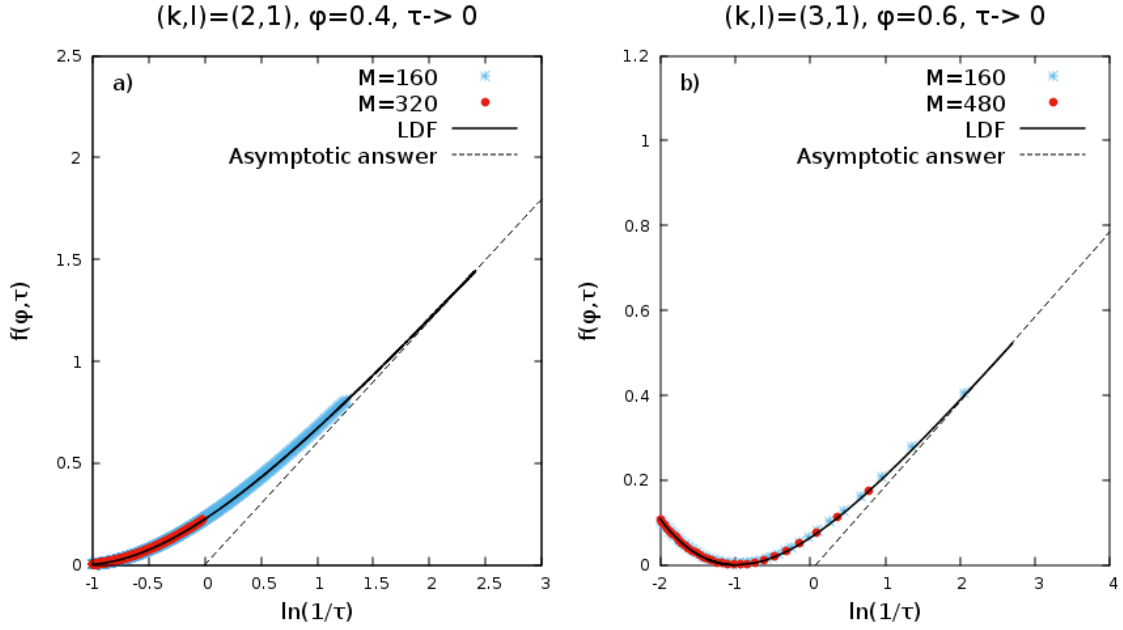$$\lim_{\tau_f \to \infty} \frac{f(\phi, \tau_f)}{\tau_f} = \frac{\phi^k}{k!}. \tag{6.39}$$

Figure 6.5: Large deviation functions $S(\phi, \tau)$ are plotted with respect to τ for a) $(k, l) = (2, 1), \phi = 0.4$ for $\tau \to \infty$, b) $(k, l) = (2, 1), \phi = 0.4$ for $\tau \to 0$, and with respect to $\ln(1/\tau)$ for c) $(k, l) = (3, 1), \phi = 0.6, \tau \to \infty$ and d) $(k, l) = (3, 1), \phi = 0.6, \tau \to 0$.

Hence, the asymptotic LDF for k-nary coalescence is the direct generalization of the constant kernel case [57]. In the short time limit, $\tau << \tau_{typ}$, the instanton energy E is large and negative. Then $|\Omega_i| >> 1$ and the equation (6.36) takes the form

$$k(1 - \phi) + O(\Omega^{-1}) = -k(k - \ell)E\tau_f.$$

The solution is

$$E = -\frac{1 - \phi}{(k - \ell)\tau_f}(1 + O(\tau_f^{1/k})). \tag{6.40}$$

Substituting this solution in the LDF (6.27) and simplifying, we obtain

$$\lim_{\tau_f \to 0} \frac{f(\phi, \tau_f)}{\ln(\tau_{typ}/\tau_f)} = \frac{1 - \phi}{k - \ell}. \tag{6.41}$$

Figures 6.1 and 6.5 show that the asymptotic answers for $\tau_f >> \tau_{typ}$ and $\tau_f << \tau_{typ}$ respectively, are in excellent agreement with the exact answers.

119

6.7 Summary

To summarize, we derived the large deviation function for the general coalescence process, $kA \to \ell A$, for arbitrary $k > \ell$ using the path integral approach. The solution minimizing the action allowed us to determine the optimal trajectory for each rare event.

For the reaction $kA \to \ell A$, it is possible to write an exact expression for $P(M, N, t)$ as a sum of exponentials. However, it is not straightforward to derive the large deviation function from this expression, neither are the scaling variables obvious. Using the Doi-Peliti-Zeldovich method helps us to circumvent these issues. First the scaling variables become obvious, second we are able to determine the exact expression for the large deviation function and third, the optimal trajectories for rare and typical events can be obtained.

The formalism used in this chapter is generalizable to reaction diffusion systems in higher dimensions, where a term related to transport of the clusters, such as a diffusion term would appear in the Euler Lagrange equations. Solvability remains an issue and a promising area for future research. The formalism can also be generalized to coalescence with input [93, 55, 68, 67], or with branching [94, 95, 60], which could exhibit interesting features such as oscillations and steady states.

Chapter 7

Conclusions and Outlook

In this thesis, we have considered the problem of irreversible cluster-cluster aggregation, focusing on the unexplored area of obtaining the probabilities of rare or atypical events. The study of this problem has a long history. Its importance stems from its ubiquitousness in various physical phenomena, as well as the mathematical challenges arising from the absence of a general formalism for out-of-equilibrium phenomena. Previous work on aggregation has largely concentrated on using the Smoluchowski equation to obtain the mass distributions for various collision kernels. However, the Smoluchowski equation can be solved exactly only for the constant, sum and product kernels, and these solutions correspond only to the typical mass distribution and moments. Lushnikov was the first to study CCA by considering the master equation as the starting point (instead of the Smoluchowski equation), and develop a Hamiltonian formalism. His most remarkable contribution in this respect was to derive an exact solution for the typical mass distribution in product kernel aggregation, which incorporated both the pre-gelation and post-gelation behaviour beautifully. Although the Doi-Peliti-Zeldovich (DPZ) method was shown to be effective in studying problems such as birth-death processes, there has not been any attempt to study large deviations in CCA analytically using this method. We

find that by combining the Hamiltonian formalism of Lushnikov, and the DPZ path integral method, we can get the explicit large deviation functions for atleast a few collision kernels.

Computing the probabilities of rare events, both numerically and analytically, is a challenging task. In our work, we have designed and implemented a numerical algorithm which establishes a large deviation principle for arbitrary collision kernels. The main success of the algorithm is that very low probabilities, of the order of 10^{-40} and smaller, can be measured. The algorithm is benchmarked with the exact answer for constant kernel aggregation. Moreover, the instanton trajectories and mass distributions for arbitrary kernels can also be computed using this algorithm. Ergodicity of the algorithm is rigorously proved. The dependence of the temporal and configurational autocorrelation times on the different parameters of the algorithm has also been characterized.

We have also developed an analytical formalism using the DPZ technique, which can in principle be used to compute the rate functions for arbitrary collision kernels. We have explicitly calculated the large deviation functions of the exactly solvable constant, sum and product kernels. This formalism is able to obtain the probabilities of rare events because the starting point is the exact master equation, and not the Smoluchowski equation which only gives the typical mass distributions.

The product kernel is a gelling kernel, and exhibits gelation for $\tau \geq 1$. We find that although the rate function itself is a continuous function and does not show a discontinuity, the second derivative of the rate function with respect to ϕ shows a jump for final time $\tau > 1$. For fixed M, the discontinuity becomes smaller with decreasing τ, and the critical ϕ_c decreases with τ. We expect that when $\tau \to 1$, $\phi_c \to 0.5$. However, to see this, we have to numerically analyse the equations for large M. But, it becomes difficult to accurately calculate the Mallows-Riordan polynomials for large values of M, limiting the maximum value of M we can study.

The exact large deviation functions for the constant, sum and product kernels have been benchmarked and found to be in excellent agreement with numerical simulations. Further, we have calculated the full mass distribution for the constant and sum kernels and benchmarked them with simulations.

We have used the formalism to calculate the large deviation function in the case of $k-$nary coalescence, where k particles collide to form l particles, at a constant rate. The large deviation function is found to be in very good agreement with the exact answer. The instanton trajectories for typical and atypical events have also been obtained.

Although stochastic aggregation models have been investigated extensively since Smoluchowski, the results have mostly been restricted to only the typical or average properties. Here, we open up unexplored avenues in this field by developing an action formalism to calculate probabilities of rare events, thus giving a complete description of the kinetics of aggregation for the first time using sophisticated analytical and numerical techniques. Our exact results for CCA and $k-$nary coalescence are also an addition to the large deviation theory literature, and generalisable to other reaction-diffusion systems such as aggregation with input, aggregation of diffusing particles, etc.

It is possible to generalise the formalism and algorithm which we have presented in this thesis, and the associated papers, to standard reaction-diffusion systems. Some generalisations of aggregation include input of particles, and full gelation ($N = 1$). The model we have considered has infinite number of degrees of freedom. It is also possible to use this formalism to study reaction-diffusion systems with other processes such as fragmentation, birth etc., especially if number of degrees of freedom are finite. Using the algorithm, it is possible to numerically compute the rate functions and instanton trajectories in the phase space of kernel parameters μ and ν, where $K(i, j) = i^\mu j^\nu + i^\nu j^\mu$. This will provide an insight into the existence and form

123

of the rate functions, as well as the convexity properties of the instanton trajectories, in extreme regions, such as those exhibiting no gelations and those exhibiting instantaneous gelation.

Bibliography

[1] MV Smoluchowski. Mathematical theory of the kinetics of the coagulation of colloidal solutions. *Z. Phys. Chem.*, 92:129–168, 1917.

[2] Nicole Riemer and AS Wexler. Droplets to drops by turbulent coagulation. *Journal of the atmospheric sciences*, 62(6):1962–1975, 2005.

[3] Bin Wang, Cunlan Guo, Zhichao Lou, and Bingqian Xu. Following the aggregation of human prion protein on au (111) surface in real-time. *Chemical Communications*, 51(11):2088–2090, 2015.

[4] Walter H Stockmayer. Theory of molecular size distribution and gel formation in branched-chain polymers. *The Journal of chemical physics*, 11(2):45–55, 1943.

[5] Alexander K Hartmann, Alexandre Krajenbrink, and Pierre Le Doussal. Probing large deviations of the kardar-parisi-zhang equation at short times with an importance sampling of directed polymers in random media. *Physical Review E*, 101(1):012134, 2020.

[6] Allan H Marcus. Stochastic coalescence. *Technometrics*, 10(1):133–143, 1968.

[7] Alex A Lushnikov. Gelation in coagulating systems. *Physica D: Nonlinear Phenomena*, 222(1-2):37–53, 2006.

[8] Georgy Th Guria, Miguel A Herrero, and Ksenia E Zlobina. A mathematical model of blood coagulation induced by activation sources. *Discrete & Continuous Dynamical Systems*, 25(1):175, 2009.

[9] Gregory Falkovich, A Fouxon, and MG Stepanov. Acceleration of rain initiation by cloud turbulence. *Nature*, 419(6903):151–154, 2002.

[10] Hans R Pruppacher and James D Klett. Microphysics of clouds and precipitation: Reprinted 1980. 2012.

[11] MMR Williams. A unified theory of aerosol coagulation. *Journal of Physics D: Applied Physics*, 21(6):875, 1988.

[12] Nikolai Brilliantov, PL Krapivsky, Anna Bodrova, Frank Spahn, Hisao Hayakawa, Vladimir Stadnichuk, and Jürgen Schmidt. Size distribution of particles in saturn's rings from aggregation and fragmentation. *Proceedings of the National Academy of Sciences*, 112(31):9536–9541, 2015.

[13] Colm Connaughton, Arghya Dutta, R Rajesh, Nana Siddharth, and Oleg Zaboronski. Stationary mass distribution and nonlocality in models of coalescence and shattering. *Physical Review E*, 97(2):022137, 2018.

[14] Adrian B Burd and George A Jackson. Particle aggregation. *Annual review of marine science*, 1:65–90, 2009.

[15] Sangeeta Benjwal, Shikha Verma, Klaus-Heinrich Röhm, and Olga Gursky. Monitoring protein aggregation during thermal unfolding in circular dichroism experiments. *Protein Science*, 15(3):635–639, 2006.

[16] Chenchong Zhang, William R Heinson, Pai Liu, Payton Beeler, Qing Li, Jingkun Jiang, and Rajan K Chakrabarty. Three-dimensional tomography reveals distinct morphological and optical properties of soot aggregates from

coal-fired residential stoves in china. *Journal of Quantitative Spectroscopy and Radiative Transfer*, 254:107184, 2020.

[17] Shuyuan Liu, Tat Leung Chan, Jianzhong Lin, and Mingzhou Yu. Numerical study on fractal-like soot aggregate dynamics of turbulent ethylene-oxygen flame. *Fuel*, 256:115857, 2019.

[18] Christopher M Sorensen, Jérôme Yon, Fengshan Liu, Justin Maughan, William R Heinson, and Matthew J Berg. Light scattering and absorption by fractal aggregates including soot. *Journal of Quantitative Spectroscopy and Radiative Transfer*, 217:459–473, 2018.

[19] Jordi Colomer, Francesc Peters, and Cèlia Marrasé. Experimental analysis of coagulation of particles under low-shear flow. *Water Research*, 39(13):2994–3000, 2005.

[20] Anvy Moly Tom, R Rajesh, and Satyavani Vemparala. Aggregation dynamics of rigid polyelectrolytes. *The Journal of Chemical Physics*, 144(3):034904, 2016.

[21] Anvy Moly Tom, Ravindran Rajesh, and Satyavani Vemparala. Aggregation of flexible polyelectrolytes: Phase diagram and dynamics. *The Journal of chemical physics*, 147(14):144903, 2017.

[22] David G Tarboton, Rafael L Bras, and Ignacio Rodriguez-Iturbe. The fractal nature of river networks. *Water resources research*, 24(8):1317–1322, 1988.

[23] Simon Heimlicher and Kavé Salamatian. Globs in the primordial soup: the emergence of connected crowds in mobile wireless networks. In *Proceedings of the eleventh ACM international symposium on Mobile ad hoc networking and computing*, pages 91–100, 2010.

[24] Nathanaël Berestycki. Recent progress in coalescent theory. *ENSAIOS MATEMÁTICOS*, 16:1–193, 2009.

[25] Dimitris Achlioptas, Raissa M D'Souza, and Joel Spencer. Explosive percolation in random networks. *science*, 323(5920):1453–1455, 2009.

[26] Raissa M D'Souza, Jesus Gómez-Gardenes, Jan Nagler, and Alex Arenas. Explosive phenomena in complex networks. *Advances in Physics*, 68(3):123–223, 2019.

[27] François Leyvraz. Scaling theory and exactly solved models in the kinetics of irreversible aggregation. *Physics Reports*, 383(2-3):95–212, 2003.

[28] David J Aldous. Deterministic and stochastic models for coalescence (aggregation and coagulation): a review of the mean-field theory for probabilists. *Bernoulli*, pages 3–48, 1999.

[29] Pavel L Krapivsky, Sidney Redner, and Eli Ben-Naim. A kinetic view of statistical physics. 2010.

[30] Jonathan AD Wattis. An introduction to mathematical models of coagulation–fragmentation processes: a discrete deterministic mean-field approach. *Physica D: Nonlinear Phenomena*, 222(1-2):1–20, 2006.

[31] John L Spouge. Exact solutions for a diffusion-reaction process in one dimension. *Physical review letters*, 60(10):871, 1988.

[32] K Kang and S Redner. Fluctuation effects in smoluchowski reaction kinetics. *Physical Review A*, 30(5):2833, 1984.

[33] Supriya Krishnamurthy, R Rajesh, and Oleg Zaboronski. Kang-redner small-mass anomaly in cluster-cluster aggregation. *Physical Review E*, 66(6):066118, 2002.

[34] Supriya Krishnamurthy, R Rajesh, and Oleg Zaboronski. Persistence properties of a system of coagulating and annihilating random walkers. *Physical Review E*, 68(4):046103, 2003.

[35] Yehuda Ben-Zion and Ilya Zaliapin. Localization and coalescence of seismicity before large earthquakes. *Geophysical Journal International*, 223(1):561–583, 2020.

[36] T Congy, GA El, G Roberti, A Tovbis, S Randoux, and P Suret. Statistics of extreme events in integrable turbulence. *Physical Review Letters*, 132(20):207201, 2024.

[37] Francesco Ragone and Freddy Bouchet. Rare event algorithm study of extreme warm summers and heatwaves over europe. *Geophysical Research Letters*, 48(12):e2020GL091197, 2021.

[38] Francesco Ragone, Jeroen Wouters, and Freddy Bouchet. Computation of extreme heat waves in climate models using a large deviation algorithm. *Proceedings of the National Academy of Sciences*, 115(1):24–29, 2018.

[39] Lucía Morales and Bernadette Andreosso-O'Callaghan. Covid19: Global stock markets "black swan". 2020.

[40] Jaclyn Iannucci, William Renehan, and Paula Grammas. Thrombin, a mediator of coagulation, inflammation, and neurotoxicity at the neurovascular interface: Implications for alzheimer's disease. *Frontiers in neuroscience*, 14:762, 2020.

[41] Hugo Touchette. The large deviation approach to statistical mechanics. *Physics Reports*, 478(1-3):1–69, 2009.

[42] Alexander K Hartmann. Large-deviation properties of largest component for random graphs. *The European Physical Journal B*, 84(4):627–634, 2011.

[43] Alexander K Hartmann and Marc Mézard. Distribution of diameters for erdős-rényi random graphs. *Physical Review E*, 97(3):032128, 2018.

[44] Lasse Ebener, Georgios Margazoglou, Jan Friedrich, Luca Biferale, and Rainer Grauer. Instanton based importance sampling for rare events in stochastic pdes. *Chaos: An Interdisciplinary Journal of Nonlinear Science*, 29(6):063102, 2019.

[45] Carsten Hartmann, Omar Kebiri, Lara Neureither, and Lorenz Richter. Variational approach to rare event simulation using least-squares regression. *Chaos: An Interdisciplinary Journal of Nonlinear Science*, 29(6):063107, 2019.

[46] Frédéric Cérou, Arnaud Guyader, and Mathias Rousset. Adaptive multilevel splitting: Historical perspective and recent results. *Chaos: An Interdisciplinary Journal of Nonlinear Science*, 29(4):043108, 2019.

[47] Freddy Bouchet, Joran Rolland, and Jeroen Wouters. Rare event sampling methods, 2019.

[48] Tobias Grafke and Eric Vanden-Eijnden. Numerical computation of rare events via large deviation theory. *Chaos: An Interdisciplinary Journal of Nonlinear Science*, 29(6):063118, 2019.

[49] AA Lushnikov. Evolution of coagulating systems. *Journal of Colloid and Interface Science*, 45(3):549–556, 1973.

[50] Alexei A Lushnikov. Coagulation in finite systems. *Journal of Colloid and interface science*, 65(2):276–285, 1978.

[51] Rahul Dandekar, R Rajesh, V Subashri, and Oleg Zaboronski. A monte carlo algorithm to measure probabilities of rare events in cluster-cluster aggregation. *Computer Physics Communications*, 288:108727, 2023.

[52] Mark Denny. Introduction to importance sampling in rare-event simulations. *European Journal of Physics*, 22(4):403, 2001.

[53] Daniel T Gillespie. An exact method for numerically simulating the stochastic coalescence process in a cloud. *Journal of Atmospheric Sciences*, 32(10):1977–1989, 1975.

[54] PGJ Van Dongen and MH Ernst. Dynamic scaling in the kinetics of clustering. *Physical review letters*, 54(13):1396, 1985.

[55] Colm Connaughton, R Rajesh, and Oleg Zaboronski. Stationary kolmogorov solutions of the smoluchowski aggregation equation with a source term. *Physical Review E*, 69(6):061114, 2004.

[56] MS Veshchunov. A new approach to the brownian coagulation theory. *Journal of aerosol science*, 41(10):895–910, 2010.

[57] R Rajesh, V Subashri, and Oleg Zaboronski. Exact calculation of the probabilities of rare events in cluster-cluster aggregation. *Physical Review Letters*, 133(9):097101, 2024.

[58] Nikolai V Brilliantov, Wendy Otieno, and PL Krapivsky. Nonextensive supercluster states in aggregation with fragmentation. *Physical Review Letters*, 127(25):250602, 2021.

[59] Aleksei Kalinov, AI Osinsky, Sergey A Matveev, W Otieno, and Nikolai V Brilliantov. Direct simulation monte carlo for new regimes in aggregation-fragmentation kinetics. *Journal of Computational Physics*, 467:111439, 2022.

[60] Robin C Ball, Colm Connaughton, Peter P Jones, R Rajesh, and Oleg Zaboronski. Collective oscillations in irreversible coagulation driven by monomer inputs and large-cluster outputs. *Physical review letters*, 109(16):168304, 2012.

[61] Masao Doi. Second quantization representation for classical many-particle system. *Journal of Physics A: Mathematical and General*, 9(9):1465, 1976.

[62] Masao Doi. Stochastic theory of diffusion-controlled reaction. *Journal of Physics A: Mathematical and General*, 9(9):1479, 1976.

[63] Luca Peliti. Path integral approach to birth-death processes on a lattice. *Journal de Physique*, 46(9):1469–1483, 1985.

[64] AA Ovchinnikov and Ya B Zeldovich. Role of density fluctuations in bimolecular reaction kinetics. *Chemical Physics*, 28(1-2):215–218, 1978.

[65] Uwe C. Täuber. *Critical Dynamics: A Field Theory Approach to Equilibrium and Non- Equilibrium Scaling Behavior*. Cambridge University Press, 2014.

[66] John Cardy. Reaction-diffusion processes. *A+ A*, 100:26, 2006.

[67] Colm Connaughton, R Rajesh, and Oleg Zaboronski. Cluster–cluster aggregation as an analogue of a turbulent cascade: Kolmogorov phenomenology, scaling laws and the breakdown of self-similarity. *Physica D: Nonlinear Phenomena*, 222(1-2):97–115, 2006.

[68] Colm Connaughton, R Rajesh, and Oleg Zaboronski. Breakdown of kolmogorov scaling in models of cluster aggregation. *Physical review letters*, 94(19):194503, 2005.

[69] Donald E Knuth. Linear probing and graphs. *Algorithmica*, 22:561–568, 1998.

[70] George M Hidy, James Rush Brock, et al. *Dynamics of aerocolloidal systems*. Pergamon Press, 1970.

[71] RL Drake. Topics in current aerosol research, vol. 3, part 2, 1972.

[72] Colm Connaughton, Arghya Dutta, R Rajesh, and Oleg Zaboronski. Universality properties of steady driven coagulation with collisional evaporation. *Europhysics Letters*, 117(1):10002, 2017.

[73] Lynn M Bekris, Chang-En Yu, Thomas D Bird, and Debby W Tsuang. Genetics of alzheimer disease. *Journal of geriatric psychiatry and neurology*, 23(4):213–227, 2010.

[74] André Pineau, Amine A Benzerga, and Thomas Pardoen. Failure of metals i: Brittle and ductile fracture. *Acta Materialia*, 107:424–483, 2016.

[75] Fahad Puthalath, Apurba Biswas, VV Prasad, and R Rajesh. Lattice models for ballistic aggregation: Cluster-shape-dependent exponents. *Physical Review E*, 108(4):044127, 2023.

[76] Luisa Andreis, Wolfgang König, and RI Patterson. A large-deviations approach to gelation. *SFB 1114 Preprint in arXiv: 1901.01876*, pages 1–22, 2019.

[77] Hannes Hinterbichler, Carole Planchette, and Günter Brenn. Ternary drop collisions. *Experiments in fluids*, 56:1–12, 2015.

[78] Benjamin P Lee. Renormalization group calculation for the reaction ka to oe. *Journal of Physics A: Mathematical and General*, 27(8):2633, 1994.

[79] Daniel Ben-Avraham. Complete exact solution of diffusion-limited coalescence, $a + a \rightarrow a$. *Physical review letters*, 81(21):4756, 1998.

[80] Daniel Ben-Avraham. Inhomogeneous steady states of diffusion-limited coalescence, $a + a \rightleftharpoons a$. *Physics Letters A*, 249(5-6):415–423, 1998.

[81] Dmytro Shapoval, Maxym Dudka, Xavier Durang, and Malte Henkel. Crossover between diffusion-limited and reaction-limited regimes in the coagulation–diffusion process. *Journal of Physics A: Mathematical and Theoretical*, 51(42):425002, 2018.

[82] Ranjiva M Munasinghe, R Rajesh, and Oleg V Zaboronski. Multiscaling of correlation functions in single species reaction-diffusion systems. *Physical Review E—Statistical, Nonlinear, and Soft Matter Physics*, 73(5):051103, 2006.

[83] Ranjiva Munasinghe, R Rajesh, Roger Tribe, and Oleg Zaboronski. Multi-scaling of the n-point density function for coalescing brownian motions. *Communications in Mathematical Physics*, 268:717–725, 2006.

[84] L Peliti. Renormalisation of fluctuation effects in the a+a to a reaction. *Journal of Physics A: Mathematical and General*, 19(6):L365, 1986.

[85] AA Lushnikov. Binary reaction $1 + 1 \rightarrow 0$ in one dimension. *Physics Letters A*, 120(3):135–137, 1987.

[86] G Oshanin, A Stemmer, S Luding, and A Blumen. Smoluchowski approach for three-body reactions in one dimension. *Physical Review E*, 52(6):5800, 1995.

[87] Yu Jiang, Hu Gang, and Ma BenKun. Critical property and universality in the generalized smoluchovski coagulation equation. *Physical Review B*, 41(13):9424, 1990.

[88] Yu Jiang. Scaling theory for multipolymer coagulation. *Physical Review E*, 50(6):4901, 1994.

[89] PL Krapivsky and Sergey A Matveev. Gelation in input-driven aggregation. *arXiv preprint arXiv:2404.01032*, 2024.

[90] Stéphan Clémençon, Anthony Cousien, Miraine Dávila Felipe, and Viet Chi Tran. On computer-intensive simulation and estimation methods for rare-event analysis in epidemic models. *Statistics in Medicine*, 34(28):3696–3713, 2015.

[91] R. Rajesh, V. Subashri, and Oleg Zaboronski. Exact calculation of the large deviation function for k-nary coalescence, 2024.

[92] Chris D Greenman. Doi–peliti path integral methods for stochastic systems with partial exclusion. *Physica A: Statistical Mechanics and its Applications*, 505:211–221, 2018.

[93] Pablo A Alemany and Daniel ben Avraham. Inter-particle distribution functions for one-species diffusion-limited annihilation, $a + a \rightarrow 0$. *Physics Letters A*, 206(1-2):18–25, 1995.

[94] Daniel Ben-Avraham. Diffusion-limited coalescence, $a + a \rightleftharpoons a$, with a trap. *Physical Review E*, 58(4):4351, 1998.

[95] Daniel ben Avraham. Fisher waves in the diffusion-limited coalescence process $a + a \rightleftharpoons a$. *Physics Letters A*, 247(1-2):53–58, 1998.